

Mechanistic insights into the interactions of HTRA1 with pathological Tau species

Dissertation

zur Erlangung des Doktorgrades

Dr. rer. nat.

der Fakultät für Biologie

an der

Universität Duisburg-Essen

vorgelegt von

Birte Hagemeier

aus Castrop-Rauxel

April 2024

DuEPublico

Duisburg-Essen Publications online

UNIVERSITÄT
DUISBURG
ESSEN

Offen im Denken

ub

universitäts
bibliothek

Diese Dissertation wird via DuEPublico, dem Dokumenten- und Publikationsserver der Universität Duisburg-Essen, zur Verfügung gestellt und liegt auch als Print-Version vor.

DOI: 10.17185/duepublico/82705

URN: urn:nbn:de:hbz:465-20250722-133634-2

Alle Rechte vorbehalten.

Die der vorliegenden Arbeit zugrunde liegenden Experimente wurden am Zentrum für Medizinische Biotechnologie an der Universität Duisburg-Essen durchgeführt.

1. Gutachter: Prof. Dr. Michael Ehrmann
2. Gutachter: Prof. Dr. Peter Bayer
3. Gutachter: Prof. Dr. Elsa Sánchez García

Vorsitzender des Prüfungsausschusses: Prof. Dr. Barbara Saccà

Tag der mündlichen Prüfung: 11.10.2024

In the context of this doctoral work, the following article was submitted for publication:

Beaufort N., Ingendahl L., Merdanovic M., Schmid A., Podlesainski D, Richter T., Neumann T., Kuszner M., Vetter I.R., Stege P., Burston S.G., Filipovic A., Ruiz-Blanco Y.B., Bravo-Rodriguez K., Mieres-Perez J., Beuck C., Uebel S., Zobawa M., Schillinger J., Malik R., Todorov-Völgyi K., Rey J., Roberti A., Hagemeyer B., Wefers B., Müller S.A., Wurst W., Sanchez-Garcia E., Zimmermann A., Hu X., Clausen T., Huber R., Lichtenthaler S.F., Schmuck C., Giese M., Kaiser M., Ehrmann M., and Dichgans M.: Rational correction of pathogenic conformational defects in HTRA1.: *Nat Commun*

Table of Contents

List of Figures	IV
List of Tables	VI
Abbreviations	VII
Abstract	1
Zusammenfassung.....	3
1. Introduction	5
1.1 Proteostasis and protein quality control.....	5
1.2 High temperature requirement A proteases.....	8
1.3 HTRA1.....	11
1.4 Microtubule-associated protein Tau.....	17
1.5 Objectives.....	23
2. Materials	25
2.1 Devices.....	25
2.2 Consumables.....	26
2.3 Chemicals and substances.....	27
2.4 Buffers and Media	27
2.5 Antibiotics	30
2.6 <i>Escherichia coli</i> strains	31
2.7 Plasmids.....	31
2.8 Primers	32
2.9 Proteins	32
2.10 Enzymes.....	33
2.11 DNA and protein standards	33
2.12 Software	34

3. Methods	35
3.1 Molecular biology methods.....	35
3.1.1 Polymerase chain reaction.....	35
3.1.2 DNA assembly.....	36
3.1.3 Agarose gel electrophoresis.....	36
3.2 Microbiology methods.....	37
3.2.1 Determination of bacterial cell density in suspension.....	37
3.2.2 Transformation.....	37
3.2.3 Isolation of plasmid DNA.....	37
3.2.4 Protein expression.....	37
3.3 Biochemical methods.....	38
3.3.1 Protein purification of recombinant Tau variants.....	38
3.3.2 Protein purification of recombinant HTRA1 variants.....	39
3.3.3 Sodium dodecyl sulfate-polyacrylamide gel electrophoresis.....	39
3.3.4 <i>In vitro</i> phosphorylation of recombinant Tau.....	40
3.3.5 Formation of Tau fibrils.....	40
3.3.6 Generation of Tau fibril seeds.....	40
3.3.7 Fibril sedimentation assay.....	41
3.3.8 Thioflavin T fluorescence.....	41
3.3.9 Atomic force microscopy imaging.....	41
3.3.10 Microtubule co-sedimentation assay.....	42
3.3.11 <i>In vitro</i> proteolysis assays.....	42
3.3.12 Time-resolved proteolysis and analysis by mass spectrometry.....	42
3.3.13 Cross-linking assay.....	43
3.3.14 HTRA1 activity assay.....	43
3.3.15 Fluorescence-labeling of HTRA1.....	44
4. Results	45
4.1 Formation of pathological Tau species.....	45
4.1.1 Hyperphosphorylation of recombinant Tau.....	45
4.1.2 Formation of Tau fibrils.....	47
4.2 Interactions of HTRA1 and Tau with microtubules.....	48
4.2.1 HTRA1 and Tau bind to microtubules simultaneously.....	49
4.2.2 Hyperphosphorylated Tau loses ability to bind to microtubules.....	50

4.3	Differences in the degradation of native, hyperphosphorylated, and fibrillar Tau by HTRA1	51
4.4	HTRA1 efficiently degrades Tau fibrils	55
4.4.1	Visualization of the Tau fibril degradation process	55
4.4.2	Spatial and temporal resolution of the degradation of Tau fibrils by HTRA1	57
4.4.3	Initial interaction sites of HTRA1 and Tau fibrils	61
4.5	N-terminal region of Tau is resistant to HTRA1 cleavage	64
4.6	Activation of HTRA1 by pathological Tau species	68
4.7	HTRA1 reduces amyloid- β plaque load in cerebral organoids	71
5.	Discussion	74
5.1	HTRA1 distinguishes between different Tau species	74
5.2	Mechanistic insights into the process of Tau fibril degradation by HTRA1	78
5.3	Model of HTRA1-Tau interactions under physiological and pathological conditions	81
5.4	Outlook	84
6.	Bibliography	86
	Appendix	101
	Danksagung	105
	Lebenslauf	106
	Eidesstattliche Erklärung	107

List of Figures

Figure 1: Overview of proteostasis	6
Figure 2: Domain structure of different HtrA proteases	8
Figure 3: Structure of HTRA1	13
Figure 4: The six different Tau isoforms of the human adult CNS	18
Figure 5: Tau in physiology and pathology	20
Figure 6: Structures of Tau fibrils	22
Figure 7: Sequential hyperphosphorylation of Tau generates AD-specific epitopes.....	46
Figure 8: <i>In vitro</i> formation of Tau fibrils	48
Figure 9: Tau and HTRA1 co-sediment with microtubules	50
Figure 10: Hyperphosphorylated Tau-ps and Tau-pg do not bind and stabilize microtubules.....	51
Figure 11: Degradation of native, hyperphosphorylated, and fibrillar Tau by HTRA1	52
Figure 12: Number of HTRA1 cleavage sites in native, hyperphosphorylated, and fibrillar Tau.....	54
Figure 13: Visualization of the Tau fibril degradation by HTRA1	56
Figure 14: Temporal and spatial resolution of HTRA1 cleavage sites within the sequence of fibrillar Tau	58
Figure 15: Evolution of HTRA1 cleavage sites within the core region of Tau fibrils.....	59
Figure 16: HTRA1 cleavage sites mapped to a structure of <i>in vitro</i> formed Tau fibrils.....	61
Figure 17: Interactions of HTRA1 and Tau fibrils.....	63
Figure 18: Tau constructs with exchanged N- and C-terminal region.....	65
Figure 19: Degradation of Tau, Tau ^{CN} , and Tau ^{CNC} fibrils by HTRA1	67

Figure 20: Activation of HTRA1 by Tau fibrils.....	69
Figure 21: Degradation of native and fibrillar Tau by HTRA1 under activating conditions	70
Figure 22: HTRA1 reduces A β deposits in cerebral organoids.....	72
Figure 23: Interaction of substrates with HTRA1 loop L3 and active site	79
Figure 24: Model of HTRA1 implications in Tau pathology.....	82
Figure 25: Relative amino acid distribution around HTRA1 cleavage sites within the Tau sequence.....	103

List of Tables

Table 1: List of devices.....	25
Table 2: List of consumables.....	26
Table 3: List of buffers and media	27
Table 4: List of antibiotics	30
Table 5: List of <i>Escherichia coli</i> strains	31
Table 6: List of plasmids.....	31
Table 7: List of primers.....	32
Table 8: List of proteins	32
Table 9: List of enzymes	33
Table 10: List of DNA and protein standards.....	33
Table 11: List of software	34
Table 12: PCR Reaction Setup	35
Table 13: PCR Cycling Parameters.....	35
Table 14: Assembly Reaction Setup	36
Table 15: Phosphorylation sites of Tau detected by LC-MS/MS	101

Abbreviations

aa	Amino acid
A β	Amyloid- β peptide
AD	Alzheimer's disease
AFM	Atomic force microscopy
AGE	Agarose gel electrophoresis
ALP	Autophagy-lysosomal pathway
AMD	Age-related macular degeneration
<i>A. thaliana</i>	<i>Arabidopsis thaliana</i>
ATP	Adenosine triphosphate
CARASIL	Cerebral autosomal dominant arteriopathy with subcortical infarcts and leukoencephalopathy
CBD	Corticobasal degeneration
CNS	Central nervous system
Cryo-EM	Cryo-electron microscopy
CTE	Chronic traumatic encephalopathy
CV	Column volumes
DNA	Deoxyribonucleic acid
DPBS	Dulbecco's phosphate-buffered saline
DTT	Dithiothreitol
ECM	Extracellular matrix
<i>E. coli</i>	<i>Escherichia coli</i>
EDTA	Ethylenediaminetetraacetic acid
EGTA	Egtazic acid

E1	Ubiquitin-activating enzyme
E2	Ubiquitin-conjugating enzyme
E3	Ubiquitin ligase
GSK3 β	Glycogen synthase kinase 3 β
HAP	Hydroxyapatite
HD	Huntington's disease (HD)
HEPES	4-(2-hydroxyethyl)-1-piperazineethanesulfonic acid
hiPSCs	Human induced pluripotent stem cells
<i>H. sapiens</i>	<i>Homo sapiens</i>
HSP	Heat-shock protein
HtrA	High temperature requirement A
IGF	Insulin-like growth factor
IGFBP	Insulin growth factor binding domain
IPTG	Isopropyl β -D-1-thiogalactopyranoside
KI	Kazal protease inhibitor domain
LC	Liquid chromatography
LC-MS/MS	Liquid chromatography tandem-mass spectrometry
MAP	Microtubule-associated protein
MOPS	3-(N-morpholino)propanesulfonic acid
MS	Mass spectrometry
MT	Microtubule
MTBD	Microtubule-binding domain
MW	Molecular weight
N	N-terminal inserts

NFTs	Neurofibrillary tangles
NHS	N-hydroxysuccinimide
OD ₆₀₀	Optical density measured at a wavelength of 600nm
PAGE	Polyacrylamide gel electrophoresis
PBS	Phosphate-buffered saline
PCR	Polymerase chain reaction
PDB	Protein Data Bank
PDZ	Postsynaptic density of 95 kDa, Discs large and zonula occludens1
PHF	Paired helical filament
PiD	Pick's disease
PIPES	Piperazine-N,N'-bis(2-ethanesulfonic acid)
PKA	cAMP-dependent protein kinase A
pNA	para-nitroaniline
PQC	Protein quality control
PSP	Progressive supranuclear palsy
R	Repeats
RFU	Relative fluorescence units
RT	Room temperature
SAPK4	Stress-activated protein kinase 4
SAXS	Small angle X ray scattering
SDS	Sodium dodecyl sulfate
SEC	Size exclusion chromatography
SF	Straight filament
SOB	Super Optimal Broth

SS	Signal sequence
TAE	Tris-acetate-EDTA
TCEP	Tris-(2-carboxyethyl)-phosphine
TGF- β	Transforming growth factor- β
ThT	Thioflavin T
TM	Transmembrane domain
Tris	Tris(hydroxymethyl)aminomethane
UPS	Ubiquitin-proteasome system
XL-MS	Chemical cross-linking mass spectrometry

Abstract

A balanced and functional set of proteins is crucial for cell viability, as proteins are the key players in biological processes that direct almost all cellular functions. Aggregation of proteins into highly ordered amyloid fibrils is associated with loss of protein function as well as gain of toxic function and is, therefore, considered a serious hazard for cells. Fibrils of the human protein Tau are a hallmark of several neurodegenerative diseases termed Tauopathies, including Alzheimer's disease as a prominent example. Despite intensive research, the underlying molecular mechanisms and cellular strategies for preventing Tauopathies are still not well understood. Recently, Tau as well as Tau fibrils were identified as substrates of the human serine protease HTRA1. Defining features such as combination of protease and chaperone function, ATP independence, and tightly regulated reversible activation make HTRA1 a remarkable factor of the protein quality control system. In this study, I investigated the interactions of HTRA1 with pathological Tau species and thus gained detailed mechanistic insights into the process of fibril degradation.

Hyperphosphorylated and fibrillar Tau were generated as disease-relevant Tau species, and their interactions with HTRA1 were analyzed using different biochemical assays. Comparison with native Tau revealed that HTRA1 distinguishes native and pathological Tau species, and specifically targets fibrils by conformation-specific recognition. Interactions between HTRA1 and Tau fibrils result in activation of HTRA1 and, subsequently, efficient degradation of the fibrils. Visualization of the degradation process by atomic force microscopy revealed a mechanism with simultaneous degradation of Tau molecules along the entire length of a fibril by multiple HTRA1 molecules. Combining time-resolved and cross-linking mass spectrometry, I identified initial interactions between loop L3 of the HTRA1 protease domain and the C-terminal region of the Tau molecules within the fibril. Subsequently, the tightly packed fibril core is completely degraded into small peptides within minutes, making reassembly seem unfeasible. Preliminary experiments indicate similar degradation of fibrils formed by amyloid- β peptide, suggesting a general role of HTRA1 in counteracting amyloid-associated pathologies. Overall, this study provides new insights into how fibrils, characterized by strong inter- and intramolecular interactions, are

degraded and contributes to a deeper understanding of the mechanisms cells have evolved to counteract protein aggregation.

Zusammenfassung

Proteine übernehmen eine zentrale Rolle in nahezu allen biologischen Prozessen und zellulären Funktionen. Daher haben die Funktionsfähigkeit sowie die richtige Konzentration und Lokalisation von Proteinen eine fundamentale Bedeutung für die Lebensfähigkeit der Zelle. Die Aggregation von Proteinen zu amyloiden Fibrillen geht mit einem Funktionsverlust sowie der Entstehung von Toxizität einher und hat daher schwerwiegende Auswirkungen auf die Zellintegrität. Fibrillen des humanen Proteins Tau sind das charakteristische Merkmal einer Reihe von neurodegenerativen Erkrankungen, die als Tauopathien bezeichnet werden. Dabei ist die Alzheimersche Krankheit wohl das bekannteste Beispiel. Trotz intensiver Forschung sind die zugrunde liegenden Prozesse von Tauopathien und dadurch ausgelöste zelluläre Reaktionen noch nicht ausreichend verstanden. Kürzlich wurden sowohl Tau als auch Tau-Fibrillen als Substrate der humanen Serinprotease HTRA1 identifiziert. Besondere Eigenschaften wie die Kombination von Protease- und Chaperonfunktion, Unabhängigkeit von ATP und die reversible Aktivierung machen HTRA1 zu einem bemerkenswerten Teil der zellulären Proteinqualitätskontrolle. Im Rahmen dieser Arbeit habe ich daher die Interaktionen von HTRA1 mit pathologischen Formen von Tau untersucht und so detaillierte mechanistische Einblicke in den Prozess des Fibrillenabbaus erhalten.

Zunächst wurde hyperphosphoryliertes und fibrilläres Tau generiert und die Interaktionen von HTRA1 mit den beiden pathologischen Tau-Formen wurde in unterschiedlichen biochemischen Verfahren analysiert. Der Vergleich mit nativem Tau ergab, dass HTRA1 zwischen nativen und pathologischen Formen von Tau unterscheidet konformationsabhängig gezielt Fibrillen erkennt und diese effizient abbaut. Die Visualisierung des Abbauprozesses mittels Rasterkraftmikroskopie zeigte, dass der Abbau entlang der gesamten Fibrille gleichzeitig durch mehrere HTRA1 Moleküle stattfindet. Weitere Details des Abbaumechanismus wurden mittels zeitaufgelöster und *cross-linking* Massenspektrometrie untersucht. Dabei wurden initiale Interaktionen zwischen dem Loop L3 der HTRA1 Proteasedomäne und der C-terminalen Tau Region identifiziert. Im Anschluss an die initiale Bindung wird der dicht gepackte Fibrillenkern innerhalb weniger Minuten vollständig in kleine Peptide gespalten. Eine erneute Aggregation der Proteolyseprodukte scheint auf Grund der geringen Größe der Peptide eher unwahrscheinlich. Vorläufige Experimente mit

Fibrillen des Amyloid- β Peptids weisen ebenfalls auf einen Abbau durch HTRA1 hin und legen daher eine generelle Funktion von HTRA1 bei der Bekämpfung von Amyloid-assoziierten Pathologien nahe. Insgesamt liefert diese Studie neue Erkenntnisse darüber wie Fibrillen abgebaut werden und trägt so zu einem tieferen Verständnis der zellulären Mechanismen bei, die der Proteinaggregation entgegenwirken.

1. Introduction

1.1 Proteostasis and protein quality control

Proteins are the key players in biological processes that direct almost all functions of the cell. Therefore, cell viability is dependent on a balanced and functional set of proteins. To be functional, proteins must fold into a three-dimensional structure known as the native state. Some proteins also need to assemble correctly into dimers and multimers. Moreover, proteins need to be at the right localization at appropriate abundance within the cell. The regulatory process that maintains all these aspects and adapts them to constantly changing requirements and tasks of the cell is known as protein homeostasis or proteostasis (Hartl et al., 2011; Jayaraj et al., 2020).

Proteostasis is conducted by an integrated network of protein quality control (PQC) factors that work in each life stage of a protein, starting with protein synthesis and folding (Figure 1). Only a minor part of proteins can self-fold during synthesis. Most proteins have complex structures and frequently show intermediate states during folding into their native state. Intermediate folding states are often unstable and expose hydrophobic amino acid residues that are typically buried in the native state. In the densely crowded environment of the cell, these proteins have a high risk of misfolding or aggregation (Ellis and Minton, 2006; Bartlett and Radford, 2009). Therefore, folding of these proteins is assisted by molecular chaperones and their regulatory cochaperones. Chaperones can assist protein folding already during synthesis or after release of the polypeptide from the ribosome. Typically, they bind to hydrophobic areas of the unfolded protein, keeping it in a folding-competent state. Then, folding is induced by an ATP-dependent cycle of binding and release (Hartl et al., 2011; Jayaraj et al., 2020).

Next to *de novo* folding, chaperones also act in conformational maintenance. They refold proteins that are misfolded or stress-denatured, prevent protein aggregation, and even dissolve protein aggregates. These chaperones, typically known as heat-shock proteins (HSPs), are induced under stress conditions when amounts of aberrant proteins are elevated (Jayaraj et al., 2020). Maintenance of conformational

integrity is of particular relevance, as the native structure of many proteins is highly flexible to allow conformational changes that are required for function. Moreover, a considerable part of proteins contain non-folding regions or are inherently disordered, making them prone to aggregation (Dunker et al., 2008).

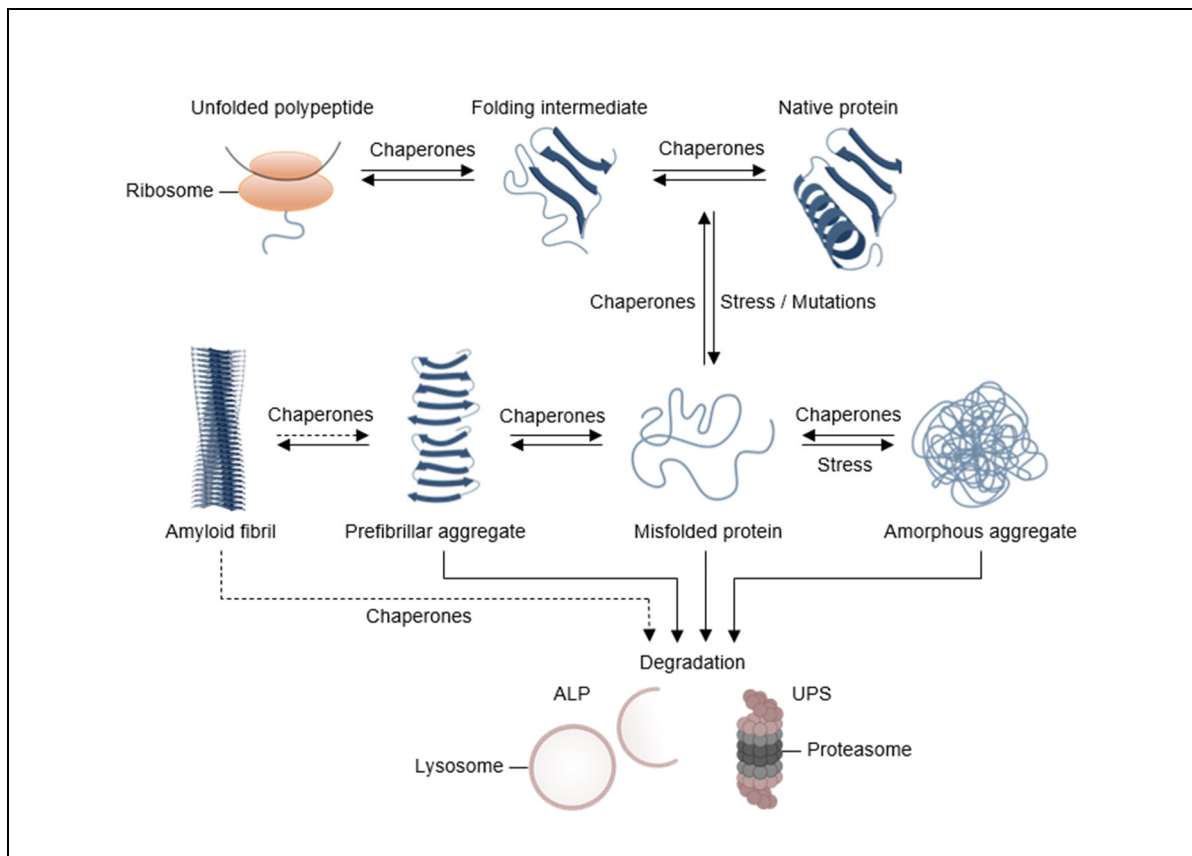


Figure 1: Overview of proteostasis

During or after synthesis, proteins must fold into their native three-dimensional structure to be functional. The folding process of the majority of proteins is highly complex and, therefore, often shows intermediate folding states. Under stress conditions or due to mutation, unfolding or misfolding of proteins can occur, which may aggregate into amorphous aggregates or also into amyloid fibrils. Cells have evolved a complex system of protein quality control factors that include a multitude of chaperones and proteases to maintain proteostasis. While chaperones assist in folding and conformational maintenance, proteases degrade misfolded and aggregated proteins. In eukaryotic cells, the ubiquitin-proteasome system (UPS) and the autophagy lysosomal pathway (ALP) represent the two main degradation pathways. Arrows indicate processes that may involve multiple steps and arrows with dashed lines represent processes of minor relevance. (Figure adapted from Tyedmers et al., 2010)

After synthesis and folding, controlled degradation is the last step in the life cycle of proteins. Degradation occurs as part of the natural turnover to keep balanced protein levels. It is also a mechanism of cell regulation. Degradation of regulatory molecules allows quick responses to external or internal stimuli. Furthermore, it is used to

eliminate damaged and misfolded proteins when (re)folding has failed. In eukaryotic cells, protein degradation is mainly achieved by two pathways, the ubiquitin-proteasome system (UPS) and the autophagy-lysosomal pathway (ALP). The UPS is based on ubiquitination of target proteins, which leads to their recognition and degradation by the proteasome. Ubiquitination is a strictly regulated multistep process that is performed by a cascade of enzymes, consisting of ubiquitin-activating enzyme (E1), ubiquitin-conjugating enzyme (E2), and ubiquitin ligase (E3). A multitude of E3 enzymes is what makes the UPS both versatile and selective. Target proteins are then transported to the proteasome, a large protein complex, where they are unfolded, translocated, deubiquitinated, and degraded. Compared to the UPS, the ALP is less selective. In a process known as autophagy, cytoplasmic proteins or whole organelles are enwrapped by an autophagic vesicle. The formed autophagosome then fuses with lysosomes that contain numerous hydrolases. These hydrolases are of low specificity and can efficiently degrade the enclosed proteins (Finley, 2009; Xie and Klionsky, 2007)

Various conditions can compromise proteostasis and lead to proteotoxic stress. These include environmental stress conditions such as heat and oxidative stress or mutations. Mutations can prevent the correct folding of proteins, increase the tendency of proteins to aggregate, or impair factors of the PQC system. Moreover, it is known that aging can cause progressive exhaustion of the PQC system. If proteotoxic stress is persistent, it can overwhelm the PQC system, and misfolded proteins and protein aggregates can accumulate. Aggregated proteins are commonly rich in β -sheets. They can have varying degrees of structure, ranging from unstructured amorphous aggregates to prefibrillar species and highly ordered amyloid fibrils (Tyedmers et al., 2010). Consequences of misfolding and aggregation are the loss of physiological protein function and, moreover, the gain of toxic function. Large deposits can result in cellular dysfunction or even cell death. Therefore, protein aggregates and fibrils are implicated in many pathologies. Prominent examples are neurodegenerative disorders, such as Alzheimer's disease, Parkinson's disease, and frontotemporal dementia, or if other tissues are affected, amyloidosis and type 2 diabetes (Louros et al., 2023; Winklhofer et al., 2008).

1.2 High temperature requirement A proteases

High temperature requirement A (HtrA) proteases are a family of evolutionarily conserved serine proteases, involved in central functions of the PQC. They are characterized by a homo-oligomeric structure and a shared domain architecture, composed of protease domain and at least one PDZ (postsynaptic density of 95 kDa, Discs large and zonula occludens1) domain (Figure 2) (Pallen and Wren, 1997; Clausen et al., 2002). HtrAs function in an ATP-independent manner and can combine the antagonistic activities of proteases and chaperones. Therefore, they act in two key aspects of PQC, protein folding and protein degradation (Spiess et al., 1999). The activity of HtrAs is regulated by several mechanisms and can be reversibly switched on and off. This allows a rapid and finely tuned response to protein folding stress, making HtrA proteases remarkable factors of the PQC system.

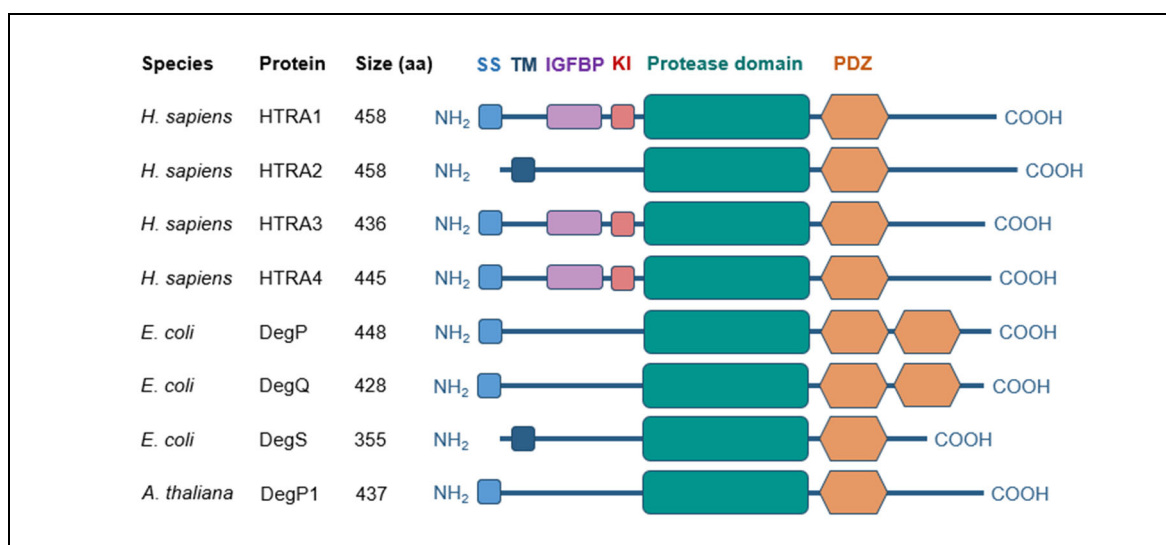


Figure 2: Domain structure of different HtrA proteases

Different HtrA proteases from various species show a conserved domain organization consisting of a protease domain and at least one C-terminal PDZ domain. The N-terminal region differs between the individual proteases and can include signal sequence (SS), transmembrane domain (TM), insulin growth factor binding domain (IGFBP) and Kazal protease inhibitor domain (KI). The size of the proteins is given in amino acids (aa). (Figure adapted from Clausen et al., 2002)

A multitude of different HtrA proteases are found in various organisms ranging from bacteria, yeast, and plants to animals. In most of these organisms, more than one homolog is expressed, e.g., three HtrAs in *Escherichia coli* (*E. coli*), 16 HtrAs in *Arabidopsis thaliana*, and four HtrAs in humans (Clausen et al., 2011). These

homologs can be found in diverse subcellular and extracellular locations, performing diverse cellular functions. For example, in *E. coli* the periplasmic DegP prevents protein-folding stress by recognizing and degrading misfolded and mislocalized proteins. Furthermore, DegP promotes folding and refolding of various substrates, protects membrane proteins from degradation during their transport through the periplasm, and contributes to the activation of a protein-folding stress pathway (Spiess et al., 1999; Isaac et al., 2005; Krojer et al., 2008b). In contrast to DegP, the membrane-bound *E. coli* protease DegS is highly specific. It initiates the σ^E unfolded protein response pathway by degrading the negative regulator RseA upon binding to the C-termini of mislocalized outer membrane proteins (Walsh et al., 2003). In addition to PQC, bacterial HtrAs are involved in virulence. The secreted *Helicobacter pylori* HtrA, for example, disrupts epithelial barriers by degrading the adhesion protein E-cadherin, allowing the bacteria to invade the host cells (Hoy et al., 2010). In plants, some of the HtrAs, such as Deg1, are located in chloroplasts, where they maintain proteostasis of the photosynthetic machinery (Kapri-Pardes et al., 2007). For the four human HtrAs (HTRA1, HTRA2, HTRA3, and HTRA4) a variety of functions have been postulated, many beyond PQC. So far, little information is available for HTRA4. Abundant expression levels of HTRA4 could only be detected in the human placenta, where it probably promotes trophoblast invasion by cleaving proteins of the extracellular matrix (ECM) such as fibronectin (Wang et al., 2012). For HTRA3, studies have also shown an involvement in placenta development. However, HTRA3 negatively regulates trophoblast invasion and, therefore, acts antagonistically to HTRA4 (Singh et al., 2011; Chen et al., 2014). Next to placentation, HTRA3 is involved in the inhibition of transforming growth factor- β (TGF- β) signaling, in the degradation of ECM proteins, in oncogenesis, and in the promotion of apoptosis (Tocharus et al., 2004; Belefond et al., 2010; Wenta et al., 2019). Furthermore, HTRA3 interacts with cytoskeleton proteins, acting either as protease or as chaperone, and promotes tubulin polymerization (Wenta et al., 2018). Unlike the other human HtrAs, which are all secreted proteins, HTRA2 is a membrane-bound protein localized in the intermembrane space of mitochondria. It acts as a PQC factor that maintains mitochondrial proteostasis (Vande Walle et al., 2008; Moisoï et al., 2009). Under stress conditions, expression of HTRA2 is upregulated and the N-terminal region of the protease is processed, resulting in its release into the cytosol. Subsequently, HTRA2 promotes apoptosis by binding and degrading the

inhibitor of apoptosis proteins (IAPs) or by degrading antiapoptotic proteins, such as HS1-associated protein X-1 (HAX-1) or Wilms tumor protein (WT1) (Gray et al., 2000; Verhagen et al., 2002; Chien, 2010). HTRA1 is the best characterized of the human HtrAs. It is broadly expressed in the human body, and numerous physiological substrates have been identified. HTRA1 is associated with a wide range of functions but also with various human diseases, which are described in detail in section 1.3 (Wang and Nie, 2021).

Despite their different functions, HtrA proteases share common structural features. The domain organization comprises a variable N-terminal region, a structurally well-conserved protease domain, and at least one PDZ domain (Figure 2). Depending on the respective localization and function of the HtrA protease, the N-terminal region can contain signal sequence (SS), transmembrane domain (TM), and additional domains such as insulin growth factor binding domain (IGFBP), and Kazal protease inhibitor domain (KI) (Clausen et al., 2002). The protease domain adopts a chymotrypsin fold consisting of two six-stranded β -barrels with additional α -helices attached and several loops (LA, LB, LC, L1, L2, L3, and LD), which connect the β -strands (β 1–12) (Figure 3B and C). The active site cleft is located at the interface of the two β -barrels and consists of the amino acids of the catalytic triad (histidine, aspartate, and serine). C-terminally connected to the protease domain by a flexible linker are the PDZ domains. PDZ domains of HtrAs are small, globular modules that comprise five β -strands (β 1–5) and two α -helices (α 2 and α 3), as well as two additional β -strands at the N- and C-termini (β N and β C) and an α -helix (α 1) within the loop between stands β 1 and β 2 (Clausen et al., 2011; Zurawa-Janicka et al., 2017). Characterized as protein-protein interaction domains, PDZs preferentially bind to three or four C-terminal amino acid residues of target proteins or peptides. However, recognition and binding to internal sequences have also been reported. Next to substrate binding, PDZ domains are also involved in oligomer assembly, localization, and activation of HtrAs (Sheng and Sala, 2001; Runyon et al., 2007).

HtrA monomers form homotrimers as basic functional units. The homotrimers are funnel-shaped with the central core formed by three protease domains while the flexible PDZ domains protrude outwards. The oligomeric mode and the PDZ domains allow a tightly controlled and reversible activation of HtrA proteases. This is a special feature compared to classical serine proteases, which are constitutively

active after cleavage of a propeptide. In HtrAs, the activation process is mediated by loops L1, L2, L3, and LD, which form the activation domain. Upon sensing an activation signal, loop L3 rearranges to form a direct interaction with loop LD* of a neighboring protomer (* designates structures of the neighboring protomer). This interaction initiates a disorder-to-order transition of the active site loops LD*, L1*, and L2*, resulting in an active conformation of the protease domain (Clausen et al., 2011; Zurawa-Janicka et al., 2017). Although this activation process of HtrAs is conserved, the mechanism by which loop L3 senses and transmits activation signals differs. One known mechanism is allosteric activation where a regulatory ligand binds to the PDZ domain, leading to reorientation of loop L3 and thus to protease activation (Wilken et al., 2004; Regt et al., 2015). Another mechanism, which is known for DegP and DegQ, is accompanied by the formation of higher-order oligomers. Upon binding of a substrate, the protease further assembles into 12- or 24-mers. This conversion results in the immobilization of the otherwise flexible first PDZ domain, which allows the interaction with loop L3 and induction of the active protease conformation (Krojer et al., 2010; Merdanovic et al., 2010; Sawa et al., 2011). Furthermore, activation mechanisms that are independent of PDZ domains have been proposed for HTRA1 (Truebestein et al., 2011; Eigenbrot et al., 2012). These are described in detail in the following section (1.3).

1.3 HTRA1

The human HTRA1 consists of polypeptide of 480 amino acids with a molecular weight of 51 kDa, which is encoded by the *HTRA1* gene located at region 10q25.3–q26.2 on chromosome 10 (Zumbrunn and Trueb, 1997). Typically for HtrA proteases, it contains a chymotrypsin-like serine protease domain (amino acids 204–364) and a C-terminal PDZ domain (amino acids 365–467). The N-terminal region comprises the SS (amino acids 1–22), a tandem module of IGFBP (amino acids 33–100), and a KI (amino acids 98–157) domain, also referred to as Mac25 domain. Besides HTRA1, this rare IGFBP-KI tandem module is only found in HTRA3 and 4 as well as in the other three human proteins. However, since the IGFBP

domain is incapable of binding to insulin-like growth factors (IGFs) and the KI domain has no effect on protease activity, neither of these two modules seems to perform its prototypic functions in HTRA1. The physiological functions of these domains, therefore, still remain to be elucidated (Eigenbrot et al., 2012). So far, no structure of the full-length HTRA1 is available. However, crystal structures of HTRA1 lacking the N-terminal region show that the protease forms the characteristic funnel-shaped homotrimer (Figure 3). Trimerization is mediated by interactions between the protease domains which form the central core. Depending on the activation state, the protease domain adopts different conformations. In the inactive state, loops L1, L2, L3 and LD of the activation domain are disordered (Figure 3C). Upon activation, a rearrangement of the loops results in an optimal conformation of the catalytic triad, consisting of H220, D250, and S328 (Truebestein et al., 2011; Eigenbrot et al., 2012). PDZ domains are not visible in the crystal structures, probably due to high flexibility. However, a model of the full-length HTRA1 that is based on small-angle-X-ray scattering (SAXS) data suggests that the PDZ domains project outward from the central core of the protease domains (Figure 3A). In this model, the N-terminal domains lie flat on the central core, pointing in the opposite direction of the active site (Eigenbrot et al., 2012).

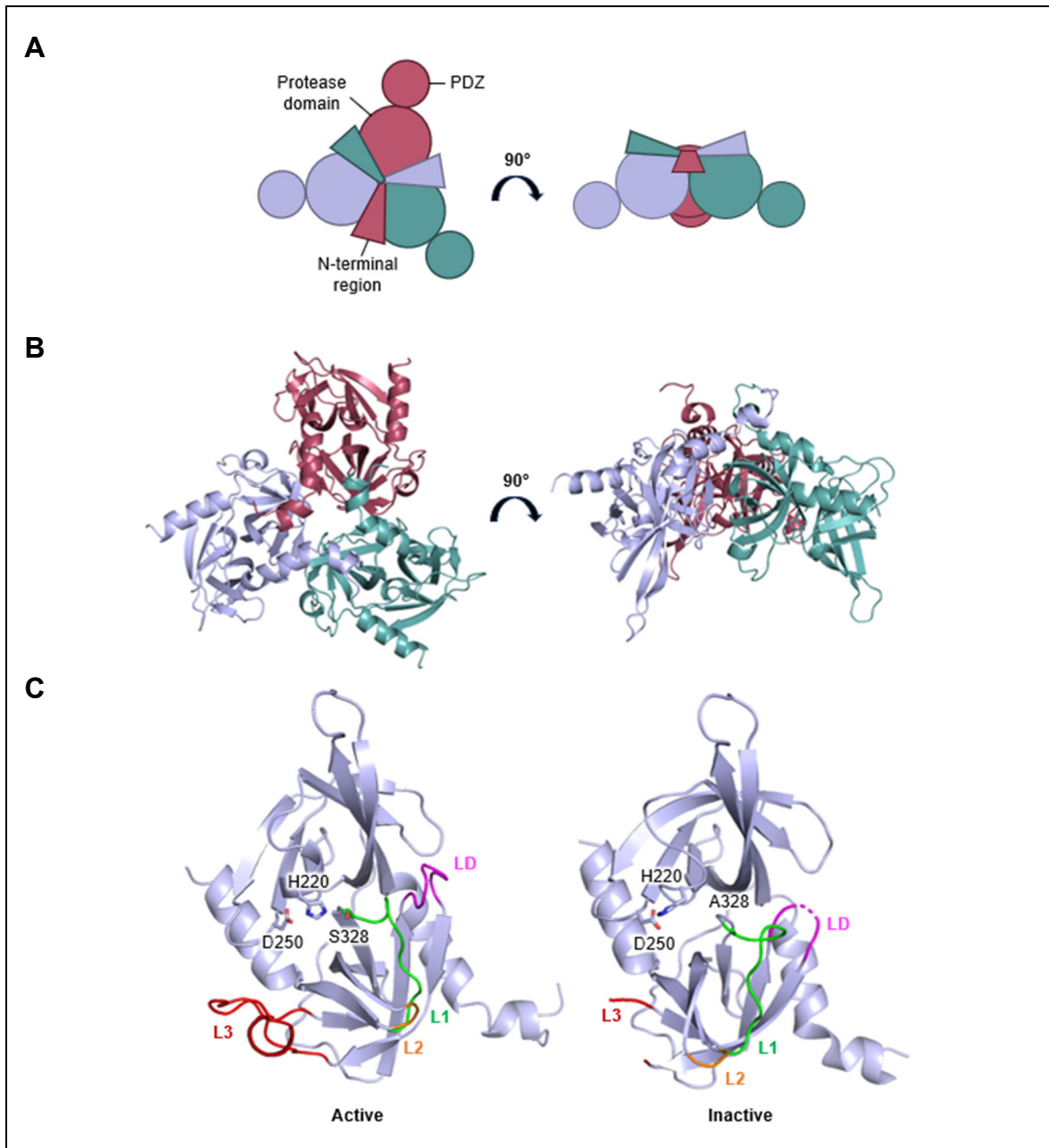


Figure 3: Structure of HTRA1

HTRA1 displays the funnel-shaped homotrimeric structure characteristic of HtrA proteases. In the figure, individual HTRA1 monomers are depicted in separate colours (red, blue, or green). (A) Simplified graphic representation of the HTRA1 architecture based on SAXS data (Eigenbrot et al., 2012). The top and side views of the trimer are shown. In the model, PDZ domains point radially outward from the central core that is formed by the three protease domains. The N-terminal regions lie flat against the top side of the core. (B) Crystal structure of the homotrimeric central core of HTRA1 formed by the protease domains. The top and side views of the structure are shown. (PDB ID: 3NZI) (C) Active and inactive conformation of the HTRA1 protease domain. Upon activation, loops L1 (green), L2 (orange), L3 (red), and LD (magenta) of the activation domain undergo a disorder-to-order transition that results in an optimal conformation of the catalytic triad, consisting of H220, D250 and S328. In the protease domain in the inactive conformation, the serine at position 328 is replaced by alanine. (PDB IDs: 3NZI (active), 3NUM (inactive)) (Figure adapted from Zurawa-Janicka et al., 2017)

The postulated activation mechanism of HTRA1 differs from the regulation scheme established for HtrA proteases (1.2). Remarkably, the PDZ domain is not required

for proteolytic activity of HTRA1. Structural and biochemical data of wild-type HTRA1 and HTRA1 lacking the PDZ domain indicate that substrates bound to the protease domain directly interact with loop L3, thus completing the activation domain and stabilizing the active state of the protease (Truebestein et al., 2011). However, this model of activation by induced-fit substrate binding is challenged by crystal structures of HTRA1, showing that the active site can adopt both conformations, the inactive and the active one, also in the absence of a substrate. Based on this, a conformational selection model for activation was proposed. Accordingly, inactive and active HTRA1 exist in equilibrium and substrates shift the equilibrium towards the active conformer (Eigenbrot et al., 2012). Furthermore, a substrate-induced assembly of HTRA1 into higher-order oligomers was observed, which is associated with increased activity. In contrast to the procaryotic HtrAs DegP and DegQ, this oligomerization is independent of the PDZ domain (Truebestein et al., 2011). In addition to these mechanisms of PDZ-independent activation, recent studies have demonstrated an allosteric regulation of HTRA1 via the PDZ domain. Binding of ligands to the PDZ domain, such as calpain 2, complement factor D, and cyclin H, can directly interact with loop L3 and thus fine-tune the proteolytic activity (Rey et al., 2022). Given these partially contradictory findings, the current understanding of HTRA1 regulation is still insufficient and requires further research for comprehensive understanding.

HTRA1 is ubiquitously expressed in the human body but with tissue-specific expression levels that can change during development and also under pathological conditions (Hu et al., 1998; De Luca et al., 2003; De Luca et al., 2004). The major fraction of the expressed HTRA1 is located in the extracellular space since it is a secreted protein. However, a fraction of approximately 20% can be detected within the cell nucleus or in the cytoplasm, where it is predominantly attached to microtubules or the plasma membrane (Clausen et al., 2011). Whether the intracellular HTRA1 is generated by re-internalization or by non-secretion remains to be elucidated. The spontaneous uptake of HTRA1, which has been observed for various cell lines in cell culture, supports the model of re-internalization (Muratoglu et al., 2013; Poepsel et al., 2015).

Secreted HTRA1 is involved in the maintenance of the ECM integrity and proteostasis by degrading and processing various ECM components. Among the known

substrates that have been identified are fibronectin (Grau et al., 2006), decorin (Hadfield et al., 2008), and aggrecan (Chamberland et al., 2009). Elevated HTRA1 levels are associated with the destruction of the ECM. This makes HTRA1 a contributory factor in the pathogenesis of several musculoskeletal diseases, such as osteoarthritis or rheumatoid arthritis (Grau et al., 2006; Tiaden and Richards, 2013). Furthermore, HTRA1 overexpression is linked to age-related macular degeneration (AMD), one of the main causes of blindness in the elderly population. Studies have identified different AMD-associated ECM proteins as targets of HTRA1 and show that their increased degradation results in an impaired elastic layer of Bruch's membrane (Vierkotten et al., 2011; Lin et al., 2018). Besides remodeling of the ECM, secreted HTRA1 sequesters or degrades various signaling molecules and thus participates in the regulation of cell proliferation. Among the target molecules are transforming growth factor- β (TGF- β) (Launay et al., 2008), insulin-like growth factor binding protein (IGFBP) 5 (Hou et al., 2005) and several TGF- β family proteins (Oka et al., 2004). Through proteolysis of the latter, HTRA1 is involved in the regulation of the TGF- β signaling pathway. Dysregulation of TGF- β signaling due to loss-of-function mutations in HTRA1 are known to cause cerebral autosomal dominant arteriopathy with subcortical infarcts and leukoencephalopathy (CARASIL), a fatal degenerative disease of the brain vasculature. So far, CARASIL is the only described monogenic disease caused by mutation of the *HTRA1* gene (Hara et al., 2009; Beaufort et al., 2014).

Within the cell, HTRA1 was shown to be localized to microtubules in a PDZ-dependent manner. It can bind to tubulins as well as microtubules and promotes microtubule assembly and stability. Downregulation of HTRA1 is associated with enhanced cell motility and thus also with increased cell migration (Chien et al., 2009a; Chien et al., 2009b). Next to cell motility, intracellular HTRA1 was shown to be involved in the regulation of cell death. The X-linked inhibitor of apoptosis protein (XIAP), an important inhibitor of apoptosis, was identified as HTRA1 substrate. By degrading XIAP, HTRA1 mediates the induction of programmed cell death (He et al., 2012). Furthermore, it was shown that HTRA1 also promotes cell death via activation of anoikis. Although the mechanism is not fully understood, it is suggested that HTRA1 induces anoikis by attenuating the activation of the epidermal growth factor receptor (EGFR)/Akt signaling pathway (He et al., 2010). The involvement of HTRA1 in cell

migration, cell death, and cell proliferation are reasons why HTRA1 is associated with oncogenesis. So far, several studies have reported downregulation of *HTRA1* expression in different cancer types, such as ovarian cancer (Chien et al., 2004), metastatic melanoma (Baldi et al., 2002), lung cancer (Esposito et al., 2006), or endometrial cancer (Mullany et al., 2011). Generally, reduced expression or even loss of *HTRA1* expression has been correlated with poor clinical prognosis, chemotherapy resistance and metastasis. Consistent with this, it has been reported that *HTRA1* overexpression inhibits tumor outgrowth and promotes cell death, suggesting a role of HTRA1 as tumor suppressor (Baldi et al., 2002; Chien et al., 2004; He et al., 2012).

HTRA1 is also highly expressed in brain tissue, and several studies have linked the protease to Alzheimer's disease (AD) (Nie et al., 2003). AD is a neurodegenerative disease associated with aggregation and abnormal deposition of the microtubule-associated protein Tau (Tau) and amyloid β peptide ($A\beta$). While aggregated and fibrillar Tau forms intracellular deposits known as neurofibrillary tangles (NFTs), $A\beta$ accumulates extracellularly as amyloid plaques. HTRA1 was found to be among the most enriched proteins in $A\beta$ plaques of AD patients, where it is suggested to reduce the deposition (Drummond et al., 2022). This assumption is supported by data showing that HTRA1 can degrade $A\beta$ and that HTRA1 inhibition results in accumulation of $A\beta$ in cell culture supernatants of astrocytes (Grau et al., 2005). In addition to $A\beta$, Tau was also identified as an HTRA1 substrate. It was demonstrated that HTRA1 not only degrades soluble Tau but also aggregated and fibrillar Tau species. With its combined chaperone and protease activity, HTRA1 is able to disintegrate tightly packed fibrils and subsequently to proteolyze them (Tennstaedt et al., 2012; Poepsel et al., 2015). Moreover, cell culture experiments have shown that overexpression of HTRA1 results in decreased Tau levels, while overexpression of Tau triggers an increased production of HTRA1. Consistent with this, an inverse correlation of HTRA1 and Tau levels has been demonstrated for brain samples of AD patients (Tennstaedt et al., 2012). All these data suggest a function of HTRA1 as PQC protease that protects the brain against amyloid deposition. Since $A\beta$ plaques and NFTs are hallmarks of AD, a disease-modifying role of HTRA1 should be considered.

1.4 Microtubule-associated protein Tau

Tau is a microtubule-associated protein (MAP) that, together with other MAPs, regulates microtubule (MT) dynamics (Weingarten et al., 1975). It is mainly expressed in neuronal cells of the central nervous system (CNS). During development, the expression and localization of Tau are differentially regulated. In mature neurons, Tau is characteristically found in the axonal compartment, where it localizes to MTs (Figure 5A) (Barbier et al., 2019). However, localization at the cell membrane and in the nucleus was also reported (Brandt et al., 1995; Brady et al., 1995). As one of the stabilizing MAPs, the main function of Tau is to promote MT assembly and protect them against depolymerization. Moreover, it was demonstrated that Tau nucleates MTs and regulates their spatial organization by inducing MT bundle formation (Weingarten et al., 1975; Chen et al., 1992; Trinczek et al., 1995; Devred et al., 2004). Thus, Tau is of critical importance for neuronal processes that rely on MT stability, such as axonal transport.

Human Tau is encoded by the gene *MAPT* located on chromosome 17q21. In total, there are six different Tau isoforms in the adult human CNS, which result from alternative splicing (Figure 4) (Neve et al., 1986; Goedert et al., 1989). The longest isoform can be divided in an N-terminal projection domain, a proline-rich region and a C-terminal microtubule-binding domain (MTBD), consisting of four similar but not identical repeats (R1–4). Other isoforms differ by the presence or absence of two N-terminal inserts (N1–2) and the inclusion of R2. Accordingly, the isoforms ranging from amino acids 352 to 441 are designated as 2N4R Tau for the longest and 0N3R Tau for the shortest form (Himmler et al., 1989; Barbier et al., 2019). So far little is known about the specific functions of individual Tau isoforms in the cellular context. However, it has been shown that they differ in their subcellular localization and in their microtubule-binding affinity. While the N-terminal inserts are suggested to affect the protein localization, the inclusion of R2 results in a higher MT binding affinity and faster MT assembly (Goedert and Jakes, 1990; Bachmann et al., 2021). Moreover, the isoforms are differentially expressed during development, with the adult CNS expressing all six isoforms (Goedert et al., 1989).

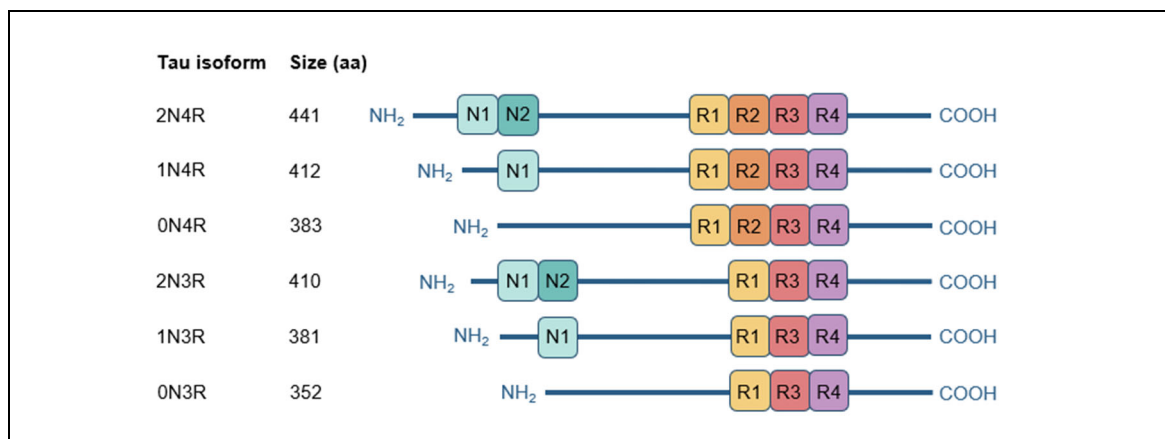


Figure 4: The six different Tau isoforms of the human adult CNS

Six different Tau isoforms are expressed in the adult human CNS. The isoforms differ by the presence or absence of two N-terminal inserts (N1–2) and by the inclusion of the second of four repeats (R) that together form the microtubule-binding domain (MTBD). Designation of the isoforms, ranging from 441 to 352 amino acids (aa), corresponds to the number of N-terminal inserts and repeats. (Figure adapted from Johnson and Stoothoff, 2004)

Tau is classified as natively unfolded or intrinsically unstructured protein. Typically for this type of protein, it is highly hydrophilic, has a low content of secondary structures, and lacks complex three-dimensional folding. These properties make Tau a highly soluble and flexible protein with variable conformations. In solution, Tau is supposed to possess a global “paperclip” fold, with contact between the N- and the C-terminus and the C-terminus folding back and interacting with the MTBD. Despite the intramolecular contacts, the mobility of the peptide chain remains (Jeganathan et al., 2006; Mukrasch et al., 2009). Upon binding to MTs, Tau adopts an extended structure in which the MTBD binds along the MT filament, linking tubulin monomers, while the N-terminal projection domain protrudes from the filament surface (Kellogg et al., 2018). Furthermore, Tau conformation is also dependent on the phosphorylation state (Jeganathan et al., 2008). Tau is defined as a phosphoprotein containing 85 potential serine, threonine, and tyrosine phosphorylation sites. Post-translational phosphorylation affects not only the structure of Tau but also its localization and is considered the predominant regulator of Tau function (Noble et al., 2013). The binding affinity of Tau to MTs was demonstrated to be reduced by phosphorylation, with different localisations and numbers of phosphorylation sites enabling finely tuned MT dynamics (Lindwall and Cole, 1984; Biernat et al., 1993; Mandelkow et al., 1995). Today, a large number of kinases and phosphatases are known that regulate Tau modification, including glycogen synthase kinase 3 (GSK3), p38 mitogen-

activated protein kinases (p38 MAPK), and protein phosphatase 2A (PP2A). Imbalances in this system can result in pathological increased phosphorylation of Tau. While approximately ten amino acid residues are phosphorylated under physiological conditions, two to four-fold higher phosphorylation levels were observed for pathological Tau species (Noble et al., 2013). This hyperphosphorylation is associated with impaired binding to MTs and with conformational changes promoting aggregation of Tau into fibrils (Figure 5B) (Biernat et al., 1993; Jeganathan et al., 2008). The loss of Tau function results in destabilization of MTs, disruption of axonal transport, and accumulation of hyperphosphorylated Tau in the cytosol. Consequently, Tau polymerization is favored, and fibrils are formed, which in turn can aggregate into larger structures known as NFTs. Toxic gain of function results in impairment of neurological functions and even in loss of neuronal cells. Thus, abnormal aggregation and deposition of Tau is a hallmark of several neurodegenerative diseases collectively referred to as tauopathies. These include Alzheimer's disease (AD), Pick's disease (PiD), chronic traumatic encephalopathy (CTE), Huntington's disease (HD), corticobasal degeneration (CBD), and progressive supranuclear palsy (PSP). It has to be mentioned that the mechanisms underlying Tau-induced neurodegeneration are still under debate and that it is not yet fully clarified how and which pathological Tau species exerts neurotoxicity (Wang and Mandelkow, 2016).

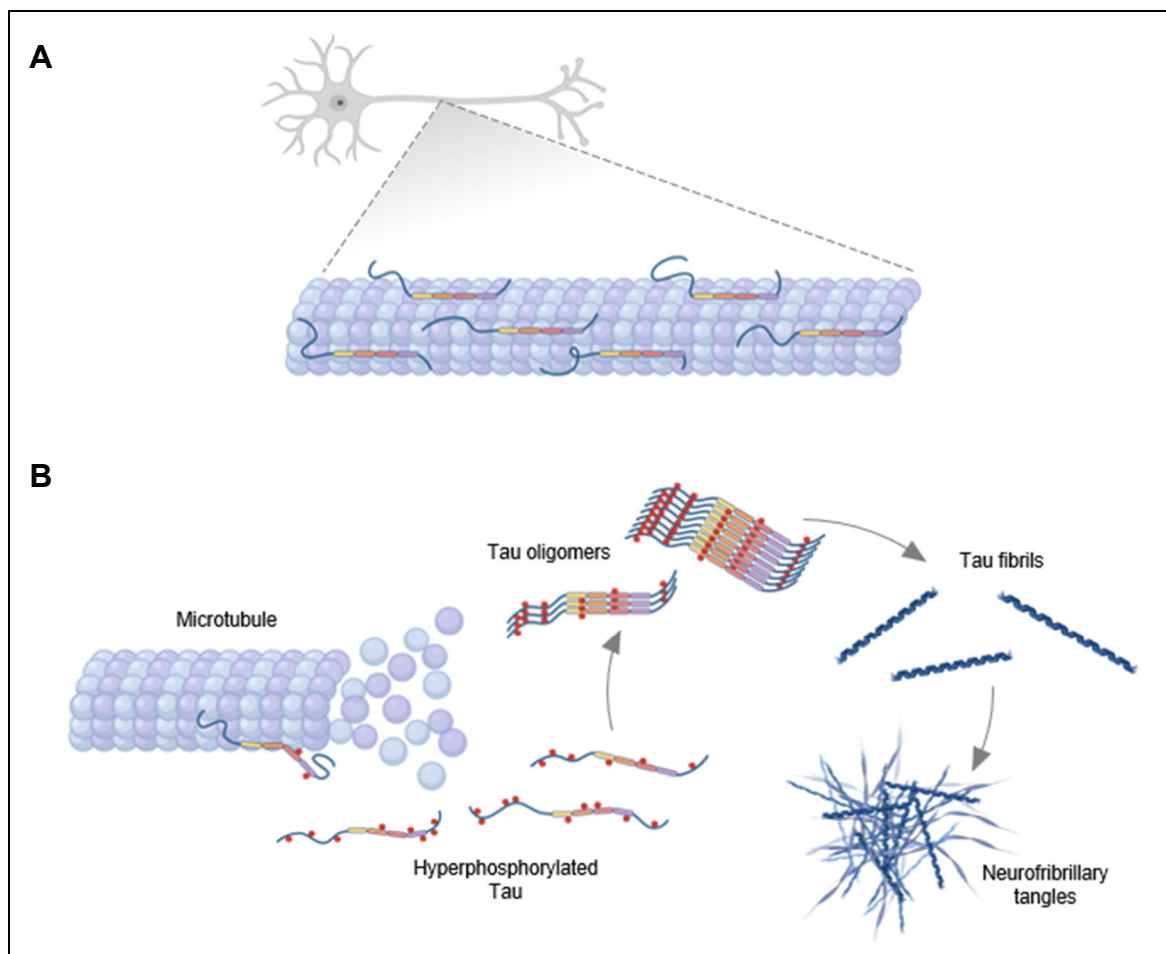


Figure 5: Tau in physiology and pathology

The MT associated protein Tau is mainly expressed in neuronal cells of the central nervous system. (A) In mature neurons, Tau is characteristically found in the axonal compartment, where it binds and stabilizes MTs. (B) Under pathological conditions, Tau can be hyperphosphorylated. This hyperphosphorylation is associated with impaired binding of Tau to MTs and with conformational changes that promote Tau assembly into oligomers. Further assembly results in the formation of Tau fibrils that can aggregate into neurofibrillary tangles. Neurofibrillary tangles are linked to impaired neurological functions and are a hallmark of tauopathies.

Recently, advances in cryo-electron microscopy (cryo-EM) have made it possible to determine structures of Tau fibrils at the atomic level (Figure 6) (Fitzpatrick et al., 2017). Since this breakthrough, multiple structures of Tau fibrils isolated from patient samples with different tauopathies have been reported. Comparison of these structures showed that each disease is defined by a specific Tau filament fold (Figure 6B) (Fitzpatrick et al., 2017; Falcon et al., 2018; Scheres et al., 2020). Several different fibril types have also been reported for *in vitro* formed fibrils of recombinant human Tau, with the structure depending on assembly conditions (Zhang et al., 2019; Lövestam et al., 2022). The basic structure of all Tau fibrils consists of an ordered, β -sheet rich core characteristic of amyloids. Stacking of the core regions

from multiple monomers creates long symmetrical filaments. Flanking N- and C-terminal regions are disordered and project away from the core, forming the so-called fuzzy coat. The ordered core is primarily built by the MTBD and a short part of the C-terminal domain. However, the exact amino acid region varies between the different filament folds. Depending on whether R1 and R2 are part of the core, there is a different isoform composition of the fibrils from the individual tauopathies. While AD and CTE fibrils consist of all six Tau isoforms, the core of CBD contains the sequence of R2, and therefore, CBD fibrils consist exclusively of 4R Tau isoforms (Scheres et al., 2020; Scheres et al., 2023). Although individual tauopathies share a specific Tau filament fold, there can be different types of fibrils in one disease (Figure 6A). In AD, for example, paired helical filaments (PHFs) and straight filaments (SFs) can be distinguished. Both filaments are formed by two identical protofilaments that show the same AD fold. The polymorphisms of the two filament types result solely from a different arrangement of the two protofilaments (Fitzpatrick et al., 2017).

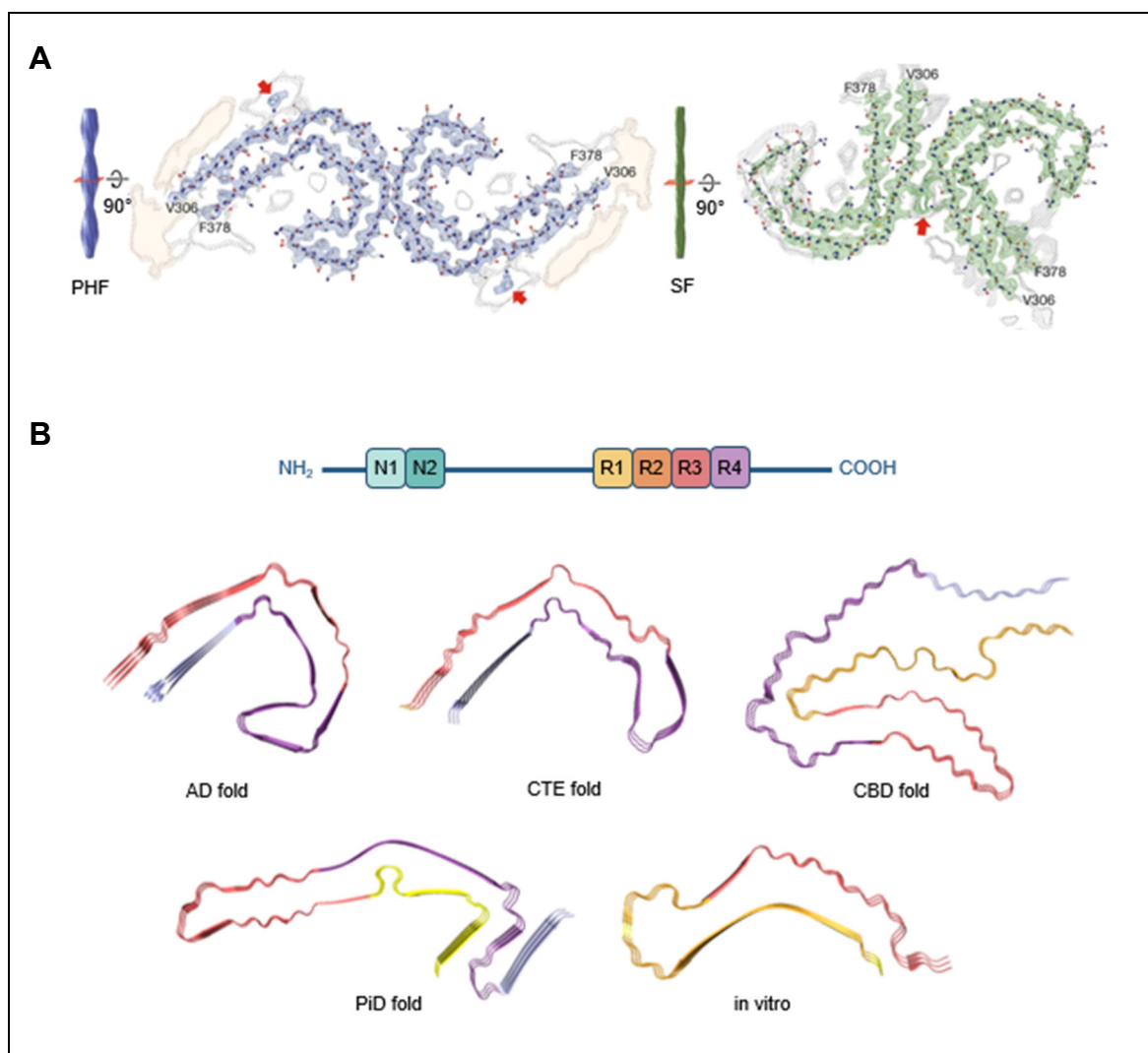


Figure 6: Structures of Tau fibrils

Tau fibrils consist of multiple Tau monomers that are stacked into long, symmetrical filaments. (A) (Fitzpatrick et al., 2017) Cryo-EM structures of the two fibril types, paired helical filament (PHF) (blue) and straight filament (SF) (green), found in AD. Shown are helical reconstructions of the fibrils (left) and cross-sectional Cryo-EM densities and atomic models (right). High-resolution densities of the fibril core are represented in blue and green, respectively, while low-resolution densities are depicted in grey and orange. Red arrows highlight extra densities that do not belong to the Tau molecules. (B) Cryo-EM structures of different Tau filament folds that are specific for different diseases. Different regions in the fibril structures are color-coded according to the schematic representation of the Tau molecule shown above the structures. (PDB IDs: 6HRE (AD fold), 8Q9M (CTE fold), 6TJO (CBD fold), 6GX5 (PiD fold), 6QJH (*in vitro*))

Tau fibrils and associated tauopathies have been the subject of extensive research for many years. Although considerable progress has been made, our understanding of pathogenic mechanisms is still insufficient, and effective therapeutic strategies are not yet available (Wang and Mandelkow, 2016; Cummings et al., 2023). One aspect that is still under investigation is how the cell deals with insoluble, highly stable fibrillar aggregates. Different strategies for removal of Tau fibrils have been described in literature, involving both UPS, ALP, and also individual proteases

(Tennstaedt et al., 2012; Cliffe et al., 2019; Jiang and Bhaskar, 2020). However, the degradation mechanisms and the contribution of the different types of degradation machinery are not fully understood. Recently, it was demonstrated that fragmentation of Tau fibrils by the proteasome generates a smaller species that has even stronger cytotoxic effects than the fibrils (Cliffe et al., 2019). These and other findings raise the question of whether hyperphosphorylated monomers, oligomers, or large filamentous aggregates represent the toxic Tau species responsible for neurodegeneration. Answering such fundamental questions would lead to a more detailed understanding of the molecular mechanism underlying Tau-mediated neurodegeneration and could provide guidance for new therapeutic approaches.

1.5 Objectives

Human Tau is an intrinsically unstructured protein that binds and stabilizes microtubules (MTs). Pathological hyperphosphorylation of Tau is associated with impaired MT-binding and conformational changes triggering ordered aggregation into amyloid fibrils. Such fibrils are a serious hazard to cells and a hallmark of several neurodegenerative diseases in humans. Previous studies have identified both soluble and fibrillar Tau as substrates of HTRA1 (Tennstaedt et al., 2012). As protease of the PQC system, HTRA1 is known to degrade misfolded and mislocalized proteins, thus maintaining proteostasis (Clausen et al., 2011). In the study presented herein, therefore, I want to investigate whether HTRA1 distinguishes between native Tau and pathological Tau species. Moreover, I want to gain detailed mechanistic insights into the process of Tau fibril degradation by HTRA1 since fibrils are considered to be rather protease-resistant.

First, I will generate recombinant Tau, which will then be phosphorylated or aggregated into fibrils. The resulting native, hyperphosphorylated, and fibrillar Tau will be used in a proteolysis assay to analyze and compare the degradation of different Tau species by HTRA1. Since HTRA1 can be activated by its substrates (Truebestein et al., 2011), I will also address different activating effects of these Tau species on HTRA1. In the next step, I will combine time-resolved and cross-linking mass

spectrometry (MS) to precisely detect interactions of HTRA1 and Tau fibrils and describe the degradation process at temporal and spatial resolution. Last, I want to extend my investigations to the interactions of HTRA1 and A β plaques using cerebral organoids as cellular models. Since Tau fibrils and A β plaques are the hallmarks of AD, a potential disease-modifying role of HTRA1 could be discussed.

2. Materials

2.1 Devices

Table 1: List of devices

Type	Designation	Manufacturer
Centrifuges and rotors	Avanti J-E	Beckmann Coulter
	Centrifuge 5424R	Eppendorf
	Centrifuge 5810R	Eppendorf
	Concentrator 5301	Eppendorf
	JA-25.50	Beckmann Coulter
	JLA-9.1000	Beckmann Coulter
	Optima MAX-XP	Beckmann Coulter
	TLA-100	Beckmann Coulter
Electrophoresis systems	Mini-PROTEAN® Tetra Cell	Bio-Rad
	Power Supply EV3020	Consort
	Sub-Cell GT	Bio-Rad
	XCell4 SureLock Midi-Cell	Thermo Fisher
French pressure cell	SLM Aminco	SLM Instruments
Imager and scanner	CanoScan LiDE 210	Canon
	Typhoon FLA 9500	GE Healthcare
Incubators	Multitron standard	Infors HT

Mass spectrometry instruments	Evosep One	Evosep Biosystems
	Orbitrap Elite	Thermo Fisher
	Orbitrap Fusion Lumos	Thermo Fisher
Microscopes	MultiMode 8	Bruker
PCR-Thermocycler	peqSTAR 96X	VWR
pH Meter	SevenCompact	Mettler-Toledo
Protein purification systems and columns	Äkta pure	GE Healthcare
	HiLoad 26/600 Superdex 200	Cytiva
Sonifier	SONOPULS mini20	Bandelin
Spectrophotometer	DS-11+	DeNovix
	SpectraMax M5	Molecular Devices

2.2 Consumables

Table 2: List of consumables

Designation	Manufacturer
Bio-Gel HT Hydroxyapatite	Bio-Rad
DyLight 633 NHS Ester	Thermo Fisher
HDGreen Plus DNA stain	Intas
Low Volume 384-well Black Flat Bottom Polystyrene NBS Microplate	Corning
Microplate, 96 well, PS, F-bottom, μ Clear, black, non-binding	Greiner

NEBuilder HiFi DNA Assembly Cloning Kit	New England Biolabs
NuPAGE 10%, Bis-Tris, Midi Protein Gels	Invitrogen
PhoX Crosslinker	Thermo Fisher
Protein LoBind Tubes	Eppendorf
POROS 50 HS Strong Cation Exchange Resin	Thermo Fisher
Slide-A-Lyzer MINI Dialysis Devices, 20K MWCO	Thermo Fisher
QIAprep Spin Miniprep Kit	Qiagen
QIAquick PCR Purification Kit	Qiagen
Strep-Tactin Superflow resin	IBA Lifesciences

2.3 Chemicals and substances

The chemicals used were purchased from the companies Sigma-Aldrich, Carl Roth, Thermo Fisher Scientific, Merck, Serva Electrophoresis GmbH, and Applichem, unless indicated otherwise. All water used was ultrapure quality (PURELAB flex water purification system, ELGA LabWater) and is hereinafter referred to as H₂O.

2.4 Buffers and Media

Table 3: List of buffers and media

Designation	Composition
Activating buffer	150 mM NaPi 380 mM NaCl pH 8.0 at 37 °C

Coomassie staining solution	25% Isopropanol 10% Acetic acid 0.05% Coomassie Blue R-250
Cross-linking buffer	100 mM HEPES 100 mM NaCl pH 7.5 at 37 °C
DNA loading dye (6x)	30% Glycerol 150 mM EDTA (pH 8.0) 30% Bromphenol blue
HAP loading buffer (HTRA1)	50 mM HEPES 10 mM K ₃ PO ₄ pH 7.8 at 4 °C
HAP loading buffer (2N4R Tau)	100 mM HEPES 10 mM K ₃ PO ₄ 2 mM DTT pH 7.8 at 4 °C
HAP elution buffer (HTRA1)	50 mM HEPES 500 mM K ₃ PO ₄ pH 7.8 at 4 °C
MOPS SDS running buffer	50 mM MOPS 50 mM Tris base 0.1% SDS 1 mM EDTA pH 7.7
PBS	137 mM NaCl 2.7 mM KCl 10 mM Na ₂ HPO ₄ 1.8 mM KH ₂ PO ₄

PEM buffer	80 mM PIPES-KOH (pH 6.8) 1 mM EGTA 1 mM MgCl ₂
Phosphorylation buffer	25 mM Tris-HCl (pH 7.4) 0.1 mM EGTA 10 mM magnesium acetate
POROS loading buffer (2N4R Tau)	50 mM HEPES 100 mM NaCl 2 mM DTT pH 7.5 at 4 °C
Proteolysis buffer	100 mM HEPES 100 mM NaCl pH 7.5 at 37 °C
SDS-PAGE loading buffer 2x	4% SDS 16% Glycerol 0.16% Bromophenol blue 120 mM Tris-HCL (pH 6.8) 200 mM DTT
SDS-PAGE running buffer	33 mM Tris-HCl 0.1 % SDS 192 mM Glycine
SDS-PAGE separation gel buffer	1.5 M Tris-HCl (pH 8.8) 0.4% SDS
SDS-PAGE stacking gel buffer	0.5 M Tris-HCl (pH 6.8) 0.4% SDS
SEC buffer (HTRA1)	10 mM HEPES 150 mM NaCl pH 7.5

SEC buffer (2N4R Tau)	10 mM HEPES 50 mM (NH ₄)SO ₄ 2 mM TCEP pH 7.5
SOB medium	5 g/l Yeast extract 20 g/l Tryptone 0.5 g/l NaCl 2.4 g/l MgSO ₄ 186 mg/l KCl pH 7.0 with NaOH
Strep loading buffer (HTRA1)	50 mM Tris-HCl 300 mM NaCl pH 7.5 at 4 °C
Strep washing buffer (HTRA1)	50 mM Tris-HCl 1 M NaCl pH 7.5 at 4 °C
TAE buffer	40 mM Tris 20 mM Acetic acid 1 mM EDTA (pH 8)

2.5 Antibiotics

Table 4: List of antibiotics

Substance	Concentration	Source
Ampicillin	200 µg/ml	Carl Roth
Chloramphenicol	30 µg/ml	Sigma-Aldrich

2.6 *Escherichia coli* strains

Table 5: List of *Escherichia coli* strains

Designation	Genotype	Source
BL21(DE3)	F ⁻ <i>ompT hsdS_B (r_B⁻ m_B⁻) gal dcm</i> (DE3)	Merck
NEB 5-alpha	<i>fhuA2Δ(argF-lacZ)U169 phoA glnV44 Φ80Δ(lacZ)M15 gyrA96 recA1 relA1 endA1 thi-1 hsdR17</i>	New England Biol

2.7 Plasmids

Table 6: List of plasmids

Designation	Description	Source
pET3d_2N4R_Tau	2N4R Tau	Poepsel et al., 2015
pET3d_2N4R_Tau ^{CN}	2N4R Tau (aa 1–40, 390–441, 99–389, 41–98)	this study
pET3d_2N4R_Tau ^{CNC}	2N4R Tau (aa 1–40, 390–441, 99–389, 41–98, 418–441)	this study
pN-StrepII_HTRA1	HTRA1 (aa 158–480) with N-term. StrepII tag	Laboratory collection
pN-StrepII_HTRA1 ^{S328A}	HTRA1 (S328A) (aa 158–480) with N-term. StrepII tag	Laboratory collection

2.8 Primers

Table 7: List of primers

Designation	Sequence (5' → 3')
pET3d_Tau1-40_fwd	gtccgtgtcaccctcttggcttgg
pET3d_Tau1-40_rev	tgaggatccggctgctaacaagcc
pET3d_Tau1-40+418_fwd	gtccgtgtcaccctcttggcttgg
pET3d_Tau1-40+418_rev	gacatgtagactcgccccagctcg
Tau41-98_CN_fwd	ggctttgtagcagccggatcctcatgggatctccgtgtgggg
Tau41-98_CNC_fwd	cgagctggggcgagtctaccatgtctgggatctccgtgtgggg
Tau41-98_CN_rev	gacagaccacggggctggcctgaaagaatctcc
Tau99-389_fwd	tffcaggccagccccgtggtctgtcttggc
Tau99-389_rev	aagcaggggttggaaggaaccacagctgaagaag
Tau390-440_fwd	ctgtggttcctccaaccctgcttgccag
Tau390-440_rev	ccaagaccaagaggggtgacacggacgcggagatcgtgtacaag

2.9 Proteins

Table 8: List of proteins

Protein	Description	MW
HTRA1	HTRA1 (aa 158–480)	36.67 kDa
HTRA1 ^{S328A}	proteolytically inactive HTRA1 (aa 158–480) with the active site serine mutated to alanine	36.67 kDa
Tau	Microtubule-associated protein tau, isoform 2N4R	45.85 kDa

Tau ^{CN}	Microtubule-associated protein tau, isoform 2N4R, with interchanged protein regions, protein sequence see Appendix C	45.85 kDa
Tau ^{CNC}	Microtubule-associated protein tau, isoform 2N4R, with interchanged protein regions, protein sequence see Appendix C	48.29 kDa
Tubulin	Obtained from Cytoskeleton Inc, purified from porcine brain	Approx. 55 kDa

2.10 Enzymes

Table 9: List of enzymes

Designation	Source
cAMP-dependent Protein Kinase A (PKA)	New England Biolabs
<i>DpnI</i>	New England Biolabs
GSK3 β , active, His tagged, human	Sigma
Q5 High-Fidelity DNA Polymerase	New England Biolabs
SAPK4, active	Merck

2.11 DNA and protein standards

Table 10: List of DNA and protein standards

Designation	Source
1 kb Plus DNA Ladder	New England Biolabs
Precision Plus Protein Unstained Protein Standard	Bio-Rad
Precision Plus Protein All Blue Prestained Protein Standard	Bio-Rad

2.12 Software

Table 11: List of software

Designation	Source
BioRender	BioRender.com
CellProfiler (Versions 4.2.5)	Open source (Carpenter et al., 2006)
Fiji (Version 2.3.0)	Open source (Schindelin et al., 2012)
GraphPad Prism (Version 10.1.0)	GraphPad Software
MaxQuant (Version 2.0.2.0)	Open Source
NanoScope (Version 1.5)	Bruker
Phoretix 1D (Version 628)	TotalLab
Proteome Discoverer (Version 2.5.0.400)	Thermo Fisher
PyMOL (Version 2.4.0)	Schrödinger
SnapGene (Version 7.2)	SnapGene
UMSAP (Version 2.1.1 (beta))	Open source (Bravo-Rodriguez et al., 2018)
xiSearch (Version 1.7.6.7)	Open source (Mendes et al., 2019)

Figures were created with BioRender.com.

3. Methods

3.1 Molecular biology methods

3.1.1 Polymerase chain reaction

Polymerase chain reactions (PCRs) were performed to amplify DNA fragments using the Q5 High-Fidelity 2x Master Mix (New England Biolabs). All reaction components were assembled on ice (Table 12), and the cycling parameters were selected according to the manufacturer's instructions, taking into consideration the melting temperature of the primers and the length of the PCR products (Table 13).

Table 12: PCR Reaction Setup

Component	Volume
Q5 High-Fidelity 2x Master Mix	25 μ l
Forward Primer (10 μ M)	2.5 μ l
Reverse Primer (10 μ M)	2.5 μ l
Template DNA	0.3 μ l
H ₂ O	19.7 μ l

Table 13: PCR Cycling Parameters

Step	Temperature	Time	
Initial Denaturation	98 °C	30 sec	
Denaturation	98 °C	10 sec	
Annealing	72 °C	20 sec	30 cycles
Extension	72 °C	3 min	
Final Extension	72 °C	2 min	

Subsequently, *DpnI* (New England Biolabs) was added to digest the DNA templates as recommended by the manufacturer. Agarose gel electrophoresis (3.1.3) was used to verify the amplified DNA fragments. The resulting PCR products were purified using the QIAquick PCR Purification Kit (Qiagen).

3.1.2 DNA assembly

The assembly of DNA fragments generated by PCR into a linearized cloning vector was performed using the NEBuilder HiFi DNA Assembly Cloning Kit (New England Biolabs) according to the manufacturer's protocol. Reactions were set up as shown in Table 14 and incubated in a thermocycler at 50 °C for 60 min. The assembly products were stored at -20 °C for subsequent transformation (3.2.2).

Table 14: Assembly Reaction Setup

Component	Volume
HiFi DNA Assembly Master Mix	10 μ l
Fragments / linearized Vector (0.2–0.5 pmol)	X μ l
H ₂ O	10–X μ l

3.1.3 Agarose gel electrophoresis

Agarose gel electrophoresis was used for the analytical separation of DNA molecules. Therefore, all DNA samples were mixed with the appropriate volume of 6x DNA loading dye and loaded into the wells of an agarose gel. The gels contained 1% (w/v) agarose in Tris-acetate-EDTA (TAE) buffer and 2 μ l of HDGreen Plus DNA stain (Intas). The electrophoretic separation was performed in TAE buffer at a constant voltage of 140 V. UV light was used to visualize the DNA. The DNA bands were compared to those of a DNA standard ladder (1 kb Plus DNA ladder, New England Biolabs) for analysis.

3.2 Microbiology methods

3.2.1 Determination of bacterial cell density in suspension

The cell density in bacterial liquid cultures was determined by measuring the optical density with a photometer at a wavelength of 600 nm (OD₆₀₀). An OD₆₀₀ of 1 corresponds to an approximate cell density of 5×10^8 cells per ml.

3.2.2 Transformation

Chemically competent *Escherichia coli* (*E. coli*) cells of strain BL21(DE3) or strain NEB 5-alpha were transformed with plasmid DNA. Therefore, 50 µl of the cells were mixed with 1 µl of plasmid DNA and incubated on ice for 30 min, followed by a 1 min heat shock at 42 °C. After cooling down on ice for 30 sec, Super Optimal Broth (SOB) medium (950 µl) was added. Phenotypic expression was carried out for 1 h at 37 °C and 900 rpm. Then, 50 µl of the cell suspension was spread on an SOB selection plate containing ampicillin according to the resistance gene in the plasmids. Plates were incubated overnight at 37 °C.

3.2.3 Isolation of plasmid DNA

Plasmid DNA was isolated from bacterial cells using the QIAprep Spin Miniprep Kit (Qiagen) according to the instructions of the manufacturer. For this purpose, a liquid overnight culture (5 ml) of transformed bacterial cells was pelleted by centrifugation (3 min at 10,000 rpm). The nucleotide sequence of the purified plasmids was confirmed by DNA sequencing conducted by Microsynth Seqlab GmbH.

3.2.4 Protein expression

Recombinant 2N4R Tau variants and HTRA1 variants were expressed in cells of the *E. coli* strain BL21(DE3). First, 30 ml SOB medium was inoculated with a colony of transformed bacteria cells. After overnight incubation (37 °C, 110 rpm), the preculture was used to inoculate 1 l SOB medium to an OD₆₀₀ of 0.07. All media

were supplemented with 200 µg/ml Ampicillin. The expression culture was incubated at 37 °C and 90 rpm. For the expression of the HTRA1 variants, the cultivation temperature was decreased to 28 °C after 2 h of incubation. Overexpression of recombinant proteins was induced when the culture reached an OD₆₀₀ of approximately 0.6 by the addition of isopropyl β-D-1-thiogalactopyranoside (IPTG) to a concentration of 0.2 mM and incubation was continued overnight. Cells were harvested by centrifugation for 20 min at 4,500 rpm and pellets were washed in PBS once. Dry cell pellets were stored at -20 °C.

3.3 Biochemical methods

3.3.1 Protein purification of recombinant Tau variants

All purification steps were carried out either on ice or at 4 °C. First, bacterial cell pellets containing overexpressed proteins were thawed in a water bath and resuspended in 10 ml lysis buffer. Cells were lysed using a French Press and the lysate was cleared by centrifugation for 45 min at 21,000 rpm. The obtained supernatant was boiled in a water bath for 15 min, followed by centrifugation (30 min, 15,000 rpm) to separate the heat-stable Tau variants from bacterial proteins. Further purification of the recombinant protein within was performed using the Äkta pure chromatography system. The cleared supernatant was applied to a POROS HS50 cation exchange column equilibrated in lysis buffer. The protein was eluted with a linear sodium chloride gradient from 100 to 1,000 mM. Fractions containing the target protein were pooled, diluted with 2 volumes of HAP loading buffer and applied to a hydroxyapatite (HAP) column. Elution was performed with a linear sodium chloride gradient (0 to 1,000 mM) and protein fractions were pooled and concentrated. The concentrated protein was further purified by size exclusion chromatography (SEC) using a HiLoad 26/600 Superdex 200 column at a constant flow rate of 1 ml/min. Fractions containing the Tau protein with high purity were pooled and concentrated, flash-frozen in liquid nitrogen and stored at -80 °C. All purification steps were analyzed by SDS-PAGE (3.3.3).

3.3.2 Protein purification of recombinant HTRA1 variants

All purification steps were carried out either on ice or at 4 °C. First, cell pellets were resuspended in lysis buffer, lysed using a French Press, and the lysate was cleared by centrifugation (45 min, 21,000 rpm). The obtained supernatant was applied to a Strep-Tactin column equilibrated in lysis buffer. Unspecifically bound proteins were removed from the column in three successive washing steps (5 column volumes (CV) lysis buffer, 5 CV washing buffer, and 2 CV lysis buffer). HTRA1 variants were eluted in lysis buffer supplemented with 2.5 mM desthiobiotin. Fractions containing the target protein were pooled, diluted with 2 volumes of HAP loading buffer, and applied to a hydroxyapatite (HAP) column. The column was washed in three successive washing steps with buffer containing 10, 15, and 17% HAP elution buffer. Elution was performed with a linear gradient of 17-50% HAP elution buffer and fractions containing the target protein were pooled and concentrated. Subsequently, the concentrated protein was applied to a pre-equilibrated HiLoad 26/600 Superdex 200 column and SEC was performed at a constant flow rate of 1 ml/min. Fractions containing the HTRA1 variant were pooled and concentrated, flash-frozen in liquid nitrogen and stored at -80 °C. All purification steps were analyzed by SDS-PAGE (3.3.3).

3.3.3 Sodium dodecyl sulfate-polyacrylamide gel electrophoresis

Protein samples were analyzed by sodium dodecyl sulfate (SDS) polyacrylamide gel electrophoresis (PAGE), an analytical method to separate proteins according to their molecular weight in an electrical field. Samples were mixed with 2x SDS-PAGE loading buffer, heated (5 min, 95 °C), and applied onto gels containing 10, 12, or 15% polyacrylamide. Electrophoresis was conducted constantly at 200 V for 50 min in SDS-PAGE running buffers. The gels were stained in Coomassie staining solution. A protein standard (Precision Plus Protein Standard, Bio-Rad) was used for evaluation of the protein size.

For certain experiments, NuPAGE 10%, Bis-Tris, Midi Protein Gels (Thermo Fisher) were used. In this case, electrophoresis was conducted at 150 V for 1.5 h in MOPS buffer.

3.3.4 *In vitro* phosphorylation of recombinant Tau

Recombinant Tau was phosphorylated in two successive steps with different kinases as described by Meng et al. (2022) with minor modifications. All phosphorylation reactions contained 200 μ M Tau in 400 μ l of phosphorylation buffer supplemented with 2 mM ATP. First, Tau was phosphorylated with the cAMP-dependent Protein Kinase A (PKA) (New England Biolabs). Therefore, 7.2 U of PKA was added and the reaction was incubated at 30 °C for 24 h. In a second phosphorylation step, 1.44 U either of GSK3 β (Sigma) or SAPK4 (Merck) was added and incubation was continued for 24 h. Following phosphorylation, kinases were inactivated by incubation at 65 °C for 20 min and the phosphorylated Tau was flash-frozen in liquid nitrogen and stored at -80 °C. Phosphorylation was confirmed by SDS-PAGE (3.3.3) and detailed mapping of phosphorylation sites was obtained by liquid chromatography tandem-mass spectrometry (LC-MS/MS) analysis conducted by the Analytics Core Facility Essen of the University Duisburg-Essen.

3.3.5 Formation of Tau fibrils

The *in vitro* assembly of Tau into fibrils was induced using polyanionic heparin, as described by (Goedert et al., 1996), with modifications. Briefly, 60 μ M Tau was incubated with 0.4 mg/ml heparin in 30 mM MOPS buffer (pH 7.2) at 37 °C and 300 rpm for up to 5 days. After incubation, the fibrils were sedimented by centrifugation (21,130 rpm, 1 h) and resuspended in 30 mM MOPS buffer (pH 7.2) to remove soluble Tau and heparin. The formation and stability of the fibrils were confirmed by atomic force microscopy (3.3.9), fibril sedimentation assay (3.3.7), and measurement of Thioflavin T fluorescence (3.3.8). For a faster formation of fibrils, 3 μ M fibril seeds (3.3.6) were added to the reaction and the incubation time was reduced to 24–48 h.

3.3.6 Generation of Tau fibril seeds

For the generation of Tau fibril seeds, 50–200 μ l of Tau fibrils were sonicated 3x for 20 s at 90% intensity with an Ultrasonic homogenizer. Between all sonication steps,

the fibrils were cooled down on ice. Fibril seeds were flash-frozen in liquid nitrogen and stored at $-80\text{ }^{\circ}\text{C}$.

3.3.7 Fibril sedimentation assay

Tau fibril sedimentation assays were performed to analyze the formation and stability of the fibrils. In particular, Tau fibrils were centrifuged for 1 h at 21,1130 rpm and samples of the total, supernatant, and pellet fractions were analyzed by SDS-PAGE (3.3.3).

3.3.8 Thioflavin T fluorescence

Thioflavin T (ThT), an amyloid-specific fluorescence dye, was used to detect the formation of Tau fibrils. For the measurement, 30 μl samples of the fibril formation reactions (3.3.5) were transferred to black, low-volume 384-well microplates (Corning). All samples were supplemented with 20 μM ThT (solved in 50 mM glycine, pH 8.5) and mixed for 1 min at 700 rpm and $37\text{ }^{\circ}\text{C}$. Fluorescence intensities were measured at excitation and emission wavelength of 440 and 480 nm with the cut-off filter set to 455 nm. Between the single measurements, microplates were incubated at $37\text{ }^{\circ}\text{C}$ and 350 rpm.

3.3.9 Atomic force microscopy imaging

Atomic force microscopy (AFM) was used to visualize Tau fibrils. Samples (10 μl) were supplemented with 5 mM magnesium chloride and deposited on freshly cleaved mica surfaces (Plano GmbH). After absorption for 3 min at room temperature (RT), samples were washed with water and dried under air flow. Using a Multi-Mode 8 microscope (Bruker) equipped with a Nanoscope V controller, samples were scanned in ScanAsyst mode with cantilevers (0.4 N/m force constant) with ScanAsyst-Air probes (Bruker). For image analysis, the NanoScope Analysis software (Bruker) and the Ridge Detection tool in Fiji (Steger, 1998) were used.

3.3.10 Microtubule co-sedimentation assay

Microtubule co-sedimentation assays were used to study the interactions of HTRA1 and different Tau species with microtubules. Therefore, microtubules were polymerized from tubulin (Cytoskeleton, Inc.) according to the instructions of the manufacturer by Jonas Neblik (University Duisburg-Essen). The microtubules were mixed with the proteins of interest at 10 μ M each in 40 μ l PEM buffer. All reactions were set up in TLA-100 tubes (Beckman Coulter) and incubated at RT for 15 min. Microtubules and bound proteins were pelleted for 20 min at 60,000 rpm and 25 °C. Supernatant and pellet fractions were analyzed by SDS-PAGE (3.3.3).

3.3.11 *In vitro* proteolysis assays

In vitro proteolysis assays were performed to investigate the degradation of different Tau species by HTRA1. Unless indicated otherwise, 1 μ M HTRA1 was mixed with 2.5 μ M of the potential substrate in proteolysis buffer and incubated at 37 ° and 350 rpm. Samples were collected at the indicated time points, and the reactions were stopped by the addition of 2x SDS-PAGE loading buffer. Analysis was carried out using SDS-PAGE (3.3.3). Subsequently, SDS-PAGE gels were scanned, and the reduction of the full-length substrate bands was quantified with Phoretix 1D software (TotalLab) using unmodified gel images.

3.3.12 Time-resolved proteolysis and analysis by mass spectrometry

Mass spectrometry (MS) experiments were performed for a temporal and spatial resolution of the degradation of different Tau species by HTRA1. For proteolysis, 10 μ M of the Tau variant was mixed with 2 μ M of HTRA1 in proteolysis buffer and incubated at 37 °C and 350 rpm, unless indicated otherwise. Samples (20 μ l) were collected at the indicated time points and directly added to 120 μ l ice-cold acetone for overnight precipitation at –80 °C. Precipitated proteins were removed by centrifugation (15,000 rpm, 1 h, 4 °C) and peptides within the supernatant were dried in a SpeedVac concentrator at 30 °C for approximately 3 h. Dried samples were stored at –80 °C. Immediately before LC-MS/MS, peptides were resuspended in 0.1%

formic acid and loaded onto Evotips (Evosep Biosystems) according to the protocol of the manufacturer. All experiments were done in quadruplicates.

Analysis of the samples was performed by LC-MS/MS conducted by the Analytics Core Facility Essen under the direction of Dr. Farnusch Kaschani. Measurements were carried out using an Orbitrap Elite (Thermo Fisher) or an Orbitrap Fusion Lumos (Thermo Fisher) mass spectrometer coupled to an Evosep One liquid chromatography (LC) system (Evosep Biosystems). Peptides and proteins were identified using the MaxQuant software. Further analysis and evaluation of the data were done using the Targeted Proteolysis module of UMSAP (Bravo-Rodriguez et al., 2018). The significance level was set to 0.05 and the minimum score value to 50. A log₂ transformation was applied to the data prior to the analysis.

3.3.13 Cross-linking assay

Cross-linking experiments were performed by Michal Strzala at the Research Institute of Molecular Pathology in Vienna. HTRA1^{S328A} and Tau fibril seeds were each diluted to 5 μM in 33 μl of cross-linking buffer and incubated for 15 min at 37 °C to allow binding. The cross-linking reaction was started by adding the chemical cross-linker PhoX (Thermo Fisher) and continued for 15 min at 37 °C until it was stopped by the addition of 100 mM Tris HCl (pH 7.5). The cross-linked samples were prepared for mass spectroscopic analysis by tryptic digestion of proteins and purification of the obtained peptides. The resulting peptides were analyzed by LC-MS/MS. Data analysis and processing were performed by the Proteomics Facility at IMP/IMBA/GMI using the VBCF instrument pool and the software Proteome Discoverer and xiSearch.

3.3.14 HTRA1 activity assay

For the determination of the proteolytic activity of recombinant HTRA1 in the presence of different Tau species, a synthetic HTRA1 substrate consisting of para-nitroaniline (pNA) coupled to the C-terminus of the peptide VFNTLPMMGKASPV was used. HTRA1 (1 μM) was mixed with different concentrations of the target Tau

species to a final volume of 100 μ l in proteolysis buffer. After incubation for 1 min at 37 °C and 700 rpm, 500 μ M of the pNA substrate was added. Cleavage of the substrate was continuously monitored, measuring the absorption at a wavelength of 405 nm every 2 min for a period of 2 h. The specific enzyme activities of HTRA1 were derived from at least three independent measurements and calculated with the following formula:

$$\text{specific enzyme activity} = \frac{\Delta A_{405} \times V}{m \times \epsilon \times t}$$

ΔA_{405} : change of absorption at $\lambda = 405$ nm

V : reaction volume (ml)

m : amount of protease (mg)

ϵ : molar extinction coefficient of pNA ($M^{-1} \times cm^{-1}$)

t : time (min)

3.3.15 Fluorescence-labeling of HTRA1

Recombinant HTRA1 and HTRA1^{S328A} were labeled with DyLight 633 NHS Ester (Thermo Fisher) according to the manufacturer's instructions. Briefly, 500 μ l of 5 mg/ml HTRA1 in DPBS (Thermo Fisher) were mixed with 50 μ g of the dye and incubated for 1 h at 350 rpm and 20 °C. Excess dye reagent was removed by dialysis using Slide-A-Lyzer MINI Dialysis Devices (Thermo Fisher). The labeled protein was flash-frozen in liquid nitrogen and stored at -80 °C in single-use aliquots.

4. Results

4.1 Formation of pathological Tau species

In order to gain mechanistic insights into the interactions of HTRA1 with different pathological Tau species, recombinant Tau was purified and afterwards phosphorylated or aggregated into fibrils. First, I expressed untagged human Tau of isoform 2N4R, subsequently referred to as Tau, in *E. coli* (3.2.4). For purification, I adopted an established four-step protocol from our laboratory (3.3.1) (Tennstaedt et al., 2012). Since Tau is a heat-stable, intrinsically unstructured protein, I could isolate it from the cleared bacterial extract by boiling. Tau was further purified using cation exchange chromatography and hydroxyapatite chromatography, followed by SEC. The obtained recombinant Tau was either phosphorylated with different kinases or aggregated into amyloid fibrils.

4.1.1 Hyperphosphorylation of recombinant Tau

Hyperphosphorylation of Tau is associated with pathological processes in Tauopathies. Following published protocols, recombinant Tau was sequentially phosphorylated by cAMP-dependent protein kinase A (PKA) and subsequently by either glycogen synthase kinase 3 β (GSK3 β) or stress-activated protein kinase 4 (SAPK4) (3.3.4) (Figure 7A) (Yoshida and Goedert, 2006; Meng et al., 2022). All three kinases have previously been linked to phosphorylation observed in Tau pathologies (Yoshida and Goedert, 2006). I confirmed successful hyperphosphorylation using SDS-PAGE analysis (Figure 7C). The band of Tau phosphorylated by PKA (Tau-p) shows the characteristic upward shift compared to the native Tau band with an apparent molecular weight (MW) of approximately 52 kDa. An even greater upward shift was observed for the bands of Tau phosphorylated with PKA and GSK3 β (Tau-pg) as well as Tau phosphorylated with PKA and SAPK4 (Tau-ps). I further analyzed all three phosphorylated Tau species by LC-MS/MS for a detailed mapping of the individual phosphorylation sites. While a total of 20 different phosphorylation sites are found in Tau-p, around twice as many amino acid residues are phosphorylated in Tau-pg and Tau-ps (Figure 7D). However, my data neither provide

information about the extent of phosphorylation per Tau molecule nor the distribution of the phosphorylation degree within the population. Relatively sharp protein bands in the SDS-PAGE analysis suggest rather similar phosphorylation degrees within the respective Tau species.

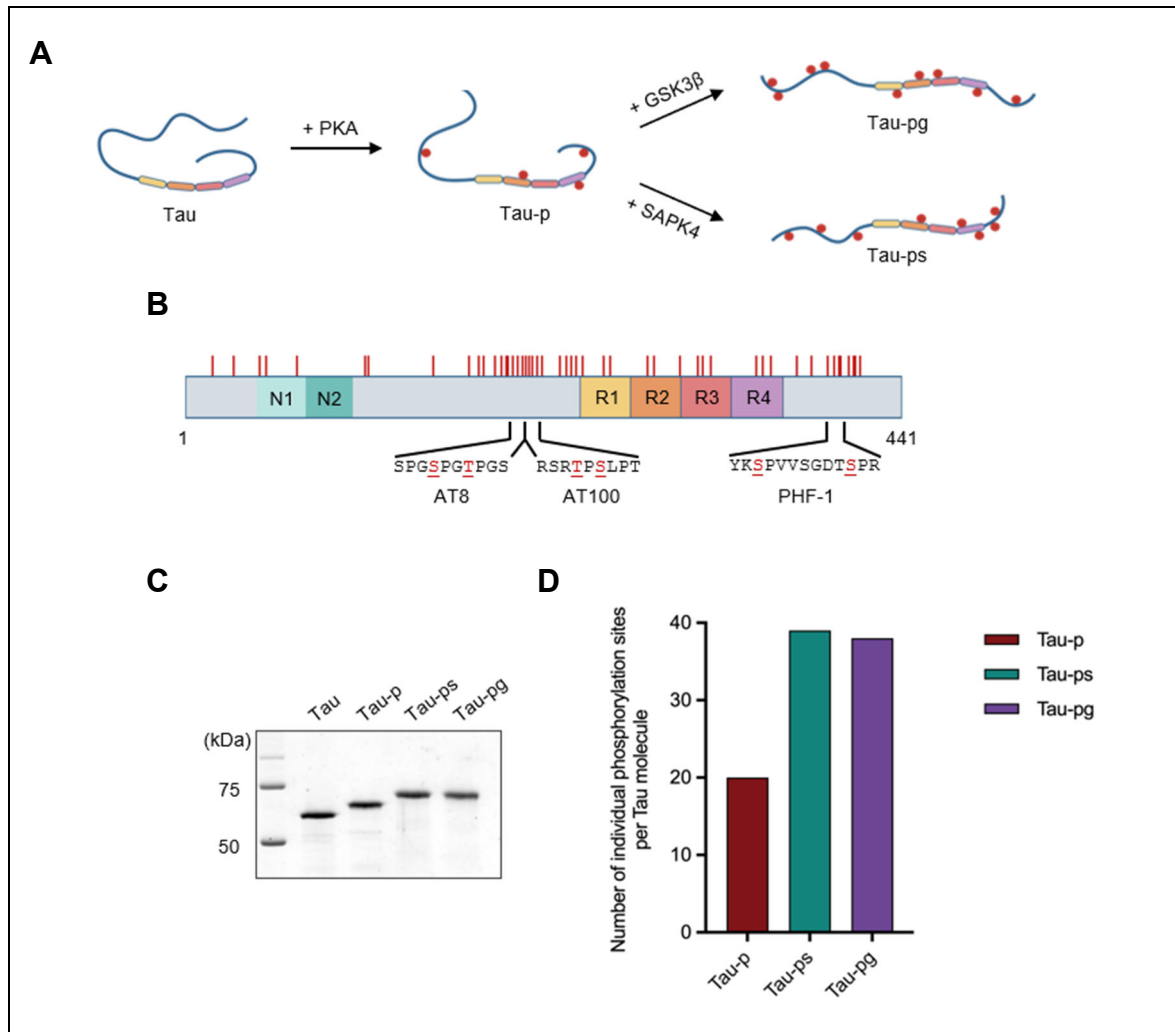


Figure 7: Sequential hyperphosphorylation of Tau generates AD-specific epitopes

Recombinant Tau was phosphorylated by PKA and subsequently either by GSK3 β or SAPK4. (A) Schematic overview of the phosphorylation process resulting in three differentially phosphorylated Tau species: Tau phosphorylated by PKA (Tau-p), Tau phosphorylated by PKA and GSK3 β (Tau-pg), and Tau phosphorylated by PKA and SAPK4 (Tau-ps). (B) All phosphorylation sites (red lines) detected by LC-MS/MS mapped to the Tau molecule. Both Tau-pg and Tau-ps, show phosphorylation at sites (amino acids highlighted in red) recognized by antibodies that detect AD-specific Tau species, such as AT8, AT100, and PHF-1. Tau-p, however, is not phosphorylated at any of these phosphorylation sites. (C) Successful phosphorylation was confirmed by SDS-PAGE analysis. Bands of phosphorylated Tau species show an upward shift compared to wild-type Tau. (D) Tau-p shows a total of 20 different phosphorylation sites, while Tau-pg and Tau-ps each have approximately twice as many individual phosphorylation sites.

In total, 49 individual serine and threonine residues were found to be phosphorylated (Figure 7B). Most of the phosphorylation sites are located in the proline-rich region and the C-terminal region, flanking the MTBD. Furthermore, sequential phosphorylation by both combinations of kinases resulted in the generation of epitopes recognized by different phosphorylation-dependent antibodies, such as AT8, AT100, and PHF-1. These antibodies are frequently used to detect Tau pathology in the human brain, for example, in AD. Thus, the hyperphosphorylated Tau generated in this work shows characteristics similar to disease-relevant Tau species. A complete list of all detected phosphorylation sites is shown in Appendix A (Table 15).

4.1.2 Formation of Tau fibrils

Aggregation of Tau into amyloid fibrils is the main characteristic of neurodegenerative Tauopathies. Several methods have already been published to reconstitute the process of Tau fibrilization *in vitro* (Goedert et al., 1996; Kampers et al., 1996). The majority of the described protocols employ the addition of polyanionic cofactors to the positively charged Tau to promote fibril formation. In this work, formation of Tau fibrils was facilitated by the addition of heparin (3.3.5). I also added Tau fibril seeds to accelerate the fibrilization process. Seeds were generated by fragmenting fibrils via sonication. They serve as nucleation cores and recruit soluble Tau into growing fibrillar assemblies. I followed the fibrillization process by measuring ThT fluorescence and confirmed the successful formation of fibrils by a sedimentation assay and atomic force microscopy (AFM) (Figure 8). ThT is an amyloid-specific fluorescence dye that gives a strong signal at approximately 480 nm upon binding to Tau fibrils. Measurements show a strong increase in fluorescence in the samples containing recombinant Tau, heparin, and seeds but not in the controls (Figure 8A). In accordance with this, the sedimentation assay shows that Tau shifts from the supernatant to the pellet fraction after 24 h under fibrillization conditions (Figure 8B). Whereas native Tau is a highly soluble protein, Tau fibrils sediment upon centrifugation. A very thin band in the supernatant fraction indicates that the majority of the protein is present as insoluble aggregate after 24 h of fibrilization. Using AFM, I confirmed that the insoluble Tau fraction shows the typical morphology of long Tau fibrils (Figure 8C).

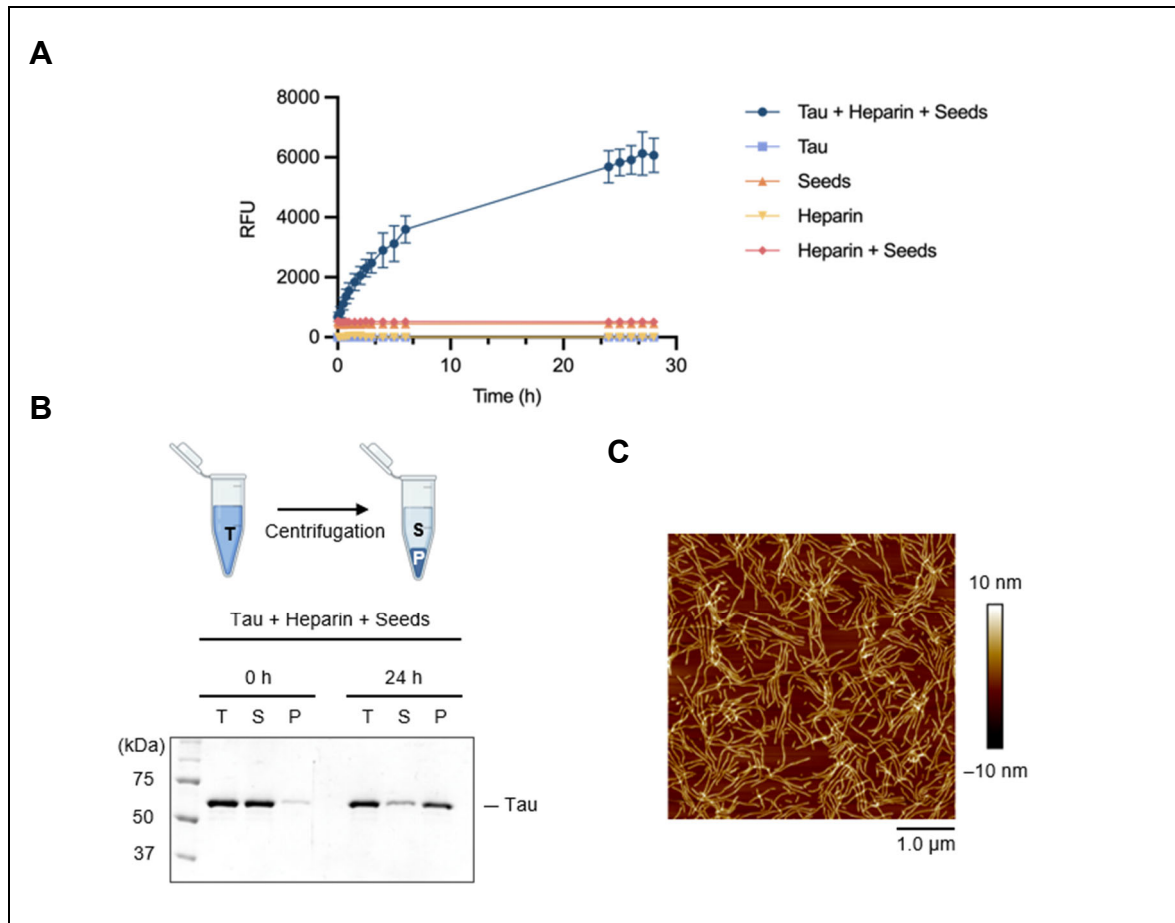


Figure 8: *In vitro* formation of Tau fibrils

Tau fibrils were generated from recombinant Tau (60 μM) by addition of polyanionic heparin (0.4 mg/ml) and Tau fibril seeds (3 μM). (A) ThT fluorescence measurement at 480 nm over a 24 h time period. A strong increase in the relative fluorescence units (RFU) can be detected in samples containing recombinant Tau with heparin and seeds but not in the control samples, indicating the generation of amyloid fibrils. Measurements were performed in triplicates. (B) In a sedimentation assay, samples before (0 h) and after 24 h of fibrillization were centrifuged to distinguish soluble wild-type Tau and insoluble aggregated Tau. After centrifugation, samples of total (T), supernatant (S), and pellet (P) fractions were analyzed by SDS-PAGE. A band shift from the S to the P fraction suggests Tau fibril formation. (C) Representative image of generated Tau fibrils acquired by AFM.

4.2 Interactions of HTRA1 and Tau with microtubules

Similar to the microtubule-associated protein Tau, a localization of HTRA1 to microtubules (MTs) is also reported (Chien et al., 2009b). I established a co-sedimentation assay to investigate the binding of HTRA1 and different Tau species to MTs. Recombinant human HTRA1 was expressed and purified from *E. coli* (3.2.4 and 3.3.2). Previous studies reported an intracellular variant of HTRA1 where the N-terminal domain is deleted. Furthermore, the N-terminal domain was shown to be dispensable for HTRA1 activity (Clawson et al., 2008; Eigenbrot et al., 2012).

Therefore, in this work, I employed a variant of HTRA1 containing only protease and PDZ domain (amino acids 158–480). Like intracellular HTRA1, the purified recombinant HTRA1 has a molecular weight of approximately 36 kDa and in the following is referred to as HTRA1. Moreover, in the co-sedimentation assays, I used a proteolytically inactive variant of HTRA1, referred to as HTRA1^{S328A}, where the active site serine is replaced by alanine to prevent degradation. MTs were assembled from tubulin and incubated with the different target proteins. After centrifugation, I analyzed supernatant and pellet fractions by SDS-PAGE to identify proteins that co-sediment with the MTs.

4.2.1 HTRA1 and Tau bind to microtubules simultaneously

I performed MT co-sedimentation assays (3.3.10) to investigate the binding behavior of Tau and HTRA1 to MTs, both separately and in combination. Analysis of the supernatant and pellet fractions shows that Tau co-sediments with MTs (Figure 9). Moreover, a substantial increase in the amount of tubulin in the pellet fraction compared to the MT control indicates that Tau, according to its endogenous function, promotes MT assembly. A minor fraction of Tau is still present in the supernatant fraction, either unbound or binding to the soluble tubulin. In samples of MTs incubated with HTRA1^{S328A}, the HTRA1^{S328A} band shifts completely from the supernatant to the pellet fraction. As in the MTs-Tau samples, an increase in the amount of tubulin in the pellet fraction can be observed, albeit to a lower extent. Consistent with previously published data, the recombinant HTRA1^{S328A} binds MTs and promotes their assembly (Chien et al., 2009b).

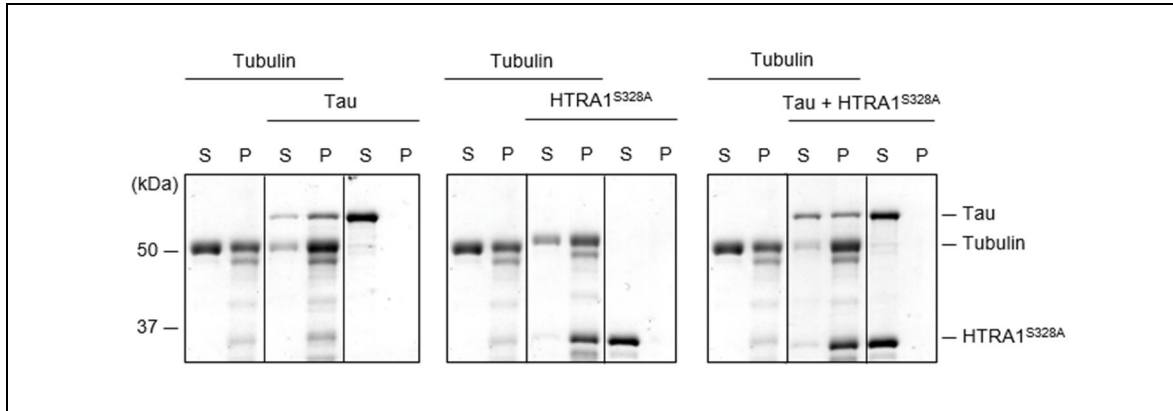


Figure 9: Tau and HTRA1 co-sediment with microtubules

The binding of Tau (10 μ M) and HTRA1^{S328A} (10 μ M) to MTs (10 μ M) was analyzed in co-sedimentation assays. Both proteins were separately or in combination incubated with MTs for 15 min. Subsequently, samples were centrifuged, and supernatant and pellet fractions were analyzed by SDS-PAGE. In all experiments, Tau and HTRA1^{S328A} co-sediment with the MTs. Therefore, both proteins bind to the MTs individually as well as simultaneously. Compared to the tubulin control, an MT-stabilizing effect of Tau and HTRA1^{S328A} can be observed. All experiments were performed in duplicate.

When a combination of Tau and HTRA1^{S328A} was tested, both proteins co-sediment with the MTs. Again, HTRA1^{S328A} shifts completely from the supernatant to the pellet fraction, while some of the Tau stays in the supernatant. It is striking that tubulin can also be detected almost exclusively in the pellet fraction. HTRA1 and Tau thus appear to bind to MTs simultaneously. Moreover, they seem to have additive effects in promoting MT assembly. In absence of MTs, Tau and HTRA1^{S328A} are only detected in the supernatant. Thus, they are soluble under the selected assay conditions.

4.2.2 Hyperphosphorylated Tau loses ability to bind to microtubules

Tau hyperphosphorylation is associated with impaired MT binding. Therefore, I analyzed binding of the hyperphosphorylated Tau species to MTs in co-sedimentation assays (3.3.10). Tau-p still co-sediments with the MTs (Figure 10). However, compared to wild-type Tau more Tau-p remains in the supernatant fraction. Furthermore, the MT stabilizing effect is less pronounced since the amount of tubulin shifted from the supernatant to the pellet fraction is lower. Phosphorylation of Tau by PKA seems to be sufficient to negatively impact MT-Tau binding interactions.

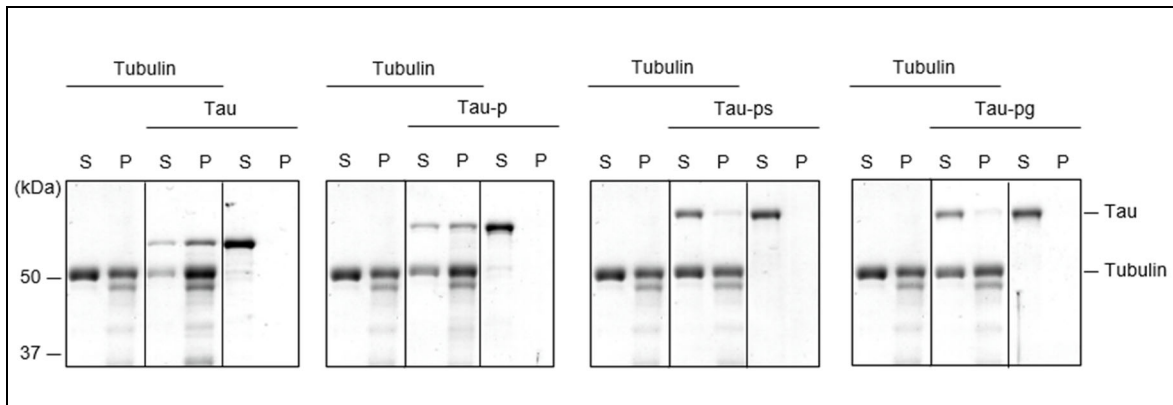


Figure 10: Hyperphosphorylated Tau-ps and Tau-pg do not bind and stabilize microtubules

Various phosphorylated Tau species were tested for their ability to bind MTs in a co-sedimentation assay. After incubation of the differently phosphorylated Tau species (10 μ M) with MTs (10 μ M), samples were centrifuged, and supernatant (S) and pellet (P) fractions were analyzed by SDS-PAGE. Unphosphorylated Tau co-sediments with MTs, thus indicating Tau-MT binding. In contrast, binding of Tau-p to MTs is impaired, and binding of Tau-ps and Tau-pg is completely abolished. All experiments were performed in duplicate.

When Tau is sequentially phosphorylated by PKA and either SAPK4 or GSK3 β , no co-sedimentation with MTs can be detected. In the SDS-PAGE analysis, bands of Tau-ps and Tau-pg are only visible in the supernatant fraction. Furthermore, the ratio of tubulin in the supernatant and pellet fraction is similar to the ratio in the tubulin control. While phosphorylation of Tau by PKA only impairs MT-binding to a certain extent, the additional phosphorylation by SAPK4 or GSK3 β completely prevents binding. Accordingly, neither Tau-ps nor Tau-pg show MT-stabilizing effects.

4.3 Differences in the degradation of native, hyperphosphorylated, and fibrillar Tau by HTRA1

Previous studies have identified soluble Tau and Tau fibrils as potential substrates of HTRA1 (Tennstaedt et al., 2012; Poepsel et al., 2015). As proteases of the PQC system, HtrAs can recognize and specifically degrade misfolded proteins (Clausen et al., 2011). I hypothesized that HTRA1 may distinguish between native and pathological Tau species. Thus, I established a proteolysis assay to test whether there are differences in the degradation of native, hyperphosphorylated, and fibrillar Tau species by HTRA1. I used the recombinantly expressed and purified Tau as native Tau species. As pathological Tau species, I tested the two hyperphosphorylated Tau variants, Tau-ps and Tau-pg (4.1.1), and the *in vitro* formed Tau fibrils (4.1.2).

Each Tau species (2.5 μM) was incubated with HTRA1 (1 μM). Samples were collected at various time points during degradation and analyzed by SDS-PAGE and LC-MS/MS.

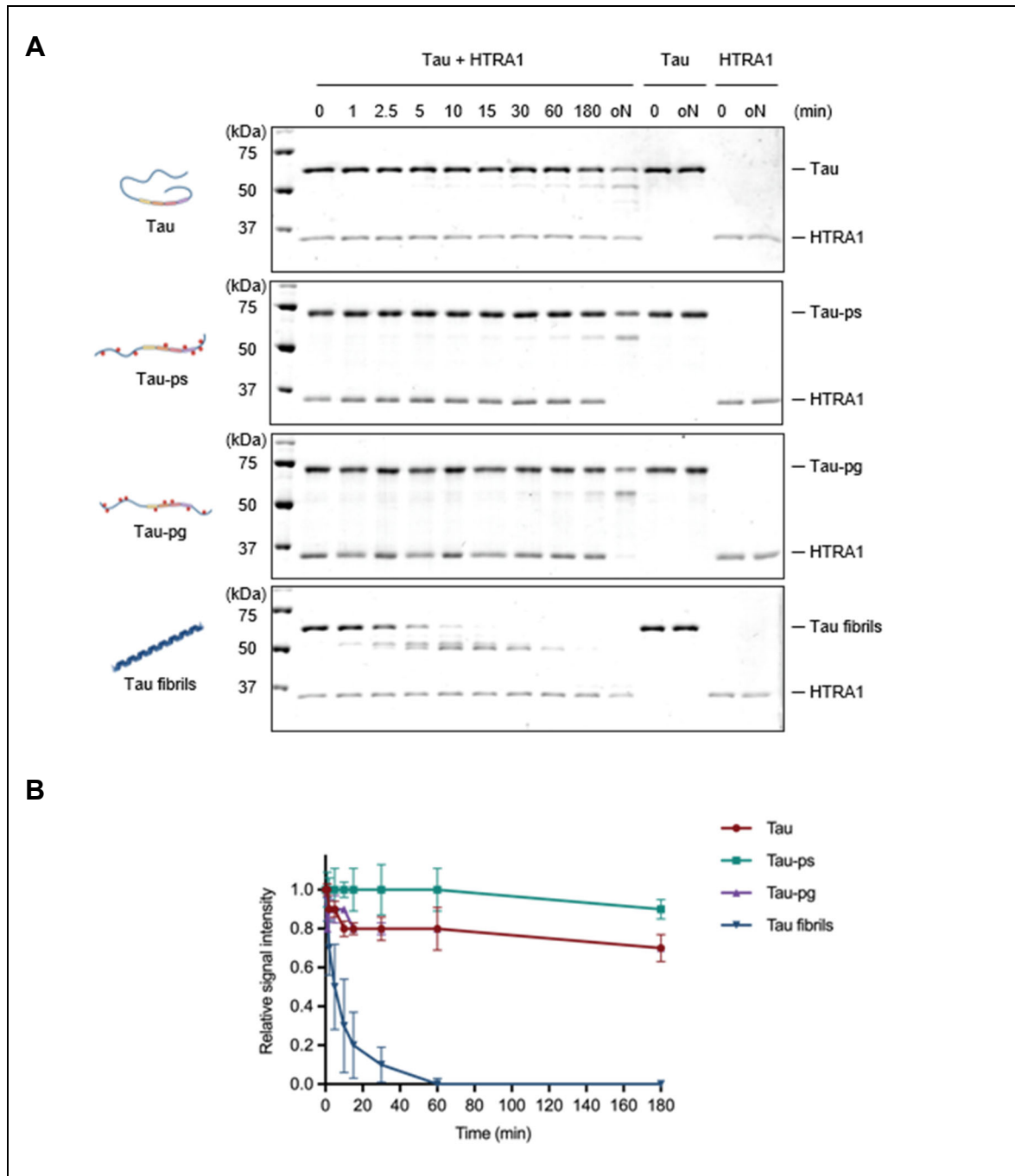


Figure 11: Degradation of native, hyperphosphorylated, and fibrillar Tau by HTRA1

A proteolysis assay was used to investigate the degradation of different Tau species by HTRA1. (A) HTRA1 (1 μM) was mixed with Tau, Tau-ps, Tau-pg, or Tau fibrils (2.5 μM) at a molar protease:substrate ratio of 1:2.5. Samples of the degradation process were collected at the indicated time points and analyzed by SDS-PAGE. All tested Tau species are substrates of HTRA1 but are degraded at varying rates. (B). The relative signal intensities of the full-length substrate bands were quantified using Phoretix 1D and are plotted against time (oN = overnight). Experiments were at least performed in duplicate.

To acquire and compare the degradation efficiencies of HTRA1 for the different Tau species, I followed the time-dependent digestion by SDS-PAGE (3.3.11) (Figure 11A). Protease and substrate were mixed at a molar ratio of 1:2.5. All experiments were performed at least in duplicate, and the relative signal intensities of the full-length substrate bands were quantified using Phoretix 1D (Figure 11B). In accordance with published data, I observed that all tested Tau species are substrates of HTRA1. Over time, a reduction of the full-length Tau is visible in all samples. Moreover, the appearance of additional bands with lower MW, which probably represent degradation products, is observed. However, under the tested conditions, native Tau, as well as hyperphosphorylated Tau, are not completely degraded by HTRA1. Full-length protein can still be detected for these Tau variants after overnight incubation. In contrast, Tau fibrils are digested by HTRA1 under the same conditions within 30 to 60 min. The resulting degradation products of the fibrils seem to be further degraded until they can no longer be detected after 180 min. In the control samples, no reduction in the amount of protein was detected. Thus, all proteins are stable under the assay conditions.

Additionally, I employed LC-MS/MS to analyze and compare the degradation of the different Tau species in more detail (3.3.12). HTRA1 (2 μ M) and the Tau substrates (10 μ M) were incubated at a molar ratio of 1:5. The resulting proteolytic products were identified by LC-MS/MS and further analyzed using the software UMSAP. For all Tau variants, increasing numbers of individual cleavage sites were detected over time (Figure 12A). Under conditions used in the assays, Tau fibrils show the highest number of individual HTRA1 cleavage sites. After an incubation time of 120 min, a total of 117 sites were detected within the 441 amino acids of the Tau sequence. At the beginning of the degradation process, the number of individual cleavage sites rapidly increases until it reaches a plateau at about 10 min. Between 10 and 120 min, only a negligible increase from 115 to 117 sites can be observed. In comparison, the number of HTRA1 cleavage sites increases at a slower rate for the other Tau species. Moreover, a plateau is not reached after 120 min. This suggests that not all possible cleavage sites of these Tau species were already detected after 120 min. A total of 35, 45, and 76 individual sites were detected for Tau, Tau-ps, and Tau-pg, respectively.

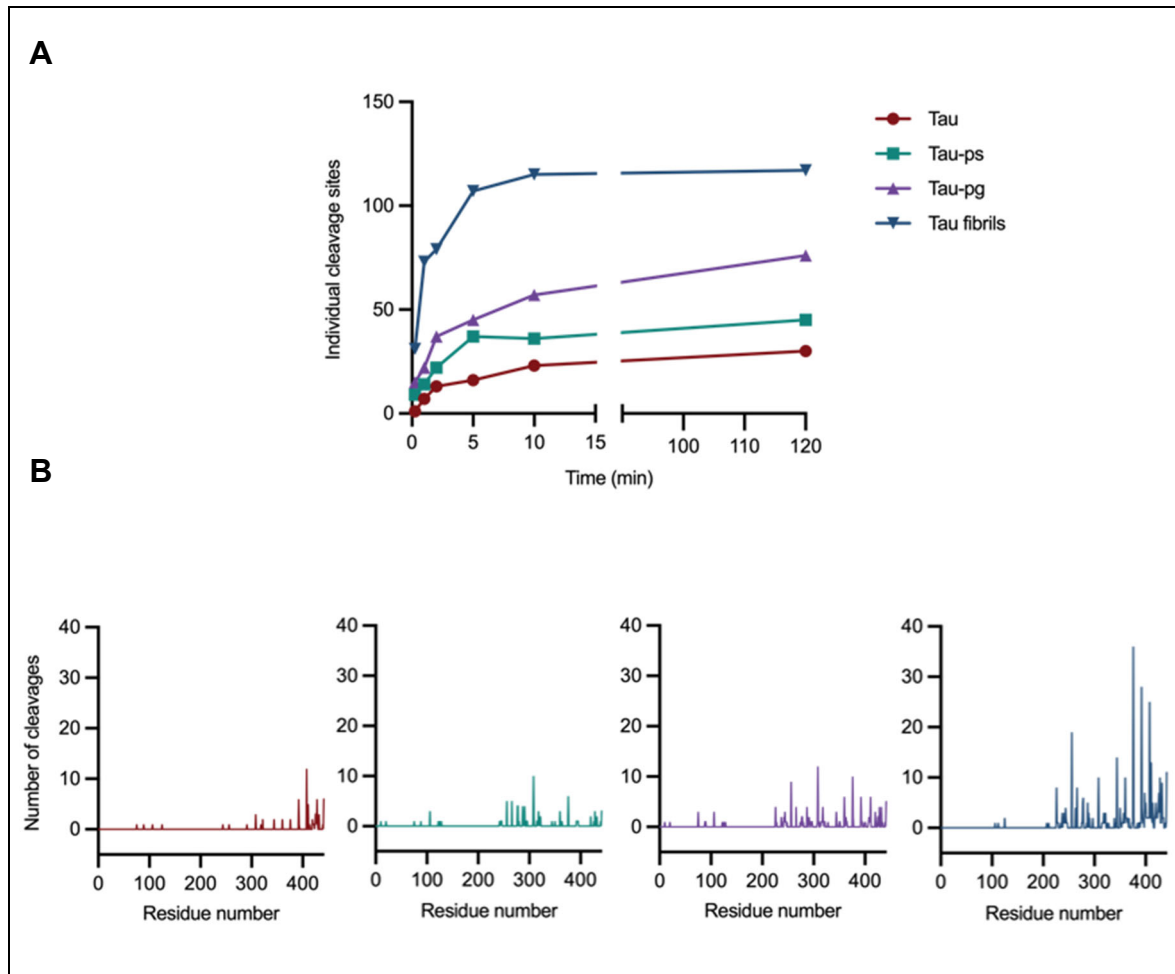


Figure 12: Number of HTRA1 cleavage sites in native, hyperphosphorylated, and fibrillar Tau

To compare the numbers of HTRA1 cleavage sites in different Tau species, HTRA1 (2 μ M) was incubated with Tau (red), Tau-ps (green), Tau-pg (purple), or Tau fibrils (blue) (10 μ M) at a molar ratio of 1:5. The resulting proteolytic products were identified by LC-MS/MS and further analyzed using the software UMSAP. (A) The numbers of individual HTRA1 cleavage sites, identified for the different Tau species, were plotted against the time of the degradation process. (B) For the last time point analyzed (120 min), the absolute numbers of identified cleavages were plotted against the amino acid residues of the Tau sequence.

In addition to the number of individual cleavage sites, I compared the absolute number of cleavages for each amino acid residue detected after 120 min of degradation (Figure 12B). Again, the highest values can be observed for the Tau fibrils, followed by Tau-pg and Tau-ps, and native Tau with the lowest values. Despite the differences in the absolute numbers, all Tau variants show a similar distribution of the cleavages within the amino acid sequence. The vast majority of cuts are found almost exclusively in the C-terminal half of the sequence. However, the two hyperphosphorylated Tau species show slight variations in the cleavage patterns.

Overall, HTRA1 seems to degrade Tau fibrils much more efficiently under the used conditions than the other Tau species. While a comparable degradation efficiency can be observed for native and hyperphosphorylated Tau in the SDS-PAGE analysis, MS data reveal some differences. Both hyperphosphorylated variants show a higher number of individual cleavage sites as well as higher absolute cleavage numbers compared to native Tau. Moreover, differences between Tau-ps and Tau-pg were observed, with more individual cleavage sites detected for Tau-pg. Thus, the conformation as well as the phosphorylation state of Tau has an impact on the proteolysis by HTRA1.

4.4 HTRA1 efficiently degrades Tau fibrils

The results of the proteolysis assay revealed that HTRA1 can efficiently degrade Tau fibrils (4.3). Since amyloid fibrils are postulated to be rather protease-resistant, I wanted to gain a deeper mechanistic understanding of how HTRA1 can degrade fibrils. Therefore, I combined AFM with time-resolved or cross-linking MS to visualize the degradation process and to uncover details of the interactions and sequential degradation of Tau fibrils by HTRA1.

4.4.1 Visualization of the Tau fibril degradation process

First, I wanted to visualize the degradation of Tau fibrils by HTRA to gain an initial understanding of the process. Therefore, I incubated Tau fibrils (2.5 μM) with HTRA1 (1 μM) under the conditions established for the proteolysis assay (4.3). At various time points, I removed aliquots from the proteolysis reaction and analyzed them by AFM. In parallel, samples of the same reaction were analyzed by SDS-PAGE to compare the morphology of the fibrils to the degradation state of the Tau molecules. In this way, I aimed to address the question of whether the degradation starts successively from one end of the fibril or occurs simultaneously along the entire fibril length. The experiment was performed in quadruplicate and the number of Tau fibrils in the individual samples was calculated using the ridge detection tool of Fiji.

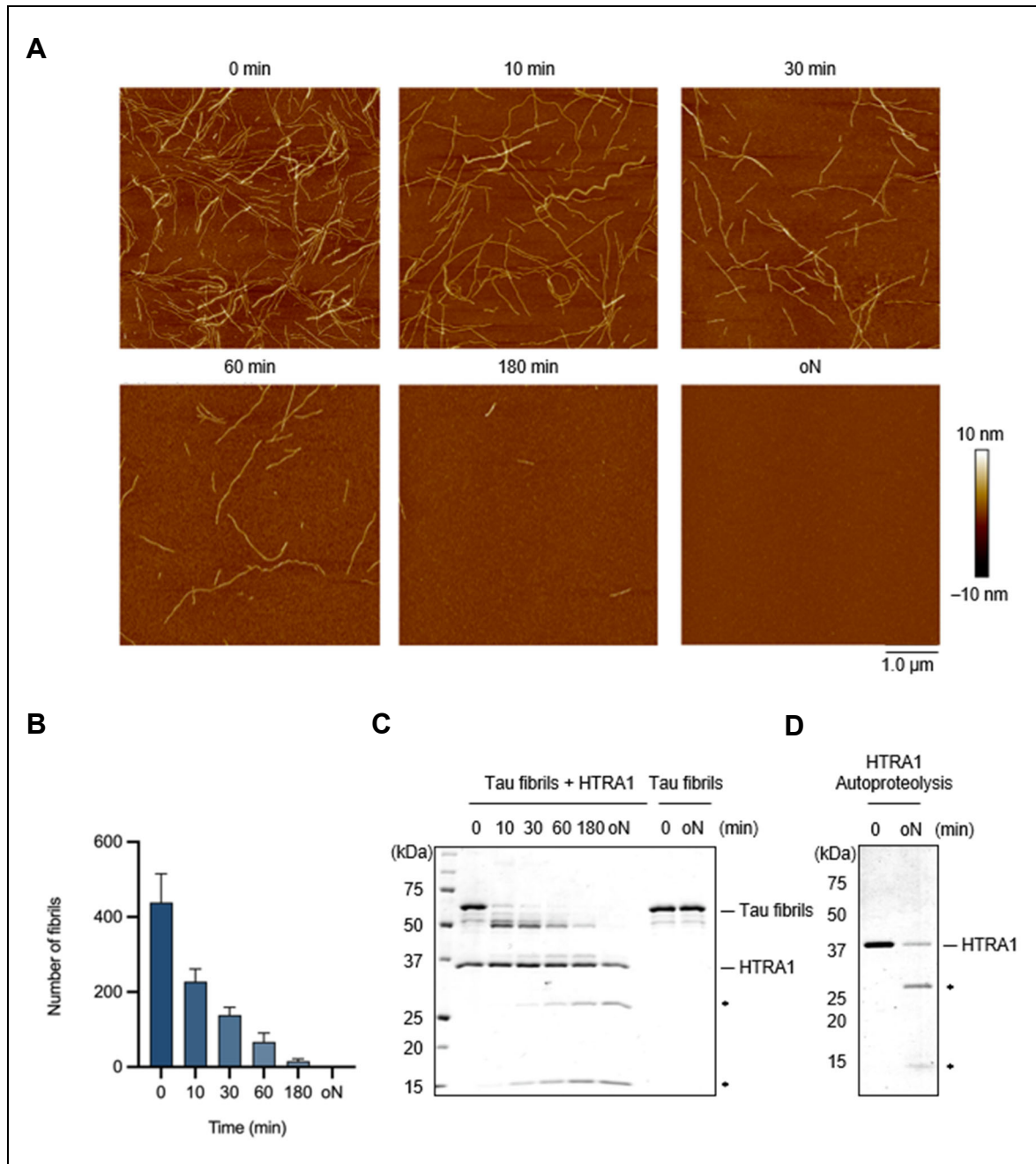


Figure 13: Visualization of the Tau fibril degradation by HTRA1

Tau fibril morphology and degradation state of the Tau molecules during the degradation process by HTRA1. (A) Samples collected at indicated time points of the proteolysis were visualized using AFM. (B) The average number of fibrils, quantified using the ridge detection tool of Fiji, plotted against time ($n=4$). A decreasing number of fibrils can be observed over time until no more fibrils are visible after overnight (oN) incubation. (C) Samples of the identical degradation reaction analyzed by SDS-PAGE. (D) SDS-PAGE samples of HTRA1 incubated overnight in buffer containing 150 mM NaPi (pH 8.0) and 380 mM NaCl show the characteristic bands resulting from HTRA1 autoproteolysis (*).

When Tau fibrils are incubated with HTRA1, the number of fibrils continuously decreases over time (Figure 13A and B). After incubation overnight, no more fibrils or remnants of fibrils are visible. Thus, HTRA1 seems to degrade Tau fibrils

completely, and the resulting proteolytic products are below the resolution limit (2 nm lateral and 0.1 nm vertical) of AFM. Accordingly, in the SDS-PAGE analysis, the protein band of the full-length Tau molecules, as well as bands of the resulting cleavage products are not detectable after overnight incubation (Figure 13C). The two bands with MWs of approximately 25 and 15 kDa visible after overnight incubation are likely fragments resulting from HTRA1 autoproteolysis since similar bands can be observed in HTRA1 control samples (Figure 13D). I suggest that HTRA1 undergoes autoproteolysis when it is highly active and no or only low amounts of substrate are present. This is supported by the fact that the bands start appearing only after the full-length Tau band becomes undetectable.

While the number of fibrils decreases over time, a significant reduction of the individual fibril length was not observed (Figure 13A). A comparison of the AFM image and SDS-PAGE analysis of the 10 min time point shows many intact fibrils still present in AFM scans, whereas almost no full-length Tau molecules can be detected by SDS-PAGE. These results suggest a simultaneous degradation of several Tau molecules by HTRA1 along the whole fibril. In a model where HTRA1 initially digests the fuzzy coat outside the fibril core, the fibrils visible in AFM scans would retain their full length, while in the SDS-PAGE analysis a degradation of Tau would be observed. Subsequent proteolytic events within the core region would destabilize the intermolecular Tau interactions and should result in dissociation of the fibril. A successive degradation starting from one end of the fibrils can very likely be excluded. Otherwise, a significant reduction of the average fibril length should be visible, and full-length Tau should be detectable as long as fibrils are visible.

4.4.2 Spatial and temporal resolution of the degradation of Tau fibrils by HTRA1

AFM analysis indicates that HTRA1 dissolves fibrils by simultaneously cleaving multiple Tau molecules within the filament. However, fibrils are characterized by strong intra- and intermolecular interactions, and it remains elusive how HTRA1 is able to degrade them. To gain molecular insights into the degradation mechanism, I combined the proteolysis assay with time-resolved MS (3.3.12). I incubated HTRA1 (2 μ M) with Tau fibrils (10 μ M) at a molar ratio of 1:5 and took samples at multiple

time points. Proteolytic products within the samples were isolated by acetone precipitation and subsequently analyzed by LC-MS/MS. The cleavage sites identified for the different time points were mapped to the Tau sequence to describe the degradation process at high temporal and spatial resolution.

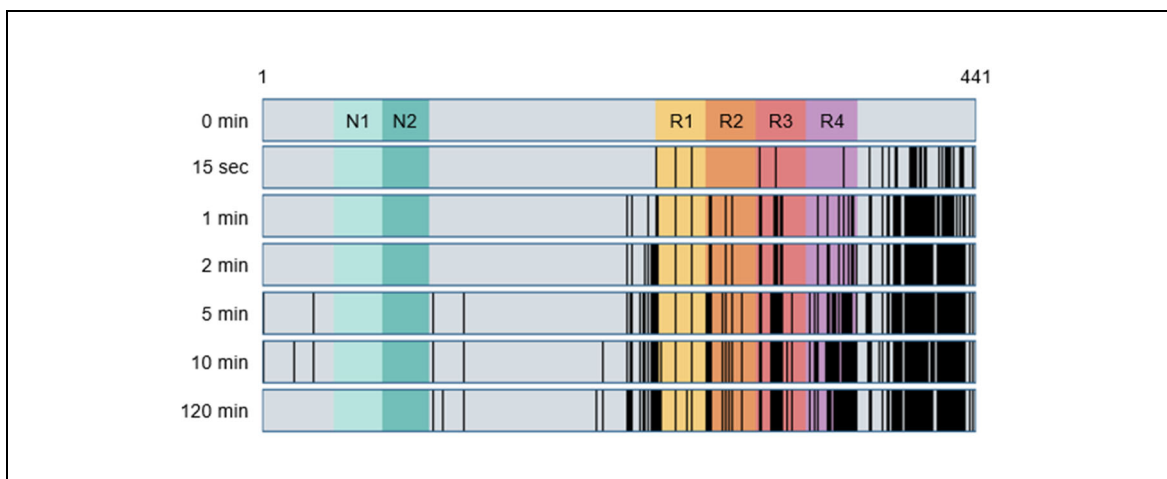


Figure 14: Temporal and spatial resolution of HTRA1 cleavage sites within the sequence of fibrillar Tau
 Degradation of Tau fibrils by HTRA1 was analyzed using time-resolved MS to gain mechanistic insights into the proteolytic process. HTRA1 (2 μ M) was incubated with Tau fibrils (10 μ M) at a molar ratio of 1:5. Samples of the reaction were taken at indicated time points, and proteolytic products were identified and analyzed using LC-MS/MS and UMSAP software. The experiment was performed in quadruplicate. Detected HTRA1 cleavage sites (black lines) were mapped to the Tau sequence for the respective time points. Within the Tau sequence, the two N-terminal inserts (N) and four repeats (R) that form the MTBD are highlighted in different colors.

Already, after a very brief incubation of the fibrils with HTRA1 for 15 s, 31 individual cleavage sites were detected within the Tau sequence (Figure 14). Six of these cleavages were within the MTBD. However, the majority of the cuts are located in the C-terminal region, indicating that HTRA1 preferentially binds and cleaves this part of the protein. The C-terminal Tau region also shows the highest density of cleavages at later time points. In contrast, no cleavage sites can be detected within the N-terminal half before the 5 min time point. After 5 min, only four individual cuts within this region were detected. Furthermore, the number of cuts did not significantly increase during the 120-min-long proteolysis experiment, indicating that the N-terminal region of Tau molecules within the fibrils is mostly resistant to HTRA1 degradation. The HTRA1 cleavage pattern looks similar at all analyzed time points but with an increasing density of the cuts. However, between the 5 min and 120 min time points, the number of cuts only slightly increases from 107 to 117. This

indicates efficient degradation of the Tau fibrils by HTRA1, with almost all individual cuts detectable within a few minutes.

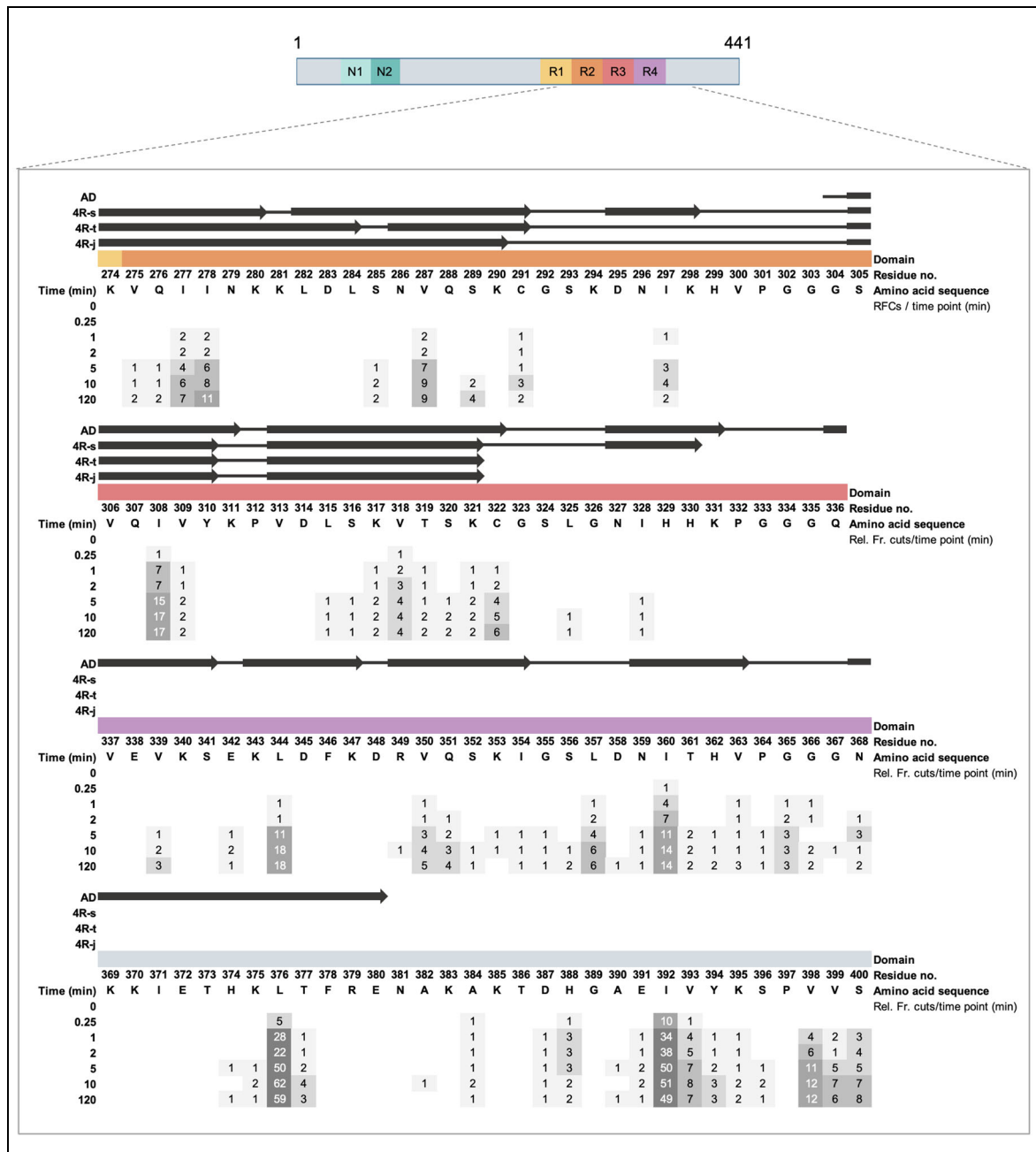


Figure 15: Evolution of HTRA1 cleavage sites within the core region of Tau fibrils

Tau fibrils (10 μ M) were degraded by HTRA1 (2 μ M), and the evolution of the proteolytic events within the fibril core was analyzed using LC-MS/MS and the software UMSAP. Shown is the amino acid sequence of the microtubule-binding repeats (R1 in yellow, R2 in orange, R3 in red, R4 in purple) and a part of the flanking C-terminal region (blue). Above the primary sequence, the β -sheet and loop regions of cryo-EM structures from AD Tau fibrils (PDB ID: 6HRE), or three different types of *in vitro* formed fibrils (PDB IDs: 6QJH (4R-s), 6QJM (4R-t), 6QJP (4R-j)) are depicted. Numbers below the individual amino acids indicate the relative frequency of cuts (RFCs) at each time point. The increasing numbers of the RFCs are highlighted gradually from light to dark grey. No number indicates that no cleavage was detected. The experiment was performed in quadruplicates.

Tau fibrils consist of a highly ordered, β -sheet rich core and a disordered fuzzy coat (Figure 6). The fibril core is formed only by a small region of the Tau molecules. This region mainly comprises the MTBD and varies between the different filament folds. Flanking N- and C-terminal regions project away from the core and build the fuzzy coat. Since the core is responsible for the assembly and stability of the fibril, I investigated the evolution of the proteolytic events in this region using the software UMSAP. The obtained data yield quantitative information on the preferred cleavage sites of HTRA1 within the Tau amino acid sequence, as well as on the spatial progression of the proteolysis over time (Figure 15). Cleavage sites detected in the first three time points were mapped to an exemplary structure of *in vitro* formed fibrils for better spatial understanding (Figure 16).

After 15 s of incubation, four HTRA1 cleavage sites (I308, V318, I360, and L376) can be detected, which originate from the degradation of the fibril core region into five peptides. Of these four cleavages, I308 and V318 are located within the part that is reported to form β -sheets within *in vitro* formed fibrils. At the following time point of 1 min, the number of different cleavages increases to 21. As a result, the entire core region is processed into 23 peptides consisting of 7 to 26 amino acid residues. The last measured time point of 120 min shows an even higher number of 45 cleavages, generating 63 peptides. Comparing the relative frequency of the cuts within the core of *in vitro* formed fibrils, I308, I278, V287, and I277 show the highest relative frequencies, reaching 17, 11, 9, and 7 cuts, respectively, after 120 min. Of these cleavage sites, only I308, which shows the highest frequency of cuts, can be detected at the first measured time point. Therefore, the proteolysis of the fibril core likely starts at I308, followed by cuts at I278, V287, and I277. Subsequently, HTRA1 presumably cleaves at less affine sites such as V318, C322, I297, C291, V309, K317, and T319, and thus efficiently degrade the fibril core.

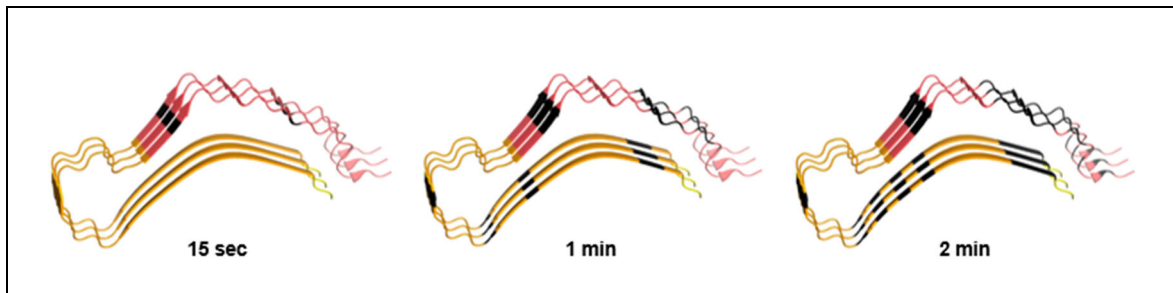


Figure 16: HTRA1 cleavage sites mapped to a structure of *in vitro* formed Tau fibrils

Degradation of Tau fibrils by HTRA1 was analyzed using LC-MS/MS and UMSAP software. HTRA1 cleavage sites identified after 15 s, 1 min, or 2 min of proteolysis were mapped to an exemplary structure of *in vitro* formed Tau fibrils (PDB ID: 6QJH). Different regions in the fibril structures are color-coded: repeat 1 in yellow, repeat 2 in orange, and repeat 3 in red. The experiment was performed in quadruplicates.

Taken together, all these data suggest that HTRA1 initiates the degradation of the fibrils at the C-termini of individual Tau molecules. The N-terminal half of Tau is mostly resistant to HTRA1, while the C-terminal half, including the fibril core, is cleaved with high efficiency. Under the conditions I tested, the fibril core is processed into 23 individual peptides within 1 min, probably starting with cleavage at residue I308 followed by I278, V287, and I277.

4.4.3 Initial interaction sites of HTRA1 and Tau fibrils

In the next step, I used chemical cross-linking mass spectrometry (XL-MS) to identify and map potential interaction sites of HTRA1 and Tau fibrils. The experiments were performed in collaboration with Michal Strzala at the Research Institute of Molecular Pathology in Vienna. In order to prevent cleavage and subsequent dissolution of fibrils during the course of the cross-linking experiment, HTRA1^{S328A} was used. This allows the identification of initial interactions between HTRA1 and Tau fibrils that take place just before the first cleavage occurs. For this purpose, HTRA1^{S328A} (5 μ M) and Tau fibril seeds (5 μ M) were incubated for 15 min at 37 °C to allow binding. The cross-linking reaction was started by addition of the crosslinker PhoX and continued for 15 min at 37 °C until it was stopped by quenching with Tris-HCl. PhoX contains an N-hydroxysuccinimide (NHS) ester at each end of a 4.3 Å spacer arm that rapidly and irreversibly reacts with primary amino groups, thus forming stable bonds between lysine residues in proteins. The cross-linked samples were prepared for mass spectroscopic analysis by performing a tryptic digestion of

proteins and purification of the obtained peptides. The resulting peptides were analyzed by LC-MS/MS, and data were processed using Proteome Discoverer and xiSearch. Data collection and analysis were performed by the Proteomics Facility at IMP/IMBA/GMI using the VBCF instrument pool. The identified intermolecular cross-links with high probability scores (>15) are schematically represented in a network map (Figure 17A). Additionally, I visualized the position of the cross-linked lysine residues within a model of HTRA1 using PyMOL (Figure 17B). The model was created using a crystal structure of the HTRA1 protease domains (PDB ID: 3NUM) and an NMR structure of the PDZ domain (PDB ID: 2JOA).

In total, I observed two cross-linked lysine residues in HTRA1 (L^{HTRA1}) and four cross-linked lysine residues in Tau (L^{Tau}) with probability scores >15 (Figure 17A). Within HTRA1, cross-links for $L261^{\text{HTRA1}}$ and $L305^{\text{HTRA1}}$ were identified (Figure 17B). $L261^{\text{HTRA1}}$ is located in a loop of the protease domain that points in the opposite direction of the active site. So far, this region of HTRA1 has not been reported to interact with substrates. Since $L261^{\text{HTRA1}}$ is highly surface-exposed, it is very likely that it forms non-specific contact with the fibrils due to its easy accessibility (Figure 17B). This is supported by the fact that $L261^{\text{HTRA1}}$ cross-links to $L163^{\text{Tau}}$ within the N-terminal half of Tau. The N-terminal half of Tau shows almost no HTRA1 cleavage sites in the proteolysis experiments (Figure 14B). Therefore, specific interactions of $L261^{\text{HTRA1}}$ with the fibrils are rather unlikely.

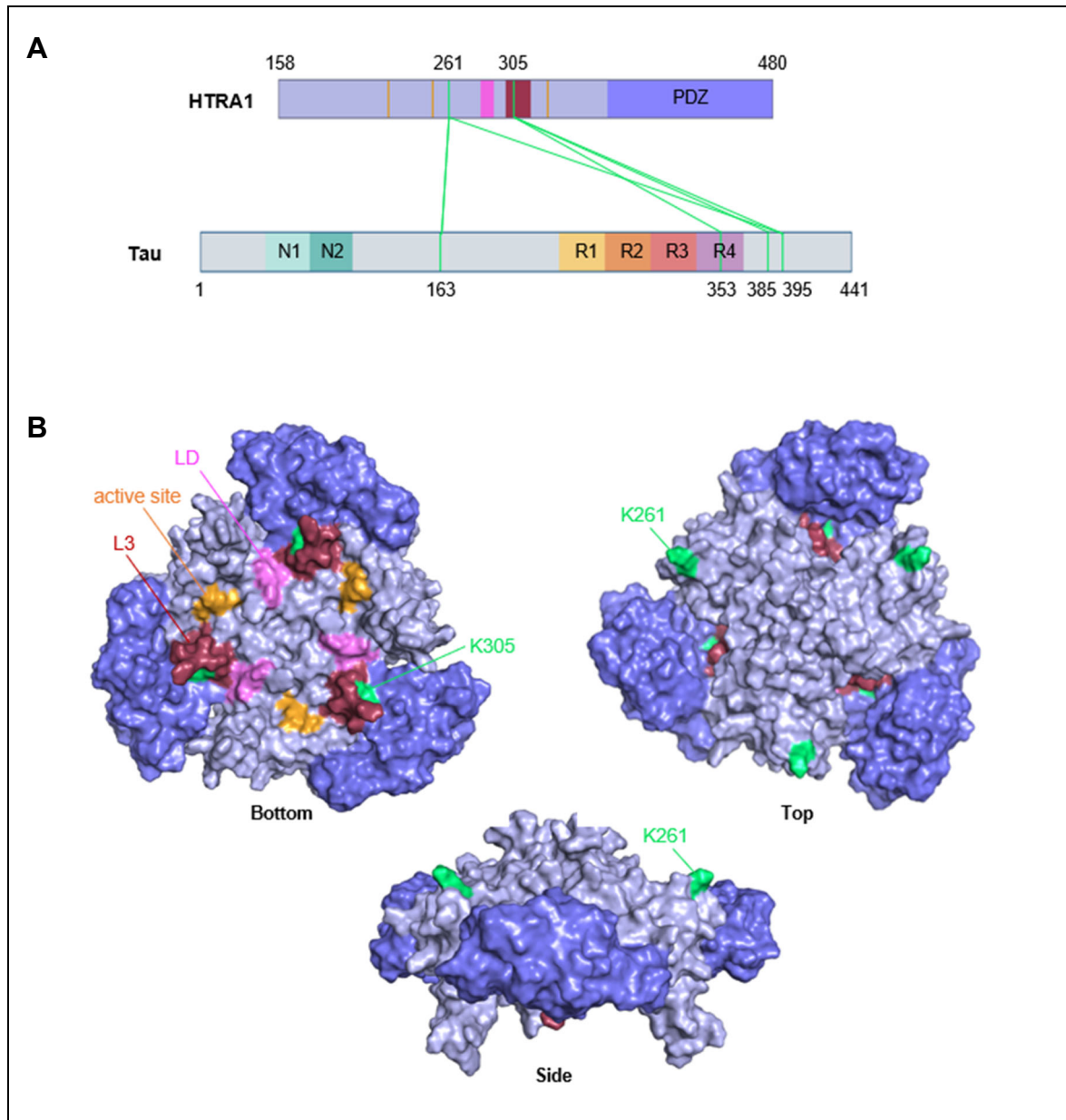


Figure 17: Interactions of HTRA1 and Tau fibrils

Cross-linking mass spectrometry identified potential interaction sites of HTRA1 and Tau fibrils. HTRA1 (5 μ M) and Tau fibril seeds (5 μ M) were cross-linked by the chemical cross-linker PhoX. Samples were analyzed by LC-MS/MS, and data were processed using Proteome Discoverer and xiSearch. (A) Identified intermolecular cross-links with high probability scores (>15) are schematically represented in a network map. Cross-linking sites (green) are labeled with the number of the amino acid residues. Active site (orange), loop L3 (red), and loop LD (magenta) of HTRA1 are color-coded. HTRA1 protease and PDZ domain are highlighted in light and dark blue, respectively. Tau is represented as described in Figure 14. (B) Visualization of cross-linking sites within an HTRA1 model containing protease domain (PDB ID: 3NUM) and PDZ domain (PDB ID: 2JOA). The model was generated using PyMOL. HTRA1 is shown in the surface representation from three different views. Colors correspond to the schematic representation in the network map.

L305^{HTRA1} is located within loop L3 of the activation domain of HTRA1. Loop L3 has been reported to directly interact with substrates bound to the protease domain. Upon binding of a substrate, loop L3 interacts with loop LD of a neighboring

protomer, resulting in the stabilization of the active state of the protease (Truebestein et al., 2011). My data shows cross-linking of L305^{HTRA1} to three different Tau lysine residues, one within repeat 4 (L353^{Tau}) and two within the C-terminal region (L385^{Tau} and L395^{Tau}). Using PyMOL, I calculated a distance of 21–26 Å between L305^{HTRA1} and the active site of HTRA1, corresponding to the length of approximately 6 to 8 amino acid residues. Amino acids located 6 to 8 residues C-terminal from the cross-linked Tau lysines (amino acid 359–361, 391–393, and 401–403) should be in spatial proximity to the HTRA1 active site. Indeed, analysis of the proteolysis experiments shows cleavage sites at I360, I392, and D402 with high relative frequencies of cuts of 14, 49, and 3, respectively, supporting this hypothesis (Figure 15). These data suggest that loop L3 of HTRA1 interacts with Tau fibrils, probably leading to activation of the protease by completing the activation domain. Furthermore, HTRA1 seems to initially interact with the C-terminal region of Tau.

4.5 N-terminal region of Tau is resistant to HTRA1 cleavage

Proteolysis experiments with HTRA1 and Tau fibrils reveal efficient degradation of the C-terminal half of Tau, with only very few cleavages detected in the N-terminal half (Figure 14). Recently published cryo-EM structures of Tau fibrils show that the N-terminal half of the Tau molecules is not part of the tightly packed fibril core but of the disordered fuzzy coat, which is postulated to be accessible for proteolysis (Scheres et al., 2020; Scheres et al., 2023). Resistance of the N-terminal Tau region to HTRA1 cleavage could be caused by inaccessibility or a non-cleavable primary sequence. To address these possibilities, I generated two different Tau constructs (Figure 18A). In the construct referred to as Tau^{CN}, I exchanged the N-terminal Tau fragment consisting of residue 41–98 (N^{41–98}) and the C-terminal fragment consisting of residue 390–441 (C^{390–441}). The selection of fragments was based on the identified HTRA1 cleavage sites within the wild-type Tau sequence (Figure 19C). In the N^{41–98} fragment, no cleavages were detected, while the C^{390–441} fragment showed the highest density of cleavages. Both fragments are located outside the protein region that forms the fibril core. The exchange should, therefore, not affect

fibrilization. In the Tau^{CNC} construct, fragments N^{41–98} and C^{390–441} were also exchanged. Additionally, residues 418–441 of the original Tau sequence were added to the C-terminus. Both Tau constructs were expressed in *E. coli* and subsequently purified following the same protocol as for wild-type Tau (4.1). Recombinant Tau^{CN} and Tau^{CNC} were assembled into fibrils and compared to wild-type Tau fibrils using AFM (3.3.5 and 3.3.9). All fibrils show the same characteristic morphology (Figure 18B).

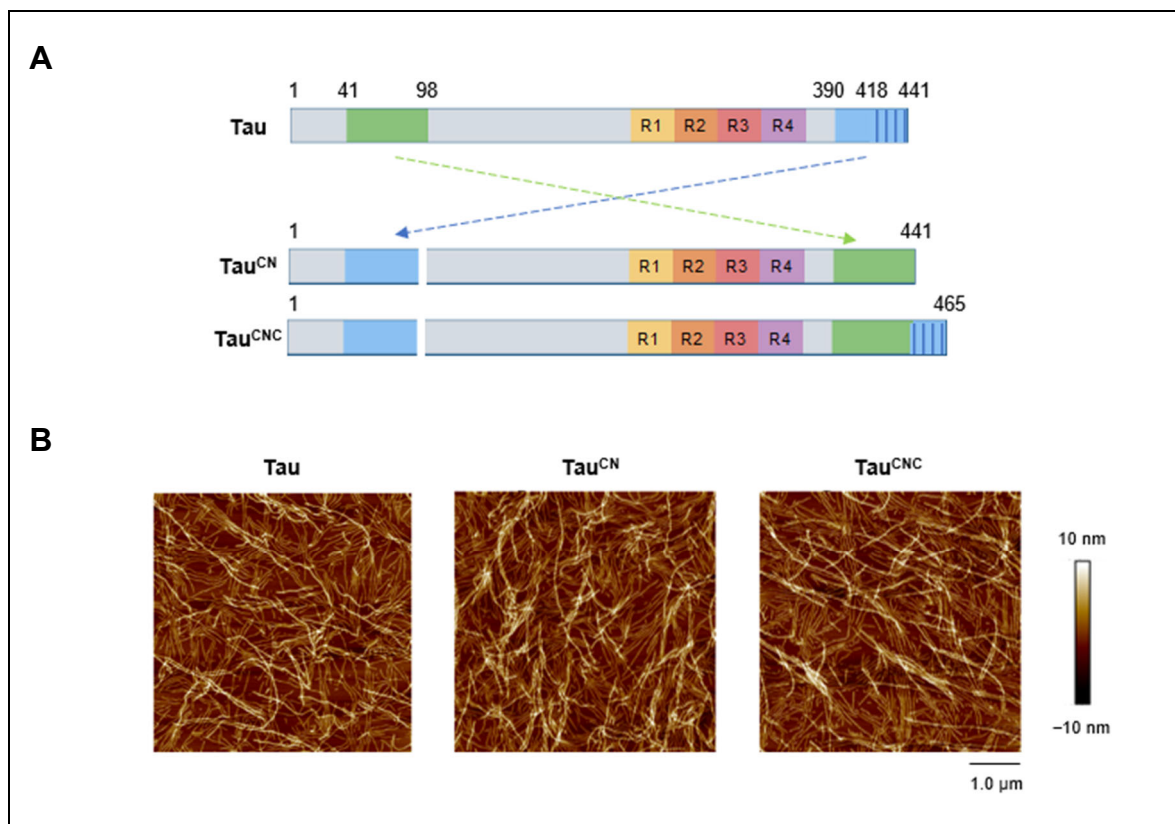


Figure 18: Tau constructs with exchanged N- and C-terminal region

Two Tau constructs with exchanged N- and C-terminal fragments were generated to address the resistance of the Tau N-terminal region to HTRA1 cleavage. (A) In the Tau^{CN} construct, the N-terminal Tau fragment consisting of residue 41–98 (green) is exchanged with the C-terminal fragment consisting of residue 390–441 (blue). In the Tau^{CNC} construct, the same N- and C-terminal fragments are exchanged. Additionally, residues 418–441 (blue with dashed lines) of the original Tau C-terminal region are added to the C terminus. The four repeats (R) that form the MTBD are highlighted in different colors. (B) AFM images of fibrils formed of Tau, Tau^{CN}, or Tau^{CNC}.

I used the established proteolysis assay to test whether there are differences in the degradation of Tau, Tau^{CN}, and Tau^{CNC} fibrils by HTRA1 (3.3.11). Fibrils (2.5 μM) and HTRA1 (1 μM) were incubated at a molar ratio of 1:2.5. Samples were collected

at different time points and analyzed by SDS-PAGE to follow the time-dependent digestion (Figure 19A). All experiments were performed at least in duplicate, and the relative signal intensities of the full-length substrate bands were quantified using Phoretix 1D (Figure 19B). The results of the experiment show that HTRA1 can degrade fibrils consisting of Tau^{CN} and Tau^{CNC}. However, in both cases proteolysis is significantly slower than with wild-type Tau fibrils. While the full-length band of wild-type Tau completely disappeared after 60 min, bands of the mutated constructs are still visible after overnight incubation. In comparison with each other, there is no significant difference in the degradation of Tau^{CN} and Tau^{CNC} fibrils. Both fibril types show similar degradation processes, and approximately 7% of the full-length bands are still detectable at the end of the proteolysis assay. These results indicate that the exchange of the N- and C-terminal fragments within the Tau sequence impairs the degradation by HTRA1. The addition of the original C-terminal region seems to have neither positive nor negative effects on the degradation efficiency.

Next, I wanted to address the question of whether the resistance of the N⁴¹⁻⁹⁸ fragment to HTRA1 cleavage is due to a low affinity to the primary amino acid sequence or to spatial inaccessibility. In the first case, fragments N⁴¹⁻⁹⁸ and C³⁹⁰⁻⁴⁴¹ should show the same degradation patterns in the constructs as in wild-type Tau. There should be no cleavages in fragment N⁴¹⁻⁹⁸ and extremely dense cleavages in fragment C³⁹⁰⁻⁴⁴¹. In the second case, fragment N⁴¹⁻⁹⁸ should show HTRA1 cleavage sites since the new position within the constructs should make it accessible for HTRA1. Fragment C³⁹⁰⁻⁴⁴¹, which is located within the N-terminal half of the constructs, on the other hand, should no longer show cleavages.

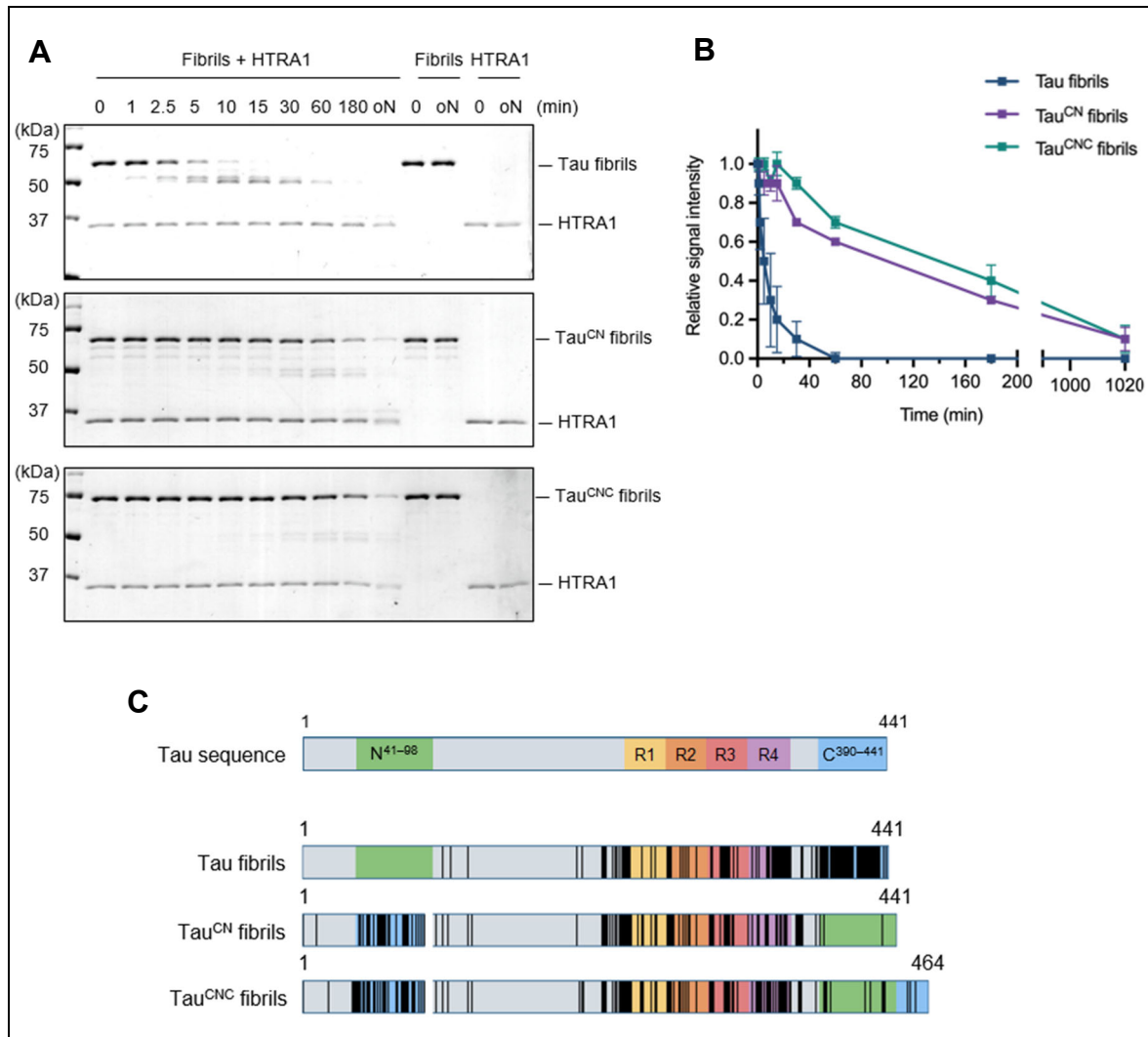


Figure 19: Degradation of Tau, Tau^{CN}, and Tau^{CNC} fibrils by HTRA1

The degradation of Tau, Tau^{CN}, or Tau^{CNC} fibrils by HTRA1 was investigated using a proteolysis assay. (A) HTRA1 (1 μ M) was mixed with fibrils (2.5 μ M) at a molar protease:substrate ratio of 1:2.5. Samples were taken at the indicated time points and analyzed by SDS PAGE. Fibrils of the two Tau constructs are degraded less efficiently by HTRA1. (B) Experiments were at least performed in duplicate. The relative signal intensities of the full-length substrate bands were quantified using Phoretix 1D and are plotted against time (oN = overnight). (C) HTRA1 cleavage sites (black lines) detected by LC-MS/MS after 120 min of proteolysis were mapped to the sequences of Tau, Tau^{CN}, and Tau^{CNC}, respectively. The four repeats (R) and the two fragments N⁴¹⁻⁹⁸ and C³⁹⁰⁻⁴⁴¹ are highlighted in different colors.

Since SDS-PAGE analysis does not provide information about cleavage sites, I analyzed the proteolysis products of Tau^{CN} and Tau^{CNC} fibrils by LC-MS/MS (Figure 19C). The analysis shows that HTRA1 efficiently cleaves fragment C³⁹⁰⁻⁴⁴¹ in both constructs. Apart from this fragment, the N-terminal half shows almost no cuts, similar to wild-type Tau fibrils. This result demonstrates that the N-terminal Tau region is generally spatially accessible for HTRA1 cleavage. Moreover, a degradation mechanism where the Tau molecules are continuously degraded starting from the

C-terminus can be excluded. Analysis of the cleavage pattern within fragment N⁴¹⁻⁹⁸ supports these assumptions. Within both Tau^{CN} and Tau^{CNC}, this fragment is not efficiently degraded by HTRA1 despite its C-terminal localization. Cleavage of the MTBD, which forms the fibril core, is not affected by the exchange of the fragments. Both Tau constructs show similar cleavage patterns to wild-type Tau in this protein region. Overall, the resistance of the N-terminal Tau region to HTRA1 cleavage seems not to be mediated by the localization within the molecule but rather by low affinity of HTRA1 to the amino acid sequence. However, it has to be mentioned that the cleavage patterns in the two fragments are not completely unaffected by the exchanged localizations. Compared to wild-type Tau, the C-terminal fragment shows a lower density of cuts. In the N-terminal fragment, which is not cleaved in the wild-type, a few cleavage sites can be detected within the constructs.

4.6 Activation of HTRA1 by pathological Tau species

XL-MS studies indicate that HTRA1 interacts with Tau fibrils via loop L3 of the protease domain (Figure 17). Previous studies have demonstrated that the binding of substrates to loop L3 induces conformational changes in the activation domain that result in the activation of HTRA1 (Truebestein et al., 2011). Therefore, I wanted to address the question of whether the presence of Tau fibrils leads to increased enzymatic activity of HTRA1. Next to the Tau fibrils, I also tested the effect of native and hyperphosphorylated Tau on HTRA1 activity since proteolysis assays showed differences in the degradation of the Tau species (4.3).

For the quantification of the proteolytic activity of HTRA1, I used a synthetic HTRA1 substrate consisting of para-nitroaniline (pNA) coupled to the C-terminus of the peptide VFNTLPMMGKASPV. This pNA-coupled peptide is a low-affinity HTRA1 substrate that shows no activating effect on HTRA1 in controls. HTRA1 activity is basal in the presence of pNA-VFNTLPMMGKASPV, thus activating effects of other ligands, such as the different Tau species, can be observed. The cleavage of the pNA substrate by HTRA1 in the presence of the different Tau species was continuously monitored measuring the absorption at 405 nm for 2 h. Specific enzymatic activities

of HTRA1 in the absence or presence of the different Tau species were calculated from at least three independent measurements. The addition of Tau fibrils causes an up to 3-fold activation of HTRA1 (Figure 20). In contrast, no significant activating effect on HTRA1 can be observed for the native Tau under the tested conditions. In the presence of the two hyperphosphorylated Tau variants, Tau-ps and Tau-pg, only a slight HTRA1 activation can be detected. The activating effects of the different Tau species thus correspond to the tendencies observed in the proteolysis assays. In these assays, the highest degradation efficiency was recorded for Tau fibrils. Hyperphosphorylated and native Tau showed only minor differences, with the degradation efficiency for hyperphosphorylated Tau being slightly higher (Figure 11 and Figure 12).

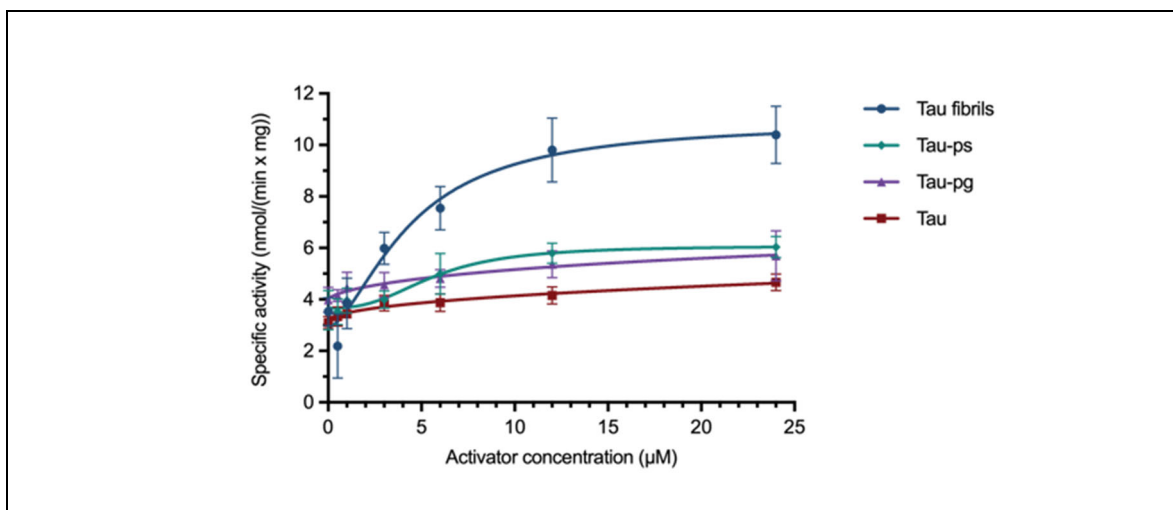


Figure 20: Activation of HTRA1 by Tau fibrils

The specific activity of HTRA1 in the presence of native (red), hyperphosphorylated (Tau-ps in green, Tau-pg in purple), and fibrillar (blue) Tau was determined using a synthetic substrate consisting of pNA coupled to the peptide VFNTLPMMGKASPV. HTRA1 (1 µM) was mixed with the pNA substrate (500 µM) and with different concentrations of the Tau species, respectively. Degradation of the pNA substrate was continuously monitored, measuring the absorption at 405 nm for 2 h and used to calculate the specific enzyme activity. The experiments were performed in triplicates.

I hypothesize that differences in degradation might be related to the activating effects of the Tau species on HTRA1. Accordingly, Tau fibrils show the strongest activating effect of the different Tau species on HTRA1 and are thus degraded with the highest efficiency. If different activating effects of the Tau species would be negligible because HTRA1 is already highly active, similar degradation efficiencies should be observed for all Tau species. To address this hypothesis, I analyzed and

compared the degradation of native and fibrillar Tau by activated HTRA1. For HTRA1 activation, I used a buffer containing high phosphate (150 mM NaPi) and high salt (380 mM NaCl) concentrations instead of the standard proteolysis buffer containing HEPES (100 mM) and a lower salt concentration (100 mM). An indicator of increased HTRA1 activity in the activating buffer is the degree of HTRA1 auto-proteolysis in the control samples. While HTRA1 is stable in standard proteolysis buffer overnight, it is almost completely degraded in activating buffer (Figure 21A).

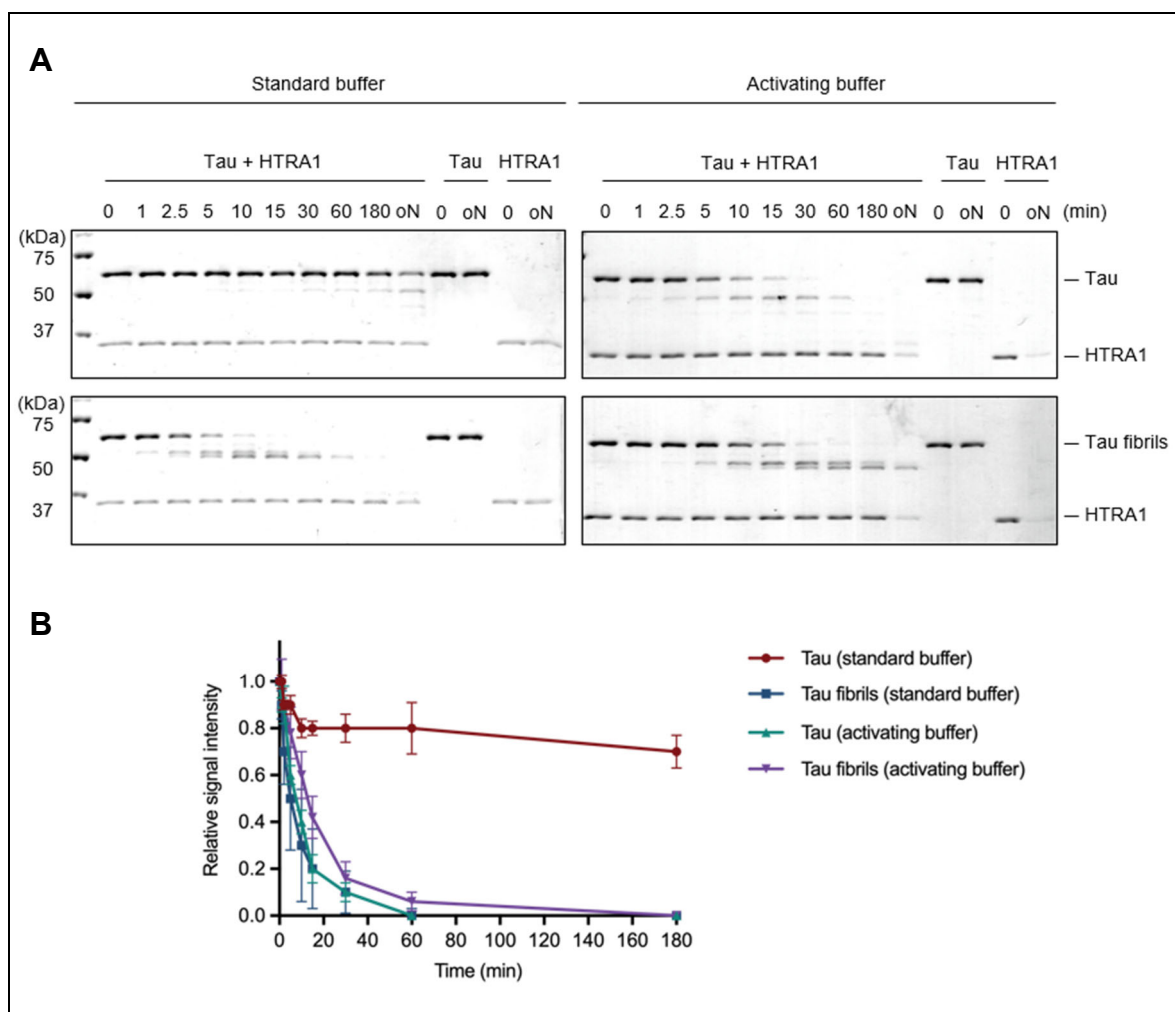


Figure 21: Degradation of native and fibrillar Tau by HTRA1 under activating conditions

A proteolysis assay was used to investigate the degradation of native and fibrillar Tau by HTRA1 under activating conditions. (A) HTRA1 (1 μ M) was incubated with native or fibrillar Tau (2.5 μ M) at a molar ratio of 1:2.5 in standard buffer (100 mM HEPES, 100 mM NaCl, pH 7.5 at 37 $^{\circ}$ C) or activating buffer (150 mM NaPi, 380 mM NaCl, pH 8.0 at 37 $^{\circ}$ C). Samples of the degradation process were taken at the indicated time points and analyzed by SDS-PAGE. Activated HTRA1 degrades both Tau species with the same efficiency. (B) Experiments were at least performed in duplicate. The relative signal intensities of the full-length substrate bands were quantified using Phoretix 1D and are plotted against time (oN = overnight).

The proteolysis assay was performed by incubating HTRA1 (1 μ M) with native or fibrillar Tau (2.5 μ M) at a molar ratio of 1:2.5. Comparing the degradation of the Tau species by HTRA1 in the activating buffer, no significant differences are visible anymore (Figure 21). Furthermore, both native and fibrillar Tau are degraded with similar efficiencies under activating conditions as the fibrillar Tau in standard buffer. These results indicate that the degradation of different Tau species depends on the activation state of HTRA1. In the presence of the fibrils, HTRA1 already shows high activity, so usage of an activating buffer has no additional effect.

4.7 HTRA1 reduces amyloid- β plaque load in cerebral organoids

Assembly and deposition of Tau fibrils are hallmarks of several neurodegenerative diseases collectively referred to as tauopathies. The most prominent tauopathy is Alzheimer's disease (AD). In addition to Tau fibrils, AD is associated with abnormal aggregation and accumulation of the amyloid- β peptide (A β) in plaques. HTRA1 was found to be among the most enriched proteins in A β plaques, where it is suggested to reduce the deposition (Drummond et al., 2022). In collaboration with the department Biochemistry II – Molecular Biochemistry from the Ruhr-Universität Bochum, we addressed the question of whether HTRA1 can degrade aggregated A β that is deposited in plaques. We used cerebral organoids containing deposited A β reminiscent of A β plaques as a state-of-the-art model for neurodegenerative diseases. Cerebral organoids are three-dimensional tissue cultures derived from human induced pluripotent stem cells (hiPSCs) that resemble the human brain. The organoids containing A β deposits were treated with HTRA1 labeled with DyLight 633 for 1 or 6 days. Since different studies demonstrate the spontaneous uptake of HTRA1 in cells (Muratoglu et al., 2013; Poepsel et al., 2015), HTRA1 was added to the organoid medium. After the treatment, organoids were fixed and processed for fluorescence-based imaging. All experiments were performed by Lucia Gallego Villarejo at the Ruhr-Universität Bochum. Data were obtained from five biological replicates for each condition. The quantification of the A β plaque load was performed by Dr. Nina Schulze at the Imaging Center Campus Essen using the software CellProfiler.

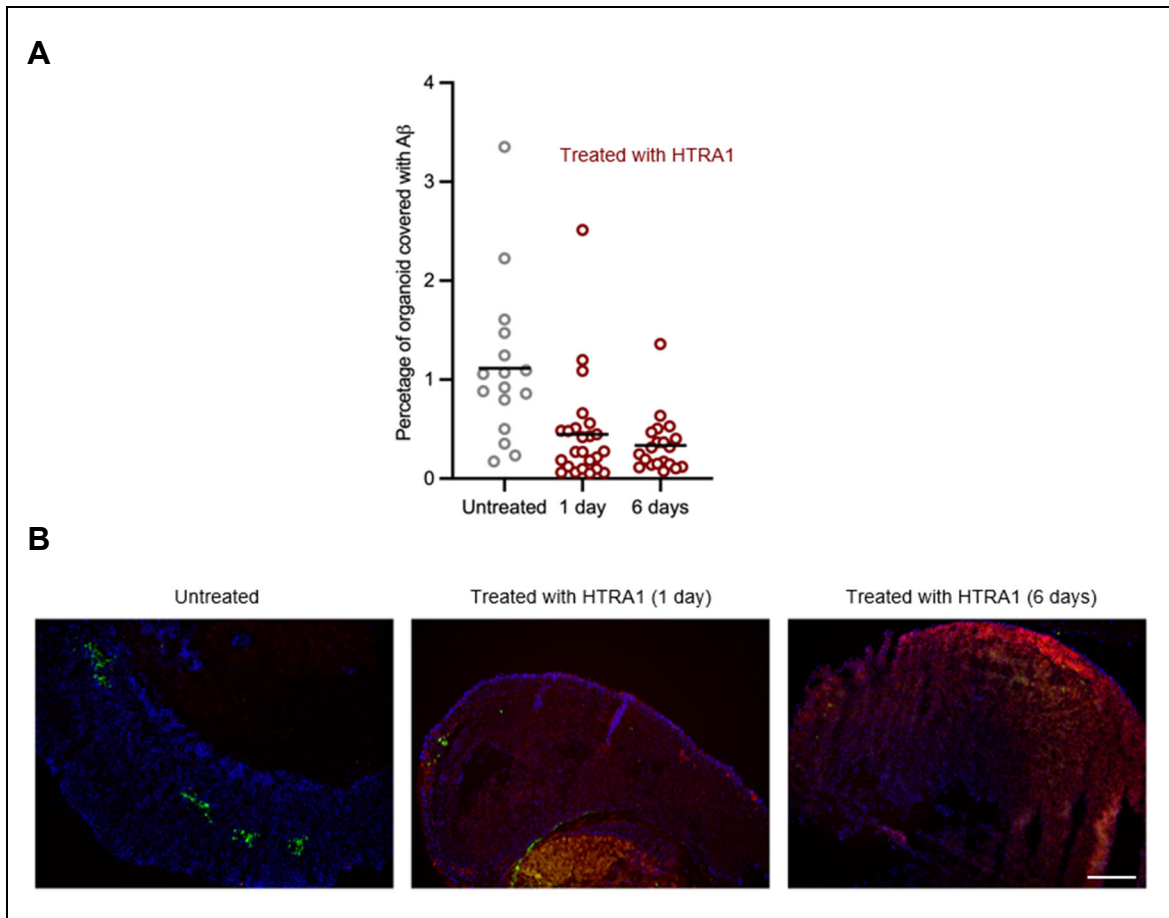


Figure 22: HTRA1 reduces A β deposits in cerebral organoids

Cerebral organoids containing A β deposits were treated with HTRA1. (A) HTRA1 labeled with DyLight 633 was added to the medium 1 or 6 days before the organoids were fixed, processed, and analyzed by fluorescence-based imaging. Data were obtained from five biological replicates. The percentage of the organoid covered with A β was quantified using CellProfiler and compared between untreated (grey) and HTRA1-treated organoids (red). (B) Representative images of the cerebral organoids untreated or treated with HTRA1. The images were processed with Fiji and show the fluorescence of HTRA1 labeled with DyLight 633 (red) and A β labeled with immunostaining (green). The DNA was stained with DAPI and the scale bar represents 200 μ M.

In the control samples not treated with HTRA1, the green-labeled A β depositions within the organoids are clearly visible (Figure 22B). Images of the organoids treated for 1 or 6 days with HTRA1 show fewer of these depositions at first glance. The red signal of the labeled HTRA1 is clearly visible and covers the entire area of the organoid. These results demonstrate that HTRA1 was spontaneously taken up by the cells, already after 1 day. Since cells located inside the organoids also show the red HTRA1 signal, it seems that HTRA1 can penetrate the tissue. Statistical analysis of the different organoid samples confirms that the HTRA1 treatment reduced the A β plaque load (Figure 22A). After 1-day of treatment, depositions are reduced by more than half. Comparison between 1-day and 6-day treatment shows no significant

differences. Possible reasons are the loss of HTRA1 activity over time or the resistance of remaining A β deposits to HTRA1 degradation.

5. Discussion

HTRA1 is a highly conserved serine protease involved in PQC that is ubiquitously expressed in the human body. Its function is ATP-independent, and due to its characteristic homotrimeric structure containing protease and PDZ domains, it can combine antagonistic protease and chaperone functions. The proteolytic activity can be reversibly switched on and off, allowing HTRA1 to respond to protein folding stress in a rapid and finely tuned manner (Clausen et al., 2011; Truebestein et al., 2011; Poepsel et al., 2015). All these features make HTRA1 a remarkable factor in the PQC system. Previous studies have identified both native Tau and Tau fibrils, which are a hallmark of several neurodegenerative diseases, as HTRA1 substrates (Tennstaedt et al., 2012). In the experimental work presented herein, I demonstrate that HTRA1 as PQC protease distinguishes between native and pathological Tau species and specifically targets and degrades fibrillar Tau. Moreover, I revealed detailed mechanistic insights into the mechanism HTRA1 utilizes to degrade fibrils.

5.1 HTRA1 distinguishes between different Tau species

HTRA1 is one of the few identified proteases capable of degrading tightly packed amyloid fibrils. Several studies demonstrate that Tau fibrils are an HTRA1 substrate. In addition, it has also been shown that HTRA1 degrades native Tau (Tennstaedt et al., 2012; Poepsel et al., 2015). As protease of the PQC system, HTRA1 is known to degrade un- or misfolded proteins (Clausen et al., 2011). Natively folded proteins should not be degraded as long as they are required for cellular function since this would compromise proteostasis and, thus, cell viability. Therefore, I wanted to address the question of whether HTRA1 distinguishes between native and pathological Tau species. This question is of particular relevance given the shared cellular localization of HTRA1 and Tau to microtubules (Tennstaedt et al., 2012).

For this purpose, I isolated and purified recombinant Tau in sufficient quantity and purity to serve as native Tau species in the experiments. MT co-sedimentation assays verified that the recombinant protein expressed in *E. coli* exhibits the physiological properties of Tau. It binds and stabilizes MTs in the assay (4.2.1). Like Tau, HTRA1 is also reported to associate with MTs and to promote their assembly (Chien et al., 2009b). Moreover, Tennstaedt et al. (2012) showed a cellular co-localization of Tau, HTRA1, and MTs in fluorescence-based microscopy experiments. Testing all three proteins in the co-sedimentation assays, I confirmed that HTRA1 binds to MTs individually and simultaneously with Tau. Furthermore, I demonstrated that HTRA1 binding has neither positive nor negative effects on the binding of Tau to MTs and vice versa. Thus, HTRA1 and Tau do not compete for binding sites on MTs. The postulated stabilizing effect of HTRA1 on MTs was also verified since HTRA1 binding increases the MT-to-tubulin ratio. Surprisingly, combining Tau and HTRA1 resulted in an almost complete assembly of the tubulin into MTs (4.2.1). Extending previous studies, I report that Tau and HTRA1 show additive effects in promoting MT assembly.

Under pathological conditions, native Tau can be hyperphosphorylated, followed by its assembly into amyloid fibrils (Jeganathan et al., 2008). Therefore, I generated hyperphosphorylated and fibrillar Tau to serve as pathological Tau species in the experiments (4.1). The *in vitro* formed fibrils show the characteristic morphology of amyloids in AFM scans (4.1.2). Tau sequentially phosphorylated by PKA and GSK3 β (Tau-pg) or by PKA and SAPK4 (Tau-ps) contains approximately 40 individual phosphorylation sites each. This corresponds to the degree of phosphorylation observed in pathological Tau species of AD brains with approximately 45 different phosphorylation sites (Noble et al., 2013). Both Tau-pg and Tau-ps also show phosphorylation at sites recognized by phosphorylation-dependent antibodies that detect AD-specific Tau species, such as AT8, AT100, and PHF1 (4.1.1). In line with previous reports (Biernat et al., 1993), hyperphosphorylation resulted in the loss of Tau function. Neither Tau-pg nor Tau-ps binds and stabilizes MTs (4.2.2). Thus, *in vitro* generated hyperphosphorylated and fibrillar Tau show characteristics similar to disease-relevant Tau species.

Recombinant native, hyperphosphorylated, and fibrillar Tau were then analyzed in proteolysis and activation assays to determine whether HTRA1 distinguishes

between physiological and pathological Tau species. To ensure comparable results, a buffer solution containing 100 mM HEPES and 100 mM NaCl was used in all assays. In this buffer, HTRA1 shows only basal activity and thus activating effects of the substrates can be observed. Indeed, I could detect significant differences in the degradation efficiencies and the activating effects of the different Tau species. Tau fibrils, which are the defining feature of tauopathies, are degraded more than 20-fold faster by HTRA1 than the other Tau species (4.3). Tau fibrils are completely degraded after overnight incubation, with neither full-length protein nor proteolysis products detectable in SDS-PAGE analysis. In contrast, native and hyperphosphorylated Tau show similar, incomplete digestion by HTRA1 under the same conditions. Interestingly, results of the activation assays show the same tendency. In the activation assays, the degradation of a low-affinity substrate that shows no activating effects on HTRA1 was continuously measured. Since HTRA1 activity is basal in the presence of this substrate, activating effects of the different Tau species could be detected. The stronger the activating effect, the faster the low-affinity synthetic substrate is degraded by HTRA1. In the absence of various Tau species, the specific activity of HTRA1 for the synthetic substrate is 3.5 nmol/(mg x min) (4.6). Tau fibrils cause significant activation of HTRA1 (10 nmol/(min x mg)), while only minor activating effects (4–6 nmol/(min x mg)) are detected for the other Tau species. These results indicate that the differences in degradation of native and fibrillar Tau are caused by the activation state of HTRA1, which in turn correlates with the binding affinity of the respective substrate. Additional proteolysis assays where activated HTRA1 was used to degrade native and fibrillar Tau confirm this hypothesis. When HTRA1 is activated, both Tau species are degraded with comparable efficiencies (4.6). The fact that HTRA1 is activated by fibrillar but not native Tau points to conformation-specific recognition of substrates by HTRA1. It is already established that HTRA1 is activated by substrates and that both the active site and PDZ domain interact with substrates via the mechanism of β -augmentation (Figure 23A) (Truebestein et al., 2011; Krojer et al., 2008a). The mechanism of β -augmentation involves the addition of an antiparallel β -strand of the substrate to a β -sheet or β -strand of the binding site of the enzyme (Remaut and Waksman, 2006). This indicates that the protease domain, as well as PDZ domain, serve as suitable docking sites that bind the β -sheet-rich Tau fibrils with high affinity. Consistent with my data and the model of activation by induced-fit substrate binding (Truebestein et al.,

2011), binding of fibrils leads to activation of HTRA1, which in turn results in efficient degradation of fibrils. This effect is probably further enhanced by the resulting proteolysis products that can serve as allosteric activators of HTRA1. Native Tau, on the other hand, is a hydrophilic, intrinsically unstructured protein with no β -sheets and thus low binding affinity for HTRA1, which prevents efficient degradation. This is further supported by a recent study demonstrating that, in the case of α -synuclein, HTRA1 also shows higher binding affinity to fibrils than to the monomeric protein (Chen et al., 2024). Interestingly, once HTRA1 is active, it degrades native Tau as efficiently as Tau fibrils (4.6). Analysis of the degradation processes shows no significant differences in the number of cleavages and cleavage patterns of the two Tau species (4.3). Apparently, differences in the degradation efficiency of native and fibrillar Tau can be overcome by HTRA1 activation.

Detailed comparison of the degradation of native and hyperphosphorylated Tau by HTRA1 reveals some differences, although these are not as significant as for Tau fibrils. Compared to native Tau, hyperphosphorylated Tau variants show slightly higher numbers of HTRA1 cleavages (4.3). Moreover, in their presence, a slight activation of HTRA1 is observed (4.6). Overall, phosphorylation of Tau affects the degradation efficiency by HTRA1 and also the binding affinity, and thus the activating effect on HTRA1 to a certain extent. A possible explanation could be conformational changes associated with hyperphosphorylation (Jeganathan et al., 2008). Interestingly, despite the different conformations, cleavage patterns generated by HTRA1 are similar for native and fibrillar Tau, whereas both hyperphosphorylated Tau variants show slightly different cleavage patterns. Thus, it seems that phosphorylation affects not only the degradation efficiency but also the specificity for distinct cleavage sites at the level of the primary sequence. Further studies are required to understand how phosphorylation affects Tau degradation by HTRA1.

In addition to the studies of different activating effects of the Tau species, experiments showed that different buffers also affect HTRA1 activity (4.6). While HTRA1 shows only basal activity in buffer solution containing 100 mM HEPES (pH 7.5) and 100 mM NaCl, it is highly active in buffer solution containing 150 mM NaPi (pH 8.0) and 380 mM NaCl. Buffer conditions obviously can have a strong impact on HTRA1 activity and, thus, on proteolysis. This likely reflects the impact of different cellular conditions *in vivo* on HTRA1 activity. Under proteotoxic stress conditions, when HTRA1

as PQC protease is highly activated, low-affinity substrates are probably also targeted. Thus, hazardous accumulation of proteins is prevented when, for example, chaperones that assist protein folding are overwhelmed.

5.2 Mechanistic insights into the process of Tau fibril degradation by HTRA1

The performed proteolysis experiments demonstrated that HTRA1 efficiently degrades Tau fibrils. A previous study reported that the proteolysis mechanism of HTRA1 for fibrils comprises not only hydrolysis of peptide bonds but also a disaggregation function. This disaggregation function is supposed to destabilize the tight interactions within the fibril to make individual molecules accessible for cleavage (Poepsel et al., 2015). Recently, a similar disaggregase activity of HTRA1 was also described for α -synuclein fibrils (Chen et al., 2024). However, the exact proteolytic mechanism by which HTRA1 can degrade amyloid fibrils generally characterized as protease-resistant remained elusive. Therefore, I aimed to gain new insights into this complex mechanism.

Using cross-linking MS, I identified interactions of HTRA1 loop L3 with the MT-binding repeat 4 and the C-terminal region of Tau (4.4.3). The experiments were performed with the catalytically inactive variant of HTRA1. Therefore, the observed interactions should represent the initial interactions between Tau and HTRA1, which occur just before the first cleavage. Although the PDZ domain of HtrA proteases is known to mediate protein-protein interaction, in the cross-linking experiments, no contacts between Tau and HTRA1 PDZ domain were detected. However, this is not surprising, given that other studies report that the PDZ domain is dispensable for disaggregation of fibrils (Poepsel et al., 2015; Chen et al., 2024). The only identified interaction site within HTRA1 is loop L3 of the protease domain. Based on a crystal structure of HTRA1 bound to a peptide that acts as substrate analog, Truebestein et al. (2011) proposed that sensor loop L3 is rearranged upon direct interactions with substrates (Figure 23A). This rearrangement ultimately results in a disorder-to-order transition of the active site loops, bringing HTRA1 into the active

conformation. According to this model of induced-fit substrate binding, the identified contact site explains how the interaction with fibrils leads to HTRA1 activation. The fibril bound to the active site via β -augmentation directly interacts with loop L3 of the HTRA1 activation domain and thus stabilizes the active conformation of the protease.

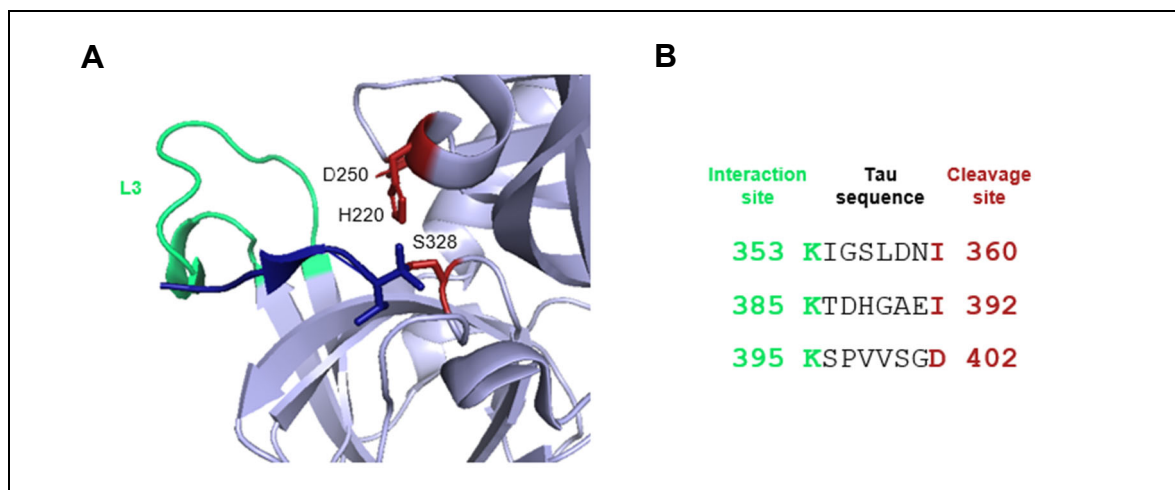


Figure 23: Interaction of substrates with HTRA1 loop L3 and active site

HTRA1 is activated via substrate-induced remodeling. (A) Crystal structure of HTRA1 (PDB ID: 3NZI) (light blue) in complex with a peptide (dark blue) covalently bound to the active site serine (S328, red). The peptide acting as a substrate analog interacts with loop L3 (green), thus stabilizing the active conformation of HTRA1. Binding of the peptide to the active site is mediated via β -augmentation. (B) Excerpts of the Tau sequence showing the HTRA1 loop L3 interaction sites (green) identified by XL-MS and HTRA1 cleavage sites (red) detected in proteolysis experiments.

The calculated distance between HTRA1 loop L3 and the active site corresponds to the length of a peptide comprising 6 to 8 amino acids. If a Tau molecule interacts simultaneously with loop L3 and the active site, it should be cleaved at a distance of 6 to 8 residues from the loop L3 interaction site. Indeed, HTRA1 cleavage sites detected in proteolysis experiments are located 7 amino acids C-terminal from loop L3-Tau interaction sites that were identified in XL-MS experiments (4.4.2 and 4.4.3) (Figure 23B). These findings further support the reliability of the identified interactions. All Tau interaction sites are in close proximity to each other and are located within repeat 4 and the flanking C-terminal region, the same area that shows a high density of HTRA1 cleavages in early time points of the proteolytic process. Therefore, it is very likely that HTRA1 degradation of the fibrils starts in this region of the

Tau molecules. AFM experiments strongly suggest a simultaneous degradation of several Tau molecules by HTRA1 along the whole fibril (4.4.1). This mechanism is further supported by negative-stain electron micrographs published by Poepsel et al. (2015) that show HTRA1 accumulation along a Tau fibril.

Initially, the fibril core was defined as the protease-resistant part of the fibril (Wischik et al., 1988; Novak et al., 1993; von Bergen et al., 2006). The core region is responsible for fibril assembly and is characterized by strong inter- and intramolecular interactions (Scheres et al., 2020). Temporal and spatial analysis of proteolysis of the fibril core by HTRA1 revealed complete degradation into small peptides within a minute (4.4.2). Within the first minute of the proteolytic process, 21 HTRA1 cleavage sites can be detected that degrade the 106 amino acids large core region into 23 peptides containing 7 to 26 residues. Comparing the relative frequency of the cuts within the core region of *in vitro* formed fibrils (PDB IDs: 6QJH, 6QJM, and 6QJP), I308, I278, V287, and I277 were identified as the cleavage sites with the highest affinity. All of these cleavage sites are located in regions that form β -sheets, supporting the preferential binding of HTRA1 to β -sheets by the mechanism of β -augmentation discussed in section 5.1.

In contrast to the fibril core region, the N-terminal half of Tau molecules that are part of the flexible, unstructured fuzzy coat is mainly resistant to HTRA1 cleavage (4.4.2). Analysis of the degradation of Tau constructs with exchanged N- and C-terminal regions (Tau^{CN} and Tau^{CNC}) indicates that the resistance is mediated by a low affinity of HTRA1 to the N-terminal amino acid sequence (4.5). Next to the discussed conformation-specificity of HTRA1 (5.1), these results indicate that further specificity exists at the level of the primary sequence. Analysis of the MS data of the fibril digestion by HTRA1 shows a preference for the hydrophobic residues leucine, valine, and isoleucine at the P1 position (Appendix B, Figure 25), consistent with previous reports (Truebestein et al., 2011; Chen et al., 2018). However, the primary sequence of the N-terminal region also contains several leucine, valine, and isoleucine residues. Thus, it is likely that another mechanism mediates the low affinity of HTRA1 to the N-terminal Tau region, which still needs to be investigated in more detail.

Taken together, I suggest that the proteolytic process is initiated by simultaneous binding of multiple HTRA1 molecules to the C-terminal regions of Tau molecules along the entire length of the fibril. Initial binding interactions mediated by the mechanism of β -sheet augmentation result in activation of HTRA1. After degradation of the fuzzy coat, binding interactions of the HTRA1 protease domain within the fibril core result in disintegration of the tightly packed region, making it accessible to proteolysis. Subsequently, HTRA1 efficiently degrades the Tau fibril core into multiple peptides of approximately 7 to 26 amino acid residues. Next to HTRA1, other cellular machinery consisting of proteases and chaperones have also been reported to target large Tau fibrils. Recent studies associate the resulting products or byproducts with enhanced aggregate seeding or cytotoxic effects. For example, it has been shown that the 26S proteasome holoenzyme fragments Tau fibrils into small aggregates that are more toxic to cells than the original fibrils (Cliffe et al., 2019). Furthermore, disaggregation of Tau fibrils by the heat shock 70 kDa protein (Hsp70) machinery or the hexameric ATPase valosin-containing protein (VCP) was demonstrated to produce seeding-competent Tau species that accelerate Tau aggregation (Nachman et al., 2020; Saha et al., 2023). So far, it cannot be excluded that the proteolytic products of Tau fibril degradation by HTRA1 are seeding-competent or possess cytotoxic effects. Considering that HTRA1 combines disaggregation of the fibril core and its proteolysis into small peptides, eliminating the need to release the substrate between these two steps, this possibility seems rather unlikely. Nevertheless, the effects of the proteolytic products on cell viability and Tau aggregation should be investigated in detail.

5.3 Model of HTRA1-Tau interactions under physiological and pathological conditions

A major challenge in PQC is the rapid and efficient removal of misfolded and damaged proteins before they accumulate and impair cellular functions. At the same time, uncontrolled degradation must be prevented, as maintaining a functional set of proteins is also crucial for cell viability. Based on the biochemical data discussed

in sections 5.1 and 5.2, I propose a model of HTRA1-Tau interactions to illustrate the implications of HTRA1 on the different life stages of Tau under physiological and pathological conditions (Figure 24). It should be noted that the interactions in this preliminary model are simplified, and further investigation is required for a comprehensive understanding.

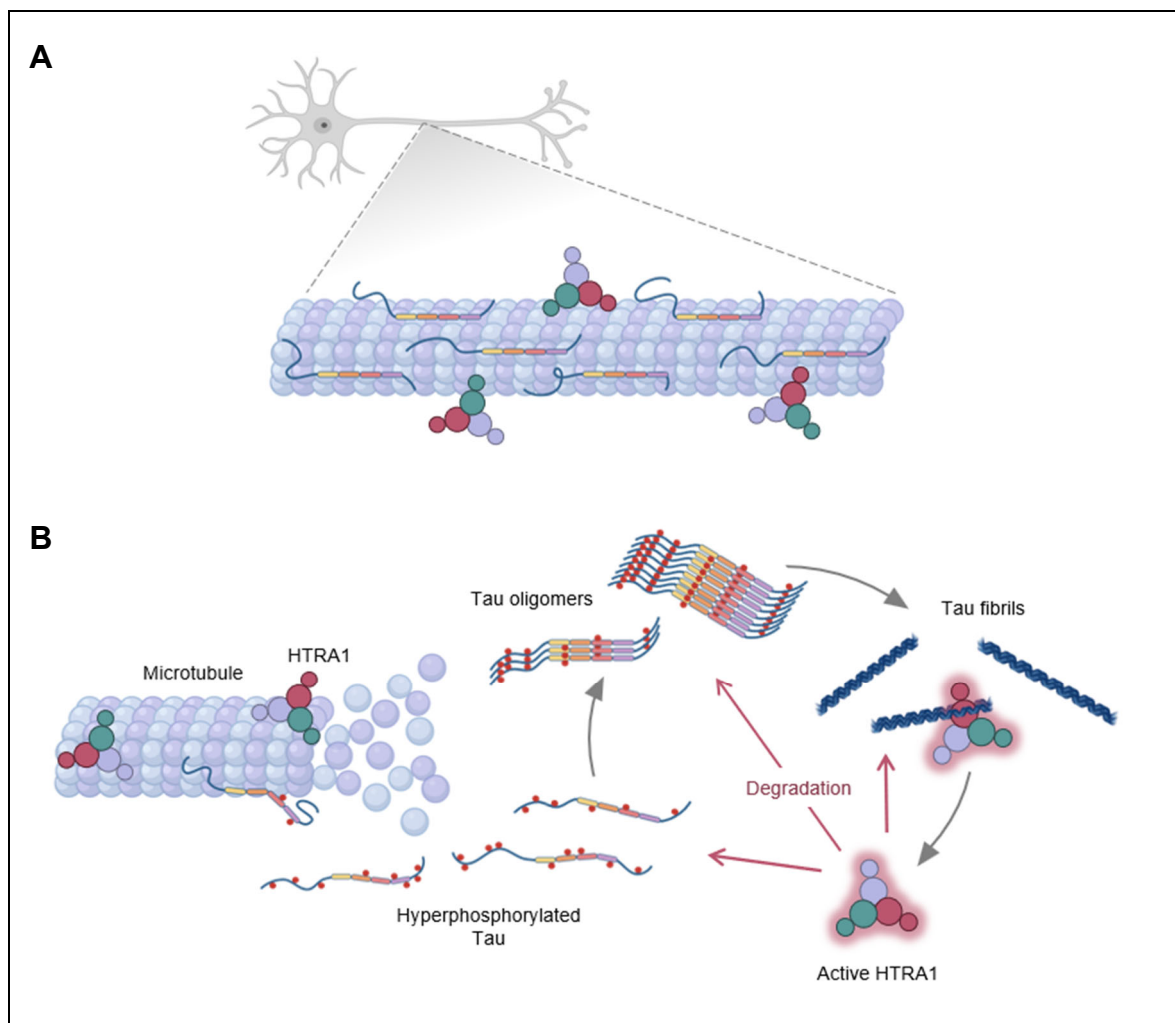


Figure 24: Model of HTRA1 implications in Tau pathology

Based on experimental data, a model of HTRA1-Tau interaction under physiological and pathological conditions is proposed. (A) Under physiological conditions, Tau and HTRA1 co-localize to MTs and native Tau is not degraded by HTRA1. (B) Pathological conditions can result in hyperphosphorylation of Tau, which is associated with impaired MT binding and subsequent aggregation into fibrils. HTRA1 recognizes and binds Tau fibrils and is thereby activated. Activated HTRA1 efficiently degrades fibrils as well as hyperphosphorylated Tau species. Thus, HTRA1 prevents further Tau aggregation and counteracts the accumulation of Tau fibrils.

Under physiological conditions, Tau and HTRA1 co-localize to MTs (Figure 24A). Despite their spatial proximity, HTRA1 does not degrade the MT-bound Tau. The

MTBD of Tau binds along the MT filament and is thus protected from proteolysis, while the N-terminal projection domain that protrudes from the filament surface is resistant to HTRA1 cleavage. The resistance is probably mediated by a low affinity of HTRA1 to the amino acid sequence of the N-terminal Tau region. Soluble Tau, not bound to MTs, is a low-affinity substrate of HTRA1. Although natively unfolded, soluble Tau is not degraded as long as HTRA1 is in an inactive state or is engaged by other substrates with higher affinities. Tau levels and functions are thus maintained under physiological conditions.

Pathological conditions can result in increased phosphorylation of Tau (Figure 24B). This hyperphosphorylation is associated with impaired MT-binding and conformational changes that promote Tau assembly. Consequently, hyperphosphorylated Tau accumulates in the cytosol and aggregates into oligomers and, finally, amyloid fibrils. Through the mechanism of conformation-specific recognition, HTRA1 senses and binds the β -sheet-rich Tau fibrils. This interaction results in activation of HTRA1. Multiple activated HTRA1 molecules are recruited and bind simultaneously along the entire fibril. By combining disaggregation and proteolysis, HTRA1 efficiently degrades fibrils into small peptides. These proteolytic products could in turn further activate HTRA1 molecules in an allosteric manner via the PDZ domain. Activated HTRA1 now also degrades hyperphosphorylated and native Tau molecules not bound to MTs. This way, further aggregation and accumulation of Tau fibrils is prevented. Tau bound to MTs should not be degraded as HTRA1 binding sites are probably covered by the interactions with the MTs. Taken together, this model illustrates how HTRA1, as a factor of the PQC system, distinguishes native and pathological Tau species and counteracts Tau fibril formation and accumulation. Moreover, it shows that the formation and deposition of amyloid fibrils are not irreversible processes and that cells have evolved efficient strategies for fibril processing and clearance.

5.4 Outlook

The results presented in this study demonstrate that the PQC protease HTRA1 has evolved a mechanism to distinguish native and pathological Tau species and specifically targets and degrades fibrillar species, which are considered the final stage of pathological Tau assembly. Moreover, the temporal and spatial resolution of the degradation process by LC-MS/MS provides insights into the mechanism utilized by HTRA1 to proteolyze Tau fibrils, which are characterized by strong inter- and intramolecular interactions. Therefore, this study contributes to a deeper understanding of how HTRA1 counteracts Tau pathology and raises the question of whether HTRA1 also targets fibrils formed by other proteins.

Preliminary results of this study show that HTRA1 can dissolve A β aggregates deposited in plaques (4.7). Together with previous studies on disaggregation or degradation of A β and α -synuclein fibrils by HTRA1, these results indicate a general role of HTRA1 in counteracting amyloid-associated pathologies (Grau et al., 2005; Chen et al., 2024). However, further studies are needed to corroborate this assumption and provide more details. As a first step, the established protocol for time-resolved MS could be used to address the degradation of A β and α -synuclein fibrils by HTRA1 at temporal and spatial resolution. Analysis and comparison of the degradation of different fibril types could reveal further details of the proteolysis process and may lead to the identification of a general mechanism utilized by HTRA1.

Furthermore, it was demonstrated that cerebral organoids are a suitable state-of-the-art model to study HTRA1 functions in the context of neuronal tissue (4.7). Organoids derived from hiPSCs of patients with, e.g., familial AD have been shown to develop Tau pathology spontaneously (Eichmüller and Knoblich, 2022). Such organoids offer cell-based platforms to investigate the interactions of HTRA1 with pathological Tau species without limitations due to *in vitro* fibril formation or protein overexpression. Moreover, function and significance of HTRA1 for the cellular response to proteotoxic stress caused by accumulation of amyloids could be investigated. Relevant aspects that could be addressed include alteration of HTRA1 levels in response to Tau pathology, effects of HTRA1 deletion or overexpression on disease pathogenesis and progression, and seeding competence or cytotoxic effects of proteolytic products from fibril degradation by HTRA1. Preliminary

experiments with cerebral organoids presented herein also demonstrated that HTRA1 was not only taken up by individual cells but also penetrated the neuronal tissue. Thus, cerebral organoids could be used to address the question of whether HTRA1 limits or even prevents the spreading of Tau pathology along neuronal networks. Overall, future studies on HTRA1 could contribute to a deeper understanding of the mechanisms cells have evolved to counteract protein aggregation and resulting diseases.

6. Bibliography

Bachmann S., Bell M., Klimek J., and Zempel H. (2021): Differential Effects of the Six Human TAU Isoforms: Somatic Retention of 2N-TAU and Increased Microtubule Number Induced by 4R-TAU. *Front Neurosci* 15: 643115. DOI: 10.3389/fnins.2021.643115.

Baldi A., Luca A. de, Morini M., Battista T., Felsani A., Baldi F., Catricalà C., Amantea A., Noonan D.M., Albini A., Natali P.G., Lombardi D., and Paggi M.G. (2002): The HtrA1 serine protease is down-regulated during human melanoma progression and represses growth of metastatic melanoma cells. *Oncogene* 21 (43): 6684–6688. DOI: 10.1038/sj.onc.1205911.

Barbier P., Zejneli O., Martinho M., Lasorsa A., Belle V., Smet-Nocca C., Tsvetkov P.O., Devred F., and Landrieu I. (2019): Role of Tau as a Microtubule-Associated Protein: Structural and Functional Aspects. *Front Aging Neurosci* 11: 204. DOI: 10.3389/fnagi.2019.00204.

Bartlett A.I., and Radford S.E. (2009): An expanding arsenal of experimental methods yields an explosion of insights into protein folding mechanisms. *Nat Struct Mol Biol* 16 (6): 582–588. DOI: 10.1038/nsmb.1592.

Beaufort N., Scharrer E., Kremmer E., Lux V., Ehrmann M., Huber R., Houlden H., Werring D., Haffner C., and Dichgans M. (2014): Cerebral small vessel disease-related protease HtrA1 processes latent TGF- β binding protein 1 and facilitates TGF- β signaling. *Proc Natl Acad Sci USA* 111 (46): 16496–16501. DOI: 10.1073/pnas.1418087111.

Beleford D., Rattan R., Chien J., and Shridhar V. (2010): High temperature requirement A3 (HtrA3) promotes etoposide- and cisplatin-induced cytotoxicity in lung cancer cell lines. *J Biol Chem* 285 (16): 12011–12027. DOI: 10.1074/jbc.M109.097790.

Biernat J., Gustke N., Drewes G., Mandelkow E.M., and Mandelkow E. (1993): Phosphorylation of Ser262 strongly reduces binding of tau to microtubules: distinction between PHF-like immunoreactivity and microtubule binding. *Neuron* 11 (1): 153–163. DOI: 10.1016/0896-6273(93)90279-z.

- Brady R.M., Zinkowski R.P., and Binder L.I. (1995): Presence of tau in isolated nuclei from human brain. *Neurobiol Aging* 16 (3): 479–486. DOI: 10.1016/0197-4580(95)00023-8.
- Brandt R., Léger J., and Lee G. (1995): Interaction of tau with the neural plasma membrane mediated by tau's amino-terminal projection domain. *J Cell Biol* 131 (5): 1327–1340. DOI: 10.1083/jcb.131.5.1327.
- Bravo-Rodriguez K., Hagemeyer B., Drescher L., Lorenz M., Rey J., Meltzer M., Kaschani F., Kaiser M., and Ehrmann M. (2018): Utilities for Mass Spectrometry Analysis of Proteins (UMSAP): Fast post-processing of mass spectrometry data. *Rapid Commun Mass Spectrom* 32 (19): 1659–1667. DOI: 10.1002/rcm.8243.
- Carpenter A.E., Jones T.R., Lamprecht M.R., Clarke C., Kang I.H., Friman O., Guertin D.A., Chang J.H., Lindquist R.A., Moffat J., Golland P., and Sabatini D.M. (2006): CellProfiler: image analysis software for identifying and quantifying cell phenotypes. *Genome Biol* 7 (10): R100. DOI: 10.1186/gb-2006-7-10-r100.
- Chamberland A., Wang E., Jones A.R., Collins-Racie L.A., LaVallie E.R., Huang Y., Liu L., Morris E.A., Flannery C.R., and Yang Z. (2009): Identification of a novel HtrA1-susceptible cleavage site in human aggrecan: evidence for the involvement of HtrA1 in aggrecan proteolysis in vivo. *J Biol Chem* 284 (40): 27352–27359. DOI: 10.1074/jbc.M109.037051.
- Chen C.-Y., Melo E., Jakob P., Friedlein A., Elsässer B., Goettig P., Kueppers V., Delobel F., Stucki C., Dunkley T., Fauser S., Schilling O., and Iacone R. (2018): N-Terminomics identifies HtrA1 cleavage of thrombospondin-1 with generation of a proangiogenic fragment in the polarized retinal pigment epithelial cell model of age-related macular degeneration. *Matrix Biol* 70: 84–101. DOI: 10.1016/j.matbio.2018.03.013.
- Chen J., Kanai Y., Cowan N.J., and Hirokawa N. (1992): Projection domains of MAP2 and tau determine spacings between microtubules in dendrites and axons. *Nature* 360 (6405): 674–677. DOI: 10.1038/360674a0.
- Chen S., Puri A., Bell B., Fritsche J., Palacios H.H., Balch M., Sprunger M.L., Howard M.K., Ryan J.J., Haines J.N., Patti G.J., Davis A.A., and Jackrel M.E. (2024): HTRA1 disaggregates α -synuclein amyloid fibrils and converts them into

non-toxic and seeding incompetent species. *Nat Commun* 15 (1): 2436. DOI: 10.1038/s41467-024-46538-8.

Chen Y.-Y., Chuang P.-Y., Chen C.-P., Chiu Y.-H., Lo H.-F., Cheong M.-L., Huang J.-Y., Kuo P.-L., and Chen H. (2014): Functional antagonism between high temperature requirement protein A (HtrA) family members regulates trophoblast invasion. *J Biol Chem* 289 (33): 22958–22968. DOI: 10.1074/jbc.M114.576744.

Chien J. (2010): WT1 as a substrate of HtrA2: a potential pathway for therapeutic targeting by HtrA proteases. *Future Oncol* 6 (8): 1233–1235. DOI: 10.2217/fon.10.84.

Chien J., He X., and Shridhar V. (2009a): Identification of tubulins as substrates of serine protease HtrA1 by mixture-based oriented peptide library screening. *J Cell Biochem* 107 (2): 253–263. DOI: 10.1002/jcb.22121.

Chien J., Ota T., Aletti G., Shridhar R., Boccellino M., Quagliuolo L., Baldi A., and Shridhar V. (2009b): Serine protease HtrA1 associates with microtubules and inhibits cell migration. *Mol Cell Biol* 29 (15): 4177–4187. DOI: 10.1128/MCB.00035-09.

Chien J., Staub J., Hu S.-I., Erickson-Johnson M.R., Couch F.J., Smith D.I., Crowl R.M., Kaufmann S.H., and Shridhar V. (2004): A candidate tumor suppressor HtrA1 is downregulated in ovarian cancer. *Oncogene* 23 (8): 1636–1644. DOI: 10.1038/sj.onc.1207271.

Clausen T., Kaiser M., Huber R., and Ehrmann M. (2011): HTRA proteases: regulated proteolysis in protein quality control. *Nat Rev Mol Cell Biol* 12 (3): 152–162. DOI: 10.1038/nrm3065.

Clausen T., Southan C., and Ehrmann M. (2002): The HtrA family of proteases: implications for protein composition and cell fate. *Mol Cell* 10 (3): 443–455. DOI: 10.1016/s1097-2765(02)00658-5.

Clawson G.A., Bui V., Xin P., Wang N., and Pan W. (2008): Intracellular localization of the tumor suppressor HtrA1/Prss11 and its association with HPV16 E6 and E7 proteins. *J Cell Biochem* 105 (1): 81–88. DOI: 10.1002/jcb.21804.

- Cliffe R., Sang J.C., Kundel F., Finley D., Klenerman D., and Ye Y. (2019): Filamentous Aggregates Are Fragmented by the Proteasome Holoenzyme. *Cell Rep* 26 (8): 2140-2149.e3. DOI: 10.1016/j.celrep.2019.01.096.
- Cummings J.L., Gonzalez M.I., Pritchard M.C., May P.C., Toledo-Sherman L.M., and Harris G.A. (2023): The therapeutic landscape of tauopathies: challenges and prospects. *Alzheimers Res Ther* 15 (1): 168. DOI: 10.1186/s13195-023-01321-7.
- De Luca A., De Falco M., De Luca L., Penta R., Shridhar V., Baldi F., Campioni M., Paggi M.G., and Baldi A. (2004): Pattern of expression of HtrA1 during mouse development. *J Histochem Cytochem* 52 (12): 1609–1617. DOI: 10.1369/jhc.4A6330.2004.
- De Luca A., De Falco M., Severino A., Campioni M., Santini D., Baldi F., Paggi M.G., and Baldi A. (2003): Distribution of the serine protease HtrA1 in normal human tissues. *J Histochem Cytochem* 51 (10): 1279–1284. DOI: 10.1177/002215540305101004.
- Devred F., Barbier P., Douillard S., Monasterio O., Andreu J.M., and Peyrot V. (2004): Tau induces ring and microtubule formation from alphabeta-tubulin dimers under nonassembly conditions. *Biochemistry* 43 (32): 10520–10531. DOI: 10.1021/bi0493160.
- Drummond E., Kavanagh T., Pires G., Marta-Ariza M., Kanshin E., Nayak S., Faustin A., Berdah V., Ueberheide B., and Wisniewski T. (2022): The amyloid plaque proteome in early onset Alzheimer's disease and Down syndrome. *Acta Neuropathol Commun* 10 (1): 53. DOI: 10.1186/s40478-022-01356-1.
- Dunker A.K., Silman I., Uversky V.N., and Sussman J.L. (2008): Function and structure of inherently disordered proteins. *Curr Opin Struct Biol* 18 (6): 756–764. DOI: 10.1016/j.sbi.2008.10.002.
- Eichmüller O.L., and Knoblich J.A. (2022): Human cerebral organoids - a new tool for clinical neurology research. *Nat Rev Neurol* 18 (11): 661–680. DOI: 10.1038/s41582-022-00723-9.
- Eigenbrot C., Ultsch M., Lipari M.T., Moran P., Lin S.J., Ganesan R., Quan C., Tom J., Sandoval W., van Lookeren Campagne M., and Kirchhofer D. (2012):

- Structural and functional analysis of HtrA1 and its subdomains. *Structure* 20 (6): 1040–1050. DOI: 10.1016/j.str.2012.03.021.
- Ellis R.J., and Minton A.P. (2006): Protein aggregation in crowded environments. *Biol Chem* 387 (5): 485–497. DOI: 10.1515/BC.2006.064.
- Esposito V., Campioni M., Luca A. de, Spugnini E.P., Baldi F., Cassandro R., Mancini A., Vincenzi B., Groeger A., Caputi M., and Baldi A. (2006): Analysis of HtrA1 serine protease expression in human lung cancer. *Anticancer Res* 26 (5A): 3455–3459.
- Falcon B., Zhang W., Schweighauser M., Murzin A.G., Vidal R., Garringer H.J., Ghetti B., Scheres S.H.W., and Goedert M. (2018): Tau filaments from multiple cases of sporadic and inherited Alzheimer's disease adopt a common fold. *Acta Neuropathol* 136 (5): 699–708. DOI: 10.1007/s00401-018-1914-z.
- Finley D. (2009): Recognition and processing of ubiquitin-protein conjugates by the proteasome. *Annu Rev Biochem* 78: 477–513. DOI: 10.1146/annurev.biochem.78.081507.101607.
- Fitzpatrick A.W.P., Falcon B., He S., Murzin A.G., Murshudov G., Garringer H.J., Crowther R.A., Ghetti B., Goedert M., and Scheres S.H.W. (2017): Cryo-EM structures of tau filaments from Alzheimer's disease. *Nature* 547 (7662): 185–190. DOI: 10.1038/nature23002.
- Goedert M., and Jakes R. (1990): Expression of separate isoforms of human tau protein: correlation with the tau pattern in brain and effects on tubulin polymerization. *EMBO J* 9 (13): 4225–4230. DOI: 10.1002/j.1460-2075.1990.tb07870.x.
- Goedert M., Jakes R., Spillantini M.G., Hasegawa M., Smith M.J., and Crowther R.A. (1996): Assembly of microtubule-associated protein tau into Alzheimer-like filaments induced by sulphated glycosaminoglycans. *Nature* 383 (6600): 550–553. DOI: 10.1038/383550a0.
- Goedert M., Spillantini M.G., Jakes R., Rutherford D., and Crowther R.A. (1989): Multiple isoforms of human microtubule-associated protein tau: sequences and localization in neurofibrillary tangles of Alzheimer's disease. *Neuron* 3 (4): 519–526. DOI: 10.1016/0896-6273(89)90210-9.

- Grau S., Baldi A., Bussani R., Tian X., Stefanescu R., Przybylski M., Richards P., Jones S.A., Shridhar V., Clausen T., and Ehrmann M. (2005): Implications of the serine protease HtrA1 in amyloid precursor protein processing. *Proc Natl Acad Sci USA* 102 (17): 6021–6026. DOI: 10.1073/pnas.0501823102.
- Grau S., Richards P.J., Kerr B., Hughes C., Caterson B., Williams A.S., Junker U., Jones S.A., Clausen T., and Ehrmann M. (2006): The role of human HtrA1 in arthritic disease. *J Biol Chem* 281 (10): 6124–6129. DOI: 10.1074/jbc.M500361200.
- Gray C.W., Ward R.V., Karran E., Turconi S., Rowles A., Viglienghi D., Southan C., Barton A., Fantom K.G., West A., Savopoulos J., Hassan N.J., Clinkenbeard H., Hanning C., Amegadzie B., Davis J.B., Dingwall C., Livi G.P., and Creasy C.L. (2000): Characterization of human HtrA2, a novel serine protease involved in the mammalian cellular stress response. *Eur J Biochem* 267 (18): 5699–5710. DOI: 10.1046/j.1432-1327.2000.01589.x.
- Hadfield K.D., Rock C.F., Inkson C.A., Dallas S.L., Sudre L., Wallis G.A., Boot-Handford R.P., and Canfield A.E. (2008): HtrA1 inhibits mineral deposition by osteoblasts: requirement for the protease and PDZ domains. *J Biol Chem* 283 (9): 5928–5938. DOI: 10.1074/jbc.M709299200.
- Hara K., Shiga A., Fukutake T., Nozaki H., Miyashita A., Yokoseki A., Kawata H., Koyama A., Arima K., Takahashi T., Ikeda M., Shiota H., Tamura M., Shimoe Y., Hirayama M., Arisato T., Yanagawa S., Tanaka A., Nakano I., Ikeda S., Yoshida Y., Yamamoto T., Ikeuchi T., Kuwano R., Nishizawa M., Tsuji S., and Onodera O. (2009): Association of HTRA1 mutations and familial ischemic cerebral small-vessel disease. *N Engl J Med* 360 (17): 1729–1739. DOI: 10.1056/NEJMoa0801560.
- Hartl F.U., Bracher A., and Hayer-Hartl M. (2011): Molecular chaperones in protein folding and proteostasis. *Nature* 475 (7356): 324–332. DOI: 10.1038/nature10317.
- He X., Khurana A., Maguire J.L., Chien J., and Shridhar V. (2012): HtrA1 sensitizes ovarian cancer cells to cisplatin-induced cytotoxicity by targeting XIAP for degradation. *Int J Cancer* 130 (5): 1029–1035. DOI: 10.1002/ijc.26044.
- He X., Ota T., Liu P., Su C., Chien J., and Shridhar V. (2010): Downregulation of HtrA1 promotes resistance to anoikis and peritoneal dissemination of ovarian cancer cells. *Cancer Res* 70 (8): 3109–3118. DOI: 10.1158/0008-5472.CAN-09-3557.

- Himmler A., Drechsel D., Kirschner M.W., and Martin D.W. (1989): Tau consists of a set of proteins with repeated C-terminal microtubule-binding domains and variable N-terminal domains. *Mol Cell Biol* 9 (4): 1381–1388. DOI: 10.1128/mcb.9.4.1381-1388.1989.
- Hou J., Clemmons D.R., and Smeekens S. (2005): Expression and characterization of a serine protease that preferentially cleaves insulin-like growth factor binding protein-5. *J Cell Biochem* 94 (3): 470–484. DOI: 10.1002/jcb.20328.
- Hoy B., Löwer M., Weydig C., Carra G., Tegtmeyer N., Geppert T., Schröder P., Sewald N., Backert S., Schneider G., and Wessler S. (2010): Helicobacter pylori HtrA is a new secreted virulence factor that cleaves E-cadherin to disrupt intercellular adhesion. *EMBO Rep* 11 (10): 798–804. DOI: 10.1038/embor.2010.114.
- Hu S.I., Carozza M., Klein M., Nantermet P., Luk D., and Crowl R.M. (1998): Human HtrA, an evolutionarily conserved serine protease identified as a differentially expressed gene product in osteoarthritic cartilage. *J Biol Chem* 273 (51): 34406–34412. DOI: 10.1074/jbc.273.51.34406.
- Isaac D.D., Pinkner J.S., Hultgren S.J., and Silhavy T.J. (2005): The extracytoplasmic adaptor protein CpxP is degraded with substrate by DegP. *Proc Natl Acad Sci USA* 102 (49): 17775–17779. DOI: 10.1073/pnas.0508936102.
- Jayaraj G.G., Hipp M.S., and Hartl F.U. (2020): Functional Modules of the Proteostasis Network. *Cold Spring Harb Perspect Biol* 12 (1). DOI: 10.1101/cshperspect.a033951.
- Jeganathan S., Hascher A., Chinnathambi S., Biernat J., Mandelkow E.-M., and Mandelkow E. (2008): Proline-directed pseudo-phosphorylation at AT8 and PHF1 epitopes induces a compaction of the paperclip folding of Tau and generates a pathological (MC-1) conformation. *J Biol Chem* 283 (46): 32066–32076. DOI: 10.1074/jbc.M805300200.
- Jeganathan S., von Bergen M., Brutlach H., Steinhoff H.-J., and Mandelkow E. (2006): Global hairpin folding of tau in solution. *Biochemistry* 45 (7): 2283–2293. DOI: 10.1021/bi0521543.

Jiang S., and Bhaskar K. (2020): Degradation and Transmission of Tau by Autophagic-Endolysosomal Networks and Potential Therapeutic Targets for Tauopathy. *Front Mol Neurosci* 13: 586731. DOI: 10.3389/fnmol.2020.586731.

Johnson G.V.W., and Stoothoff W.H. (2004): Tau phosphorylation in neuronal cell function and dysfunction. *J Cell Sci* 117 (24): 5721–5729. DOI: 10.1242/jcs.01558.

Kampers T., Friedhoff P., Biernat J., Mandelkow E.M., and Mandelkow E. (1996): RNA stimulates aggregation of microtubule-associated protein tau into Alzheimer-like paired helical filaments. *FEBS Lett* 399 (3): 344–349. DOI: 10.1016/s0014-5793(96)01386-5.

Kapri-Pardes E., Naveh L., and Adam Z. (2007): The thylakoid lumen protease Deg1 is involved in the repair of photosystem II from photoinhibition in Arabidopsis. *Plant Cell* 19 (3): 1039–1047. DOI: 10.1105/tpc.106.046573.

Kellogg E.H., Hejab N.M.A., Poepsel S., Downing K.H., DiMaio F., and Nogales E. (2018): Near-atomic model of microtubule-tau interactions. *Science* 360 (6394): 1242–1246. DOI: 10.1126/science.aat1780.

Krojer T., Pangerl K., Kurt J., Sawa J., Stingl C., Mechtler K., Huber R., Ehrmann M., and Clausen T. (2008a): Interplay of PDZ and protease domain of DegP ensures efficient elimination of misfolded proteins. *Proc Natl Acad Sci USA* 105 (22): 7702–7707. DOI: 10.1073/pnas.0803392105.

Krojer T., Sawa J., Huber R., and Clausen T. (2010): HtrA proteases have a conserved activation mechanism that can be triggered by distinct molecular cues. *Nat Struct Mol Biol* 17 (7): 844–852. DOI: 10.1038/nsmb.1840.

Krojer T., Sawa J., Schäfer E., Saibil H.R., Ehrmann M., and Clausen T. (2008b): Structural basis for the regulated protease and chaperone function of DegP. *Nature* 453 (7197): 885–890. DOI: 10.1038/nature07004.

Launay S., Maubert E., Lebeurrier N., Tennstaedt A., Campioni M., Docagne F., Gabriel C., Dauphinot L., Potier M.C., Ehrmann M., Baldi A., and Vivien D. (2008): HtrA1-dependent proteolysis of TGF-beta controls both neuronal maturation and developmental survival. *Cell Death Differ* 15 (9): 1408–1416. DOI: 10.1038/cdd.2008.82.

- Lin M.K., Yang J., Hsu C.W., Gore A., Bassuk A.G., Brown L.M., Colligan R., Sengillo J.D., Mahajan V.B., and Tsang S.H. (2018): HTRA1, an age-related macular degeneration protease, processes extracellular matrix proteins EFEMP1 and TSP1. *Aging Cell* 17 (4): e12710. DOI: 10.1111/ace1.12710.
- Lindwall G., and Cole R.D. (1984): Phosphorylation affects the ability of tau protein to promote microtubule assembly. *J Biol Chem* 259 (8): 5301–5305. DOI: 10.1016/S0021-9258(17)42989-9.
- Louros N., Schymkowitz J., and Rousseau F. (2023): Mechanisms and pathology of protein misfolding and aggregation. *Nat Rev Mol Cell Biol* 24 (12): 912–933. DOI: 10.1038/s41580-023-00647-2.
- Lövestam S., Koh F.A., van Knippenberg B., Kotecha A., Murzin A.G., Goedert M., and Scheres S.H.W. (2022): Assembly of recombinant tau into filaments identical to those of Alzheimer's disease and chronic traumatic encephalopathy. *Elife* 11: e76494. DOI: 10.7554/eLife.76494.
- Mandelkow E.M., Biernat J., Drewes G., Gustke N., Trinczek B., and Mandelkow E. (1995): Tau domains, phosphorylation, and interactions with microtubules. *Neurobiol Aging* 16 (3): 355-363. DOI: 10.1016/0197-4580(95)00025-a.
- Mendes M.L., Fischer L., Chen Z.A., Barbon M., O'Reilly F.J., Giese S.H., Bohlke-Schneider M., Belsom A., Dau T., Combe C.W., Graham M., Eisele M.R., Baumeister W., Speck C., and Rappsilber J. (2019): An integrated workflow for crosslinking mass spectrometry. *Mol Syst Biol* 15 (9): e8994. DOI: 10.15252/msb.20198994.
- Meng J.X., Zhang Y., Saman D., Haider A.M., De S., Sang J.C., Brown K., Jiang K., Humphrey J., Julian L., Hidari E., Lee S.F., Balmus G., Floto R.A., Bryant C.E., Benesch J.L.P., Ye Y., and Klenerman D. (2022): Hyperphosphorylated tau self-assembles into amorphous aggregates eliciting TLR4-dependent responses. *Nat Commun* 13 (1): 2692. DOI: 10.1038/s41467-022-30461-x.
- Merdanovic M., Mamant N., Meltzer M., Poepsel S., Auckenthaler A., Melgaard R., Hauske P., Nagel-Steger L., Clarke A.R., Kaiser M., Huber R., and Ehrmann M. (2010): Determinants of structural and functional plasticity of a widely conserved protease chaperone complex. *Nat Struct Mol Biol* 17 (7): 837–843. DOI: 10.1038/nsmb.1839.

Moisoi N., Klupsch K., Fedele V., East P., Sharma S., Renton A., Plun-Favreau H., Edwards R.E., Teismann P., Esposti M.D., Morrison A.D., Wood N.W., Downward J., and Martins L.M. (2009): Mitochondrial dysfunction triggered by loss of HtrA2 results in the activation of a brain-specific transcriptional stress response. *Cell Death Differ* 16 (3): 449–464. DOI: 10.1038/cdd.2008.166.

Mukrasch M.D., Bibow S., Korukottu J., Jeganathan S., Biernat J., Griesinger C., Mandelkow E., and Zweckstetter M. (2009): Structural polymorphism of 441-residue tau at single residue resolution. *PLoS Biol* 7 (2): e34. DOI: 10.1371/journal.pbio.1000034.

Mullany S.A., Moslemi-Kebria M., Rattan R., Khurana A., Clayton A., Ota T., Mariani A., Podratz K.C., Chien J., and Shridhar V. (2011): Expression and functional significance of HtrA1 loss in endometrial cancer. *Clin Cancer Res* 17 (3): 427–436. DOI: 10.1158/1078-0432.CCR-09-3069.

Muratoglu S.C., Belgrave S., Hampton B., Migliorini M., Coksaygan T., Chen L., Mikhailenko I., and Strickland D.K. (2013): LRP1 protects the vasculature by regulating levels of connective tissue growth factor and HtrA1. *Arterioscler Thromb Vasc Biol* 33 (9): 2137–2146. DOI: 10.1161/ATVBAHA.113.301893.

Nachman E., Wentink A.S., Madiona K., Bousset L., Katsinelos T., Allinson K., Kampinga H., McEwan W.A., Jahn T.R., Melki R., Mogk A., Bukau B., and Nussbaum-Krammer C. (2020): Disassembly of Tau fibrils by the human Hsp70 disaggregation machinery generates small seeding-competent species. *J Biol Chem* 295 (28): 9676–9690. DOI: 10.1074/jbc.RA120.013478.

Neve R.L., Harris P., Kosik K.S., Kurnit D.M., and Donlon T.A. (1986): Identification of cDNA clones for the human microtubule-associated protein tau and chromosomal localization of the genes for tau and microtubule-associated protein 2. *Brain Res* 387 (3): 271–280. DOI: 10.1016/0169-328x(86)90033-1.

Nie G.-Y., Hampton A., Li Y., Findlay J.K., and Salamonsen L.A. (2003): Identification and cloning of two isoforms of human high-temperature requirement factor A3 (HtrA3), characterization of its genomic structure and comparison of its tissue distribution with HtrA1 and HtrA2. *Biochem J* 371 (1): 39–48. DOI: 10.1042/BJ20021569.

- Noble W., Hanger D.P., Miller C.C.J., and Lovestone S. (2013): The importance of tau phosphorylation for neurodegenerative diseases. *Front Neurol* 4: 83. DOI: 10.3389/fneur.2013.00083.
- Novak M., Kabat J., and Wischik C.M. (1993): Molecular characterization of the minimal protease resistant tau unit of the Alzheimer's disease paired helical filament. *EMBO J* 12 (1): 365–370. DOI: 10.1002/j.1460-2075.1993.tb05665.x.
- Oka C., Tsujimoto R., Kajikawa M., Koshiba-Takeuchi K., Ina J., Yano M., Tsuchiya A., Ueta Y., Soma A., Kanda H., Matsumoto M., and Kawaichi M. (2004): HtrA1 serine protease inhibits signaling mediated by Tgfbeta family proteins. *Development* 131 (5): 1041–1053. DOI: 10.1242/dev.00999.
- Pallen M.J., and Wren B.W. (1997): The HtrA family of serine proteases. *Mol Microbiol* 26 (2): 209–221. DOI: 10.1046/j.1365-2958.1997.5601928.x.
- Poepsel S., Sprengel A., Sacca B., Kaschani F., Kaiser M., Gatsogiannis C., Raunser S., Clausen T., and Ehrmann M. (2015): Determinants of amyloid fibril degradation by the PDZ protease HTRA1. *Nat Chem Biol* 11 (11): 862–869. DOI: 10.1038/nchembio.1931.
- Regt A.K. de, Baker T.A., and Sauer R.T. (2015): Steric clashes with bound OMP peptides activate the DegS stress-response protease. *Proc Natl Acad Sci USA* 112 (11): 3326–3331. DOI: 10.1073/pnas.1502372112.
- Remaut H., and Waksman G. (2006): Protein-protein interaction through beta-strand addition. *Trends Biochem Sci* 31 (8): 436–444. DOI: 10.1016/j.tibs.2006.06.007.
- Rey J., Breiden M., Lux V., Bluemke A., Steindel M., Ripkens K., Möllers B., Bravo-Rodriguez K., Boisguerin P., Volkmer R., Mieres-Perez J., Clausen T., Sanchez-Garcia E., and Ehrmann M. (2022): An allosteric HTRA1-calpain 2 complex with restricted activation profile. *Proc Natl Acad Sci USA* 119 (14): e2113520119. DOI: 10.1073/pnas.2113520119.
- Runyon S.T., Zhang Y., Appleton B.A., Sazinsky S.L., Wu P., Pan B., Wiesmann C., Skelton N.J., and Sidhu S.S. (2007): Structural and functional analysis of the PDZ domains of human HtrA1 and HtrA3. *Protein Sci* 16 (11): 2454–2471. DOI: 10.1110/ps.073049407.

- Saha I., Yuste-Checa P., Da Silva Padilha M., Guo Q., Körner R., Holthusen H., Trinkaus V.A., Dudanova I., Fernández-Busnadiego R., Baumeister W., Sanders D.W., Gautam S., Diamond M.I., Hartl F.U., and Hipp M.S. (2023): The AAA+ chaperone VCP disaggregates Tau fibrils and generates aggregate seeds in a cellular system. *Nat Commun* 14 (1): 560. DOI: 10.1038/s41467-023-36058-2.
- Sawa J., Malet H., Krojer T., Canellas F., Ehrmann M., and Clausen T. (2011): Molecular adaptation of the DegQ protease to exert protein quality control in the bacterial cell envelope. *J Biol Chem* 286 (35): 30680–30690. DOI: 10.1074/jbc.M111.243832.
- Scheres S.H., Zhang W., Falcon B., and Goedert M. (2020): Cryo-EM structures of tau filaments. *Curr Opin Struct Biol* 64: 17–25. DOI: 10.1016/j.sbi.2020.05.011.
- Scheres S.H.W., Ryskeldi-Falcon B., and Goedert M. (2023): Molecular pathology of neurodegenerative diseases by cryo-EM of amyloids. *Nature* 621 (7980): 701–710. DOI: 10.1038/s41586-023-06437-2.
- Schindelin J., Arganda-Carreras I., Frise E., Kaynig V., Longair M., Pietzsch T., Preibisch S., Rueden C., Saalfeld S., Schmid B., Tinevez J.-Y., White D.J., Hartenstein V., Eliceiri K., Tomancak P., and Cardona A. (2012): Fiji: an open-source platform for biological-image analysis. *Nat Methods* 9 (7): 676–682. DOI: 10.1038/nmeth.2019.
- Sheng M., and Sala C. (2001): PDZ domains and the organization of supramolecular complexes. *Annu Rev Neurosci* 24: 1–29. DOI: 10.1146/annurev.neuro.24.1.1.
- Singh H., Endo Y., and Nie G. (2011): Decidual HtrA3 negatively regulates trophoblast invasion during human placentation. *Hum Reprod* 26 (4): 748–757. DOI: 10.1093/humrep/der019.
- Spiess C., Beil A., and Ehrmann M. (1999): A temperature-dependent switch from chaperone to protease in a widely conserved heat shock protein. *Cell* 97 (3): 339–347. DOI: 10.1016/s0092-8674(00)80743-6.
- Steger C. (1998): An unbiased detector of curvilinear structures. *IEEE Trans Pattern Anal Mach Intell* 20 (2): 113–125. DOI: 10.1109/34.659930.

- Tennstaedt A., Pöpsel S., Truebestein L., Hauske P., Brockmann A., Schmidt N., Irle I., Sacca B., Niemeyer C.M., Brandt R., Ksiezak-Reding H., Tirniceriu A.L., Egensperger R., Baldi A., Dehmelt L., Kaiser M., Huber R., Clausen T., and Ehrmann M. (2012): Human high temperature requirement serine protease A1 (HTRA1) degrades tau protein aggregates. *J Biol Chem* 287 (25): 20931–20941. DOI: 10.1074/jbc.M111.316232.
- Tiaden A.N., and Richards P.J. (2013): The emerging roles of HTRA1 in musculoskeletal disease. *Am J Pathol* 182 (5): 1482–1488. DOI: 10.1016/j.ajpath.2013.02.003.
- Tocharus J., Tsuchiya A., Kajikawa M., Ueta Y., Oka C., and Kawaichi M. (2004): Developmentally regulated expression of mouse HtrA3 and its role as an inhibitor of TGF-beta signaling. *Dev Growth Differ* 46 (3): 257–274. DOI: 10.1111/j.1440-169X.2004.00743.x.
- Trinczek B., Biernat J., Baumann K., Mandelkow E.M., and Mandelkow E. (1995): Domains of tau protein, differential phosphorylation, and dynamic instability of microtubules. *Mol Biol Cell* 6 (12): 1887–1902. DOI: 10.1091/mbc.6.12.1887.
- Truebestein L., Tennstaedt A., Mönig T., Krojer T., Canellas F., Kaiser M., Clausen T., and Ehrmann M. (2011): Substrate-induced remodeling of the active site regulates human HTRA1 activity. *Nat Struct Mol Biol* 18 (3): 386–388. DOI: 10.1038/nsmb.2013.
- Tyedmers J., Mogk A., and Bukau B. (2010): Cellular strategies for controlling protein aggregation. *Nat Rev Mol Cell Biol* 11 (11): 777–788. DOI: 10.1038/nrm2993.
- Vande Walle L., Lamkanfi M., and Vandenabeele P. (2008): The mitochondrial serine protease HtrA2/Omi: an overview. *Cell Death Differ* 15 (3): 453–460. DOI: 10.1038/sj.cdd.4402291.
- Verhagen A.M., Silke J., Ekert P.G., Pakusch M., Kaufmann H., Connolly L.M., Day C.L., Tikoo A., Burke R., Wrobel C., Moritz R.L., Simpson R.J., and Vaux D.L. (2002): HtrA2 promotes cell death through its serine protease activity and its ability to antagonize inhibitor of apoptosis proteins. *J Biol Chem* 277 (1): 445–454. DOI: 10.1074/jbc.M109891200.

- Vierkotten S., Muether P.S., and Fauser S. (2011): Overexpression of HTRA1 leads to ultrastructural changes in the elastic layer of Bruch's membrane via cleavage of extracellular matrix components. *PLoS One* 6 (8): e22959. DOI: 10.1371/journal.pone.0022959.
- von Bergen M., Barghorn S., Müller S.A., Pickhardt M., Biernat J., Mandelkow E.-M., Davies P., Aebi U., and Mandelkow E. (2006): The core of tau-paired helical filaments studied by scanning transmission electron microscopy and limited proteolysis. *Biochemistry* 45 (20): 6446–6457. DOI: 10.1021/bi052530j.
- Walsh N.P., Alba B.M., Bose B., Gross C.A., and Sauer R.T. (2003): OMP peptide signals initiate the envelope-stress response by activating DegS protease via relief of inhibition mediated by its PDZ domain. *Cell* 113 (1): 61–71. DOI: 10.1016/s0092-8674(03)00203-4.
- Wang L.-J., Cheong M.-L., Lee Y.-S., Lee M.-T., and Chen H. (2012): High-temperature requirement protein A4 (HtrA4) suppresses the fusogenic activity of syncytin-1 and promotes trophoblast invasion. *Mol Cell Biol* 32 (18): 3707–3717. DOI: 10.1128/MCB.00223-12.
- Wang Y., and Mandelkow E. (2016): Tau in physiology and pathology. *Nat Rev Neurosci* 17 (1): 5–21. DOI: 10.1038/nrn.2015.1.
- Wang Y., and Nie G. (2021): Overview of Human HtrA Family Proteases and Their Distinctive Physiological Roles and Unique Involvement in Diseases, Especially Cancer and Pregnancy Complications. *Int J Mol Sci* 22 (19): 10756. DOI: 10.3390/ijms221910756.
- Weingarten M.D., Lockwood A.H., Hwo S.Y., and Kirschner M.W. (1975): A protein factor essential for microtubule assembly. *Proc Natl Acad Sci USA* 72 (5): 1858–1862. DOI: 10.1073/pnas.72.5.1858.
- Wenta T., Rychlowski M., Jurewicz E., Jarzab M., Zurawa-Janicka D., Filipek A., and Lipinska B. (2019): The HtrA3 protease promotes drug-induced death of lung cancer cells by cleavage of the X-linked inhibitor of apoptosis protein (XIAP). *FEBS J* 286 (22): 4579–4596. DOI: 10.1111/febs.14977.
- Wenta T., Zurawa-Janicka D., Rychlowski M., Jarzab M., Glaza P., Lipinska A., Bienkowska-Szewczyk K., Herman-Antosiewicz A., Skorko-Glonek J., and

- Lipinska B. (2018): HtrA3 is a cellular partner of cytoskeleton proteins and TCP1 α chaperonin. *J Proteomics* 177: 88–111. DOI: 10.1016/j.jprot.2018.02.022.
- Wilken C., Kitzing K., Kurzbauer R., Ehrmann M., and Clausen T. (2004): Crystal structure of the DegS stress sensor: How a PDZ domain recognizes misfolded protein and activates a protease. *Cell* 117 (4): 483–494. DOI: 10.1016/s0092-8674(04)00454-4.
- Winklhofer K.F., Tatzelt J., and Haass C. (2008): The two faces of protein misfolding: gain- and loss-of-function in neurodegenerative diseases. *EMBO J* 27 (2): 336–349. DOI: 10.1038/sj.emboj.7601930.
- Wischik C.M., Novak M., Thøgersen H.C., Edwards P.C., Runswick M.J., Jakes R., Walker J.E., Milstein C., Roth M., and Klug A. (1988): Isolation of a fragment of tau derived from the core of the paired helical filament of Alzheimer disease. *Proc Natl Acad Sci USA* 85 (12): 4506–4510. DOI: 10.1073/pnas.85.12.4506.
- Xie Z., and Klionsky D.J. (2007): Autophagosome formation: core machinery and adaptations. *Nat Cell Biol* 9 (10): 1102–1109. DOI: 10.1038/ncb1007-1102.
- Yoshida H., and Goedert M. (2006): Sequential phosphorylation of tau protein by cAMP-dependent protein kinase and SAPK4/p38delta or JNK2 in the presence of heparin generates the AT100 epitope. *J Neurochem* 99 (1): 154–164. DOI: 10.1111/j.1471-4159.2006.04052.x.
- Zhang W., Falcon B., Murzin A.G., Fan J., Crowther R.A., Goedert M., and Scheres S.H. (2019): Heparin-induced tau filaments are polymorphic and differ from those in Alzheimer's and Pick's diseases. *Elife* 8: e43584. DOI: 10.7554/eLife.43584.
- Zumbrunn J., and Trueb B. (1997): Localization of the gene for a serine protease with IGF-binding domain (PRSS11) to human chromosome 10q25.3-q26.2. *Genomics* 45 (2): 461–462. DOI: 10.1006/geno.1997.4953.
- Zurawa-Janicka D., Wenta T., Jarzab M., Skorko-Glonek J., Glaza P., Gieldon A., Ciarkowski J., and Lipinska B. (2017): Structural insights into the activation mechanisms of human HtrA serine proteases. *Arch Biochem Biophys* 621: 6–23. DOI: 10.1016/j.abb.2017.04.004.

Appendix

Appendix A:

Table 15: Phosphorylation sites of Tau detected by LC-MS/MS

Recombinant Tau (Tau) was phosphorylated by PKA (Tau-p) and subsequently by GSK3 β (Tau-pg) or SAPK4 (Tau-ps). Phosphorylation sites were identified by LC-MS-MS analysis.

Amino Acid	Site	Tau	Tau-p	Tau-pg	Tau-ps
T	17			X	X
T	30		X	X	X
S	46			X	X
T	50			X	X
T	69			X	
T	111				X
S	113		X	X	
T	153				X
T	175			X	X
T	181			X	X
S	184				X
S	191			X	X
S	195	X		X	
S	198			X	
S	199				X
S	202			X	X
T	205			X	X
S	208		X	X	X
S	210		X	X	
T	212			X	X
S	214		X	X	X
T	217			X	X
T	220				X
T	231			X	X
S	235				X
S	238				X
S	241			X	
T	245		X	X	X
S	258			X	
S	262		X	X	X
S	285			X	
S	289		X	X	X
S	305	X	X	X	X
S	316			X	X

T	319		X	X	X
S	324		X	X	X
S	352		X	X	X
S	356	X	X	X	X
T	361				X
T	377		X	X	X
T	386		X	X	X
S	396	X	X	X	X
S	400		X	X	X
T	403				X
S	404			X	X
S	409		X	X	X
S	412		X	X	
S	413				X
S	416		X		

Appendix B:

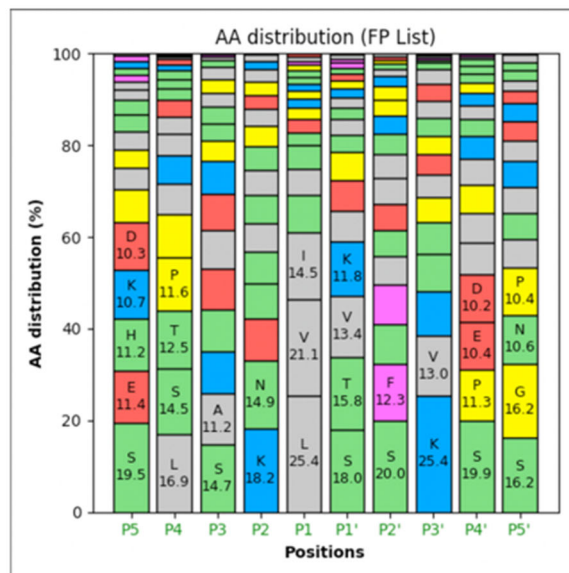


Figure 25: Relative amino acid distribution around HTRA1 cleavage sites within the Tau sequence

Relative amino acid distribution at positions P1–5 and P1'–5' within the Tau sequence detected after cleavage by HTRA1 for 120 min. Amino acids are color-coded according to their properties (positively charged (blue), negatively charged (red), polar (green), non-polar (grey), aromatic (magenta), and G and P in yellow). Amino acids that make up more than 10% within a certain position are labeled with the one-letter code for the amino acid and the respective percentage value.

Appendix C: Protein sequences

Tau^{CN}

```

1 MAEPRQEFEV MEDHAGTYGL GDRKDQGGYT MHQDQEGDTD AEIVYKSPVV
51 SGDTSPRHLS NVSSTGSIDM VDSPQLATLA DEVSASLAKQ GLEGTAAEEA
101 GIGDTPSLED EAAGHVQTQAR MVSKSKDGTG SDDKKAKGAD GGTKIATPRG
151 AAPPGQKGQA NATRIPAKTP PAPKTPPSSG EPPKSGDRSG YSSPGSPGTP
201 GSRSRTPSLP TPPTREPKKV AVVRTPPKSP SSAKSRLQTA PVPMPDLKNV
251 KSKIGSTENL KHQPGGGKVQ IINKKLDLSN VQSKCGSKDN IKHVPGGGSV
301 QIVYKPV DLS KVT SKCGSLG NIHHKPGGGQ VEVKSEK LDF KDRVQSKIGS
351 LDNITHVPGG GNKKIETHKL TFRENAKAKT DHGAGLKESP LQTP TEDGSE
401 EPGSETSDAK STPTAEDVTA PLVDEGAPGK QAAAQPHT EI P*

```

Tau^{CNC}

```

1 MAEPRQEFEV MEDHAGTYGL GDRKDQGGYT MHQDQEGDTD AEIVYKSPVV
51 SGDTSPRHLS NVSSTGSIDM VDSPQLATLA DEVSASLAKQ GLEGTAAEEA
101 GIGDTPSLED EAAGHVQTQAR MVSKSKDGTG SDDKKAKGAD GGTKIATPRG
151 AAPPGQKGQA NATRIPAKTP PAPKTPPSSG EPPKSGDRSG YSSPGSPGTP
201 GSRSRTPSLP TPPTREPKKV AVVRTPPKSP SSAKSRLQTA PVPMPDLKNV
251 KSKIGSTENL KHQPGGGKVQ IINKKLDLSN VQSKCGSKDN IKHVPGGGSV
301 QIVYKPV DLS KVT SKCGSLG NIHHKPGGGQ VEVKSEK LDF KDRVQSKIGS
351 LDNITHVPGG GNKKIETHKL TFRENAKAKT DHGAGLKESP LQTP TEDGSE
401 EPGSETSDAK STPTAEDVTA PLVDEGAPGK QAAAQPHT EI PDMVDS PQLA
451 TLADEV SASL AKQGL*

```

Danksagung

Zunächst möchte ich mich sehr herzlich bei Prof. Michael Ehrmann bedanken für die Aufnahme in der Arbeitsgruppe und die Möglichkeit an diesem spannenden Projekt zu arbeiten. Vielen Dank für die außergewöhnliche Unterstützung, die vielen anregenden Diskussionen und vor allem für die große Handlungsfreiheit und das damit entgegengebrachte Vertrauen.

Vielen Dank auch an Prof. Markus Kaiser, Dr. Farnusch Kaschani für die Unterstützung mit den massenspektroskopischen Analysen. Ebenso bedanke ich mich bei Michal Strzala und der IMP/IMBA/GMI Proteomics Facility für die Durchführung der Cross-Linking Experimente. Vielen Dank an Lucia Gallego Villarejo und Dr. Nina Schulze für die Durchführung und Analyse der Organoid Experimente und an Jonas Neblik für das Bereitstellen der Mikrotubuli.

Ein besonderer Dank gilt der gesamten Arbeitsgruppe Ehrmann. Vielen Dank Anto, Basti, Hai, Helmut, Kamilla, Lara, Lucas, Melisa, Michael, Michael, Michal, Michelle, Mina und Svenja! Ihr habt das Projekt Doktorarbeit nicht nur fachlich hervorragend unterstützt, sondern auch für eine großartige und unvergessliche Zeit gesorgt. Insbesondere möchte ich mich bei Melisa bedanken, die mich, beginnend mit der Projektfindung, über die Höhen und Tiefen der Forschungsarbeit bis zum Zusammenschreiben der Ergebnisse unaufhörlich unterstützt hast. Einen besonderen Dank auch an Michelle, die mir nicht nur während des Forschens und Schreibens immer beigestanden hat, sondern auch eine meiner besten Freundinnen geworden ist. Und natürlich auch ein großer Dank an Helmut, der nicht nur für einen reibungslosen Ablauf im Labor sorgt, sondern sich auch stets hingebungsvoll um alle sozialen und gesellschaftlichen Belange der Arbeitsgruppe kümmert.

Mein besonderer Dank gilt meiner Familie. Insbesondere danke ich meinen Eltern und meiner Oma Helene, für ihre liebevolle Unterstützung und dafür, dass sie mich immer ermutigt und es mir ermöglicht haben meine Ziele zu verfolgen. Weiterhin bedanke ich mich bei meinen Freunden, besonders bei Anja die mir in der Schreibphase den Rücken freigehalten hat.

Zuletzt möchte ich mich bei meinem Partner Tim bedanken, der mit mir alle Höhen und Tiefen der Doktorarbeit durchgestanden hat. Vielen Dank für alles!

Lebenslauf

Der Lebenslauf ist in der Online-Version aus Gründen des Datenschutzes nicht enthalten.

Eidesstattliche Erklärung

Erklärung:

Hiermit erkläre ich, gem. § 7 Abs. (2) d) + f) der Promotionsordnung der Fakultät für Biologie zur Erlangung des Dr. rer. nat., dass ich die vorliegende Dissertation selbstständig verfasst und mich keiner anderen als der angegebenen Hilfsmittel bedient, bei der Abfassung der Dissertation nur die angegebenen Hilfsmittel benutzt und alle wörtlich oder inhaltlich übernommenen Stellen als solche gekennzeichnet habe.

Essen, den 10.04.2024

Birte Hagemeyer

Erklärung:

Hiermit erkläre ich, gem. § 7 Abs. (2) e) + g) der Promotionsordnung der Fakultät für Biologie zur Erlangung des Dr. rer. nat., dass ich keine anderen Promotionen bzw. Promotionsversuche in der Vergangenheit durchgeführt habe und dass diese Arbeit von keiner anderen Fakultät/Fachbereich abgelehnt worden ist.

Essen, den 10.04.2024

Birte Hagemeyer

Erklärung:

Hiermit erkläre ich, gem. § 6 Abs. (2) g) der Promotionsordnung der Fakultät für Biologie zur Erlangung der Dr. rer. nat., dass ich das Arbeitsgebiet, dem das Thema „*Mechanistic insights into the interactions of HTRA1 with pathological Tau species*“ zuzuordnen ist, in Forschung und Lehre vertrete und den Antrag von Birte Hagemeyer befürworte und die Betreuung auch im Falle eines Weggangs, wenn nicht wichtige Gründe dem entgegenstehen, weiterführen werde.

Essen, den 10.04.2024

Prof. Dr. Michael Ehrmann